

NOTICE: This document contains information of a preliminary nature and is not intended for release. It is subject to revision or correction and therefore does not represent a final report.

ORNL/TM-2020/?

BWR Progression Problems



Chase Lawing, NCSU
Scott Palmtag, NCSU
Mehdi Asgari, ORNL

Draft. Not for public release.

June 15, 2020

DOCUMENT AVAILABILITY

Reports produced after January 1, 1996, are generally available free via US Department of Energy (DOE) SciTech Connect.

Website: www.osti.gov/

Reports produced before January 1, 1996, may be purchased by members of the public from the following source:

National Technical Information Service
5285 Port Royal Road
Springfield, VA 22161
Telephone: 703-605-6000 (1-800-553-6847)
TDD: 703-487-4639
Fax: 703-605-6900
E-mail: info@ntis.gov
Website: <http://classic.ntis.gov/>

Reports are available to DOE employees, DOE contractors, Energy Technology Data Exchange representatives, and International Nuclear Information System representatives from the following source:

Office of Scientific and Technical Information
PO Box 62
Oak Ridge, TN 37831
Telephone: 865-576-8401
Fax: 865-576-5728
E-mail: report@osti.gov
Website: <http://www.osti.gov/contact.html>

This report was prepared as an account of work sponsored by an agency of the United States Government. Neither the United States Government nor any agency thereof, nor any of their employees, makes any warranty, express or implied, or assumes any legal liability or responsibility for the accuracy, completeness, or usefulness of any information, apparatus, product, or process disclosed, or represents that its use would not infringe privately owned rights. Reference herein to any specific commercial product, process, or service by trade name, trademark, manufacturer, or otherwise, does not necessarily constitute or imply its endorsement, recommendation, or favoring by the United States Government or any agency thereof. The views and opinions of authors expressed herein do not necessarily state or reflect those of the United States Government or any agency thereof.

Reactor and Nuclear Systems Division

BWR Progression Problems

Authors

Chase Lawing, NCSU
Scott Palmtag, NCSU
Mehdi Asgari, ORNL

Date Published: June 15, 2020

Prepared by
OAK RIDGE NATIONAL LABORATORY
Oak Ridge, TN 37831-6283
managed by
UT-Battelle, LLC
for the
US DEPARTMENT OF ENERGY
under contract DE-AC05-00OR22725

CONTENTS

LIST OF FIGURES	vii
LIST OF TABLES	ix
ACRONYMS	xi
1. INTRODUCTION	1
2. 2D BWR PROGRESSION PROBLEMS	3
2.1 Peach Bottom Assembly Type 6	4
2.2 GE-9 Lattice	7
2.3 Representative GE-14 Lattice	11
2.4 GE-14 Lattice with Vanished Rods	15
2.5 Mini-core	16
2.6 Control Blade Description	18
3. 3D BWR PROGRESSION PROBLEMS	21
4. RESULTS	27
4.1 Peach Bottom 6	27
4.1.1 Normalized Fission Rate Monte Carlo Results	27
4.2 GE-9	34
4.2.1 Normalized Fission Rate Monte Carlo Results	35
4.3 GE-14	41
4.3.1 Normalized Fission Rate Monte Carlo Results	42
4.4 GE-14 With Vanished Rods	48
4.4.1 Normalized Fission Rate Monte Carlo Results	49
4.5 2D Mini-Core	55
4.5.1 Normalized Fission Rate Monte Carlo Results	56
4.6 3D GE14 Bundle	59
5. CONCLUSION	65
6. REFERENCES	67
Appendices	69
A Number Densities For all Materials	69
A.1 Structural Material for the Peach Bottom 6 Lattice	70
A.2 Structural Materials for all Problems Problems except the Peach Bottom 6 Lattice	70
A.3 Fuels	72
A.3.1 Peach Bottom Type 6	72
A.3.2 GE9	72
A.3.3 GE14	73
A.4 Smeared Grid and Nozzle Number Densities	75
A.4.1 Smeared Structures for 3D HZP Case	75
A.4.2 Smeared Structures for 3D HFP 40% Case	77
A.5 Coolant Number Densities	79

LIST OF FIGURES

1	Dimensions for the Peach Bottom type 6 bundle design. All dimensions are in centimeters.	4
2	Dimensions for the Peach Bottom type 6 bundle fuel pin (left) and water rod (right). Dimensions are in centimeters and are not to scale.	5
3	Fuel layout for the Peach Bottom type 6 bundle	5
4	Dimensions for the GE-9 lattice. All dimensions are in centimeters.	7
5	Dimensions for the GE-9 fuel pin (left) and water rod (right). These two figures are not to scale. All dimensions are in centimeters.	8
6	Fuel layout for the GE-9 bundle	8
7	Dimensions for the GE-14 bundle design. All dimensions are in centimeters.	11
8	Dimensions for the GE-14 bundle fuel pin (left) and water rod (right). These two figures are not to scale. All dimensions are in centimeters.	12
9	Fuel layout for the GE-14 bundle	12
10	Fuel layout for the GE-14 lattice with vanished rods.	15
11	Geometry of the mini-core progression problem with the control blade inserted in the north west corner.	16
12	Void distribution for the uncontrolled multi-bundle case at 20% (left) and 60% (right) system averaged void.	17
13	Void distribution for the controlled multi-bundle case at 20% (left) and 60% (right) system averaged void.	17
14	Dimensions for the original equipment manufacturer (OEM) control blade. All dimensions are in centimeters.	19
15	Fuel layout in NAT region: a natural blanket at the base of the bundle.	22
16	Fuel layout in the PSZ region (power shaping zone).	22
17	Fuel layout in the DOM region (dominate zone).	23
18	Fuel layout in the VAN region: the part length rods “vanish” in this region.	23
19	Fuel layout in the PLE region: the plenum region for part length rods.	23
20	Fuel layout in the NV region: natural blanket in the top of the bundle where only full length rods exist.	23
21	Fuel layout in the NT region: similar to the NV region, however, full length rods containing gadolinium at lower levels are now empty rods containing helium and no fuel inside the clad.	24
22	Fuel layout in the PLEN region: plenum region for the full length rods containing only helium inside the cladding.	24
23	Normalized fission rates from MCNP (top left), Serpent (top right), differences between MPACT and MCNP (bottom left), and differences between MPACT and Serpent (bottom right) for the Peach Bottom 6 Uncontrolled case at 0% Void	29
24	Normalized fission rates from MCNP (top left), Serpent (top right), differences between MPACT and MCNP (bottom left), and differences between MPACT and Serpent (bottom right) for the Peach Bottom 6 Uncontrolled case at 40% Void	30
25	Normalized fission rates from MCNP (top left), Serpent (top right), differences between MPACT and MCNP (bottom left), and differences between MPACT and Serpent (bottom right) for the Peach Bottom 6 Uncontrolled case at 80% Void	31

26	Normalized fission rates from MCNP (top left), Serpent (top right), differences between MPACT and MCNP (bottom left), and differences between MPACT and Serpent (bottom right) for the Peach Bottom 6 Controlled case at 0% Void	32
27	Normalized fission rates from MCNP (top left), Serpent (top right), differences between MPACT and MCNP (bottom left), and differences between MPACT and Serpent (bottom right) for the Peach Bottom 6 Controlled case at 40% Void	33
28	Normalized fission rates from MCNP (top left), Serpent (top right), differences between MPACT and MCNP (bottom left), and differences between MPACT and Serpent (bottom right) for the Peach Bottom 6 Controlled case at 80% Void	34
29	Normalized fission rates from MCNP (top left), Serpent (top right), differences between MPACT and MCNP (bottom left), and differences between MPACT and Serpent (bottom right) for the GE-9 Uncontrolled case at 0% Void	36
30	Normalized fission rates from MCNP (top left), Serpent (top right), differences between MPACT and MCNP (bottom left), and differences between MPACT and Serpent (bottom right) for the GE-9 Uncontrolled case at 40% Void	37
31	Normalized fission rates from MCNP (top left), Serpent (top right), differences between MPACT and MCNP (bottom left), and differences between MPACT and Serpent (bottom right) for the GE-9 Uncontrolled case at 80% Void	38
32	Normalized fission rates from MCNP (top left), Serpent (top right), differences between MPACT and MCNP (bottom left), and differences between MPACT and Serpent (bottom right) for the GE-9 Controlled case at 0% Void	39
33	Normalized fission rates from MCNP (top left), Serpent (top right), differences between MPACT and MCNP (bottom left), and differences between MPACT and Serpent (bottom right) for the GE-9 Controlled case at 40% Void	40
34	Normalized fission rates from MCNP (top left), Serpent (top right), differences between MPACT and MCNP (bottom left), and differences between MPACT and Serpent (bottom right) for the GE-9 Controlled case at 80% Void	41
35	Normalized fission rates from MCNP (top left), Serpent (top right), differences between MPACT and MCNP (bottom left), and differences between MPACT and Serpent (bottom right) for the GE-14 Uncontrolled case at 0% Void	43
36	Normalized fission rates from MCNP (top left), Serpent (top right), differences between MPACT and MCNP (bottom left), and differences between MPACT and Serpent (bottom right) for the GE-14 Uncontrolled case at 40% Void	44
37	Normalized fission rates from MCNP (top left), Serpent (top right), differences between MPACT and MCNP (bottom left), and differences between MPACT and Serpent (bottom right) for the GE-14 Uncontrolled case at 80% Void	45
38	Normalized fission rates from MCNP (top left), Serpent (top right), differences between MPACT and MCNP (bottom left), and differences between MPACT and Serpent (bottom right) for the GE-14 Controlled case at 0% Void	46
39	Normalized fission rates from MCNP (top left), Serpent (top right), differences between MPACT and MCNP (bottom left), and differences between MPACT and Serpent (bottom right) for the GE-14 Controlled case at 40% Void	47
40	Normalized fission rates from MCNP (top left), Serpent (top right), differences between MPACT and MCNP (bottom left), and differences between MPACT and Serpent (bottom right) for the GE-14 Controlled case at 80% Void	48

41	Normalized fission rates from MCNP (top left), Serpent (top right), differences between MPACT and MCNP (bottom left), and differences between MPACT and Serpent (bottom right) for the Uncontrolled GE-14 case with vanished rods at 0% Void	50
42	Normalized fission rates from MCNP (top left), Serpent (top right), differences between MPACT and MCNP (bottom left), and differences between MPACT and Serpent (bottom right) for the Uncontrolled GE-14 case with vanished rods at 40% Void	51
43	Normalized fission rates from MCNP (top left), Serpent (top right), differences between MPACT and MCNP (bottom left), and differences between MPACT and Serpent (bottom right) for the Uncontrolled GE-14 case with vanished rods at 80% Void	52
44	Normalized fission rates from MCNP (top left), Serpent (top right), differences between MPACT and MCNP (bottom left), and differences between MPACT and Serpent (bottom right) for the Controlled GE-14 case with vanished rods at 0% Void	53
45	Normalized fission rates from MCNP (top left), Serpent (top right), differences between MPACT and MCNP (bottom left), and differences between MPACT and Serpent (bottom right) for the Controlled GE-14 case with vanished rods at 40% Void	54
46	Normalized fission rates from MCNP (top left), Serpent (top right), differences between MPACT and MCNP (bottom left), and differences between MPACT and Serpent (bottom right) for the Controlled GE-14 case with vanished rods at 80% Void	55
47	Normalized fission rates from MCNP (left) and differences between MPACT and MCNP (right) for the Uncontrolled mini-core at 0% system averaged void	57
48	Normalized fission rates from MCNP (left) and differences between MPACT and MCNP (right) for the Uncontrolled mini-core at 20% system averaged void	57
49	Normalized fission rates from MCNP (left) and differences between MPACT and MCNP (right) for the Uncontrolled mini-core at 60% system averaged void	58
50	Normalized fission rates from MCNP (left) and differences between MPACT and MCNP (right) for the Controlled mini-core at 0% system averaged void	58
51	Normalized fission rates from MCNP (left) and differences between MPACT and MCNP (right) for the Controlled mini-core at 20% system averaged void	59
52	Normalized fission rates from MCNP (left) and differences between MPACT and MCNP (right) for the Controlled mini-core at 60% system averaged void	59
53	Normalized fission rate distribution throughout the HFP GE14 Bundle from MCNP calculations.	60
54	Normalized fission rate distribution throughout the HZP GE14 Bundle from MCNP calculations.	61
55	Relative standard deviation in the most limiting pin for the HZP (left) and HFP (right) cases. The errors are in percent.	61
56	Radial view of normalized fission rates at the axial peak for the HFP (left) and HZP (right) cases.	62
57	Axial distribution of fission rates for the HFP case in a part length rod (left) and the hottest rod (right).	62
58	Axial distribution of fission rates for the HZP case in a part length rod (left) and the hottest rod (right).	63

LIST OF TABLES

1	Case matrix for lattice progression problems	3
2	Coolant density as a function of void.	3
3	Fuel descriptions for Peach Bottom bundle type 6	6
4	Input parameters for the Peach Bottom type 6 lattice.	6
5	Fuel descriptions for the GE-9 lattice	9
6	Input parameters for the GE-9 lattice.	10
7	Fuel descriptions for the GE-14 lattice	13
8	Input parameters for the GE-14 lattice.	14
9	Input parameters for the GE OEM control blade.	20
10	Axial Description of the GE-14 Bundle.	21
11	Description of Grids and Nozzles for the GE-14 Bundle.	21
12	Axial locations of spacer grids.	22
13	Input parameters for the 3D hot zero power (HZP) GE-14 bundle.	24
14	Input parameters for the 3D hot full power (HFP) GE-14 bundle.	25
15	Eigenvalues from MCNP, Serpent, and MPACT for the Peach Bottom lattice 6.	27
16	Summary of maximum and minimum differences in normalized fission rates between MPACT and Monte Carlo results for the Peach Bottom 6 lattice.	28
17	Eigenvalues from MCNP, Serpent, and MPACT for the GE-9 lattice.	35
18	Summary of maximum and minimum differences in normalized fission rates between MPACT and Monte Carlo results for the GE-9 lattice.	35
19	Eigenvalues from MCNP, Serpent, and MPACT for the GE-14 lattice.	42
20	Summary of maximum and minimum differences in normalized fission rates between MPACT and Monte Carlo results for the GE-14 lattice.	42
21	Eigenvalues from MCNP, Serpent, and MPACT for the GE-14 lattice with vanished rods.	49
22	Summary of maximum and minimum differences in normalized fission rates between MPACT and Monte Carlo results for the GE-14 lattice with vanished rods.	49
23	Eigenvalues from MCNP and MPACT for the 16 bundle mini-core.	56
24	Summary of maximum and minimum differences in normalized fission rates between MPACT and Monte Carlo results for the 16 bundle mini-core.	56
25	Eigenvalues from MCNP for the 3D GE14 bundle problems.	60

ACRONYMS

BWR boiling water reactor

CASL Consortium for the Advanced Simulation of Light Water Reactors

HFP hot full power

HZP hot zero power

NCSU North Carolina State University

OEM original equipment manufacturer

ORNL Oak Ridge National Laboratory

PWR pressurized water reactor

VERA Virtual Environment for Reactor Applications

1. INTRODUCTION

This report outlines a series of boiling water reactor (BWR) progression problems which were created to guide the development of the BWR capabilities in VERA. These progression problems were developed with collaboration between North Carolina State University (NCSU) and Oak Ridge National Laboratory (ORNL).

When starting a large software development process, one of the first things that is usually done is to define a set of software requirements. The software requirements define all the features in the final product, but they usually do not specify the order (or priority) that features should be developed. To help with this, a set of progression problems has been defined to supplement the requirements and aid the developers by providing an order in which features are implemented. The order is chosen to be able to provide users with useful capabilities as soon as possible, and also provide capabilities that can be validated during the development process. The ability to receive user feedback and validate intermediate results helps to speed up the development process and deliver quality software.

In addition to helping the developers, the ability to model the progression problems provides a useful milestones to track the progress of development.

The BWR progression problems are influenced by the pressurized water reactor (PWR) progression problems used in the early Virtual Environment for Reactor Applications (VERA) development [5]. The progressions start with a single 2D assembly and progressively add more complexity, as shown in the following list.

1. 2D BWR Lattice
2. 2D Mini-core (4x4)
3. 3D Single Bundle (no TH feedback)
4. 3D Single Bundle (with TH feedback)
5. 3D Control Cell
6. 3D Mini-core
7. Full BWR core model (no TH feedback)
8. Full BWR core model (with TH feedback)

Section 2. of this document provides the specifications for the 2D progression problems, Section 3. provides the specifications for the 3D progression problems, and Section 4. provides reference Monte Carlo results for all the progression problems.

This is a draft version of the document. Later versions will include additional specifications.

2. 2D BWR PROGRESSION PROBLEMS

Four lattice types are considered in the 2D lattice progression problems. The lattices are based on an 8×8 bundle from cycle 2 of the Peach Bottom unit 2 reactor, an 8×8 GE-9 bundle, and a 10×10 GE-14 bundle. In the case of the GE-14 bundle two lattices are considered, one of which includes vanished rods. The geometry and material specifications for these lattices can be found in section 2.1, section 2.2, section 2.3, and section 2.4. For each lattice there are 6 progression problems made up from the state points shown in Table 1 each with a controlled and an uncontrolled version. In addition to the four BWR lattice geometries, one 4×4 bundle configuration is considered and is described in section 2.5. In this problem, all bundles are the GE-14 bundle described in section 2.3. The control blade used for each controlled case is described in section 2.6.

Table 1. Case matrix for lattice progression problems

Moderator Temperature [K]	600
Fuel Temperature [K]	900
Pressure [psia]	1040
Void [%]	0.0, 40.0, 80.0

For the 4×4 case, a similar case matrix was used, however, the system average voids were 0%, 20%, and 60% and the assembly void distributions are described in section 2.5. A coolant density table which represents the densities used in all of the progression problems is shown in Table 2. The coolant density is defined as a function of void in increments of 5% void and was developed assuming $\rho_l = 0.73669 \text{ g/cc}$ and $\rho_g = 0.037523 \text{ g/cc}$ [6]. All moderator, water flowing outside of the channel box and through the water rods, is assumed to be at 0% void.

Table 2. Coolant density as a function of void.

Void [%]	Density [g/cc]	Void[%]	Density [g/cc]
0	0.73669000	55	0.35214815
5	0.70173165	60	0.31718980
10	0.66677330	65	0.28223145
15	0.63181495	70	0.24727310
20	0.59685660	75	0.21231475
25	0.56189825	80	0.17735640
30	0.52693990	85	0.14239805
35	0.49198155	90	0.10743970
40	0.45702320	95	0.07248135
45	0.42206485	100	0.03752300
50	0.38710650		

2.1 Peach Bottom Assembly Type 6

This section describes the geometry and material composition of the 8×8 Peach Bottom assembly type 6 specified in the *Boiling Water Reactor Turbine Trip Benchmark, Volume I: Final Specifications* [11]. The dimensions for the lattice are depicted in Figure 1. The radii for the fuel pins and water rods are shown in Figure 2. The fuel layout is described in Figure 3 and the corresponding compositions are listed in Table 3. A concise listing of input parameters used in modeling the lattice is provided in Table 4. The Zircaloy densities shown in Table 4 were obtained from [11].

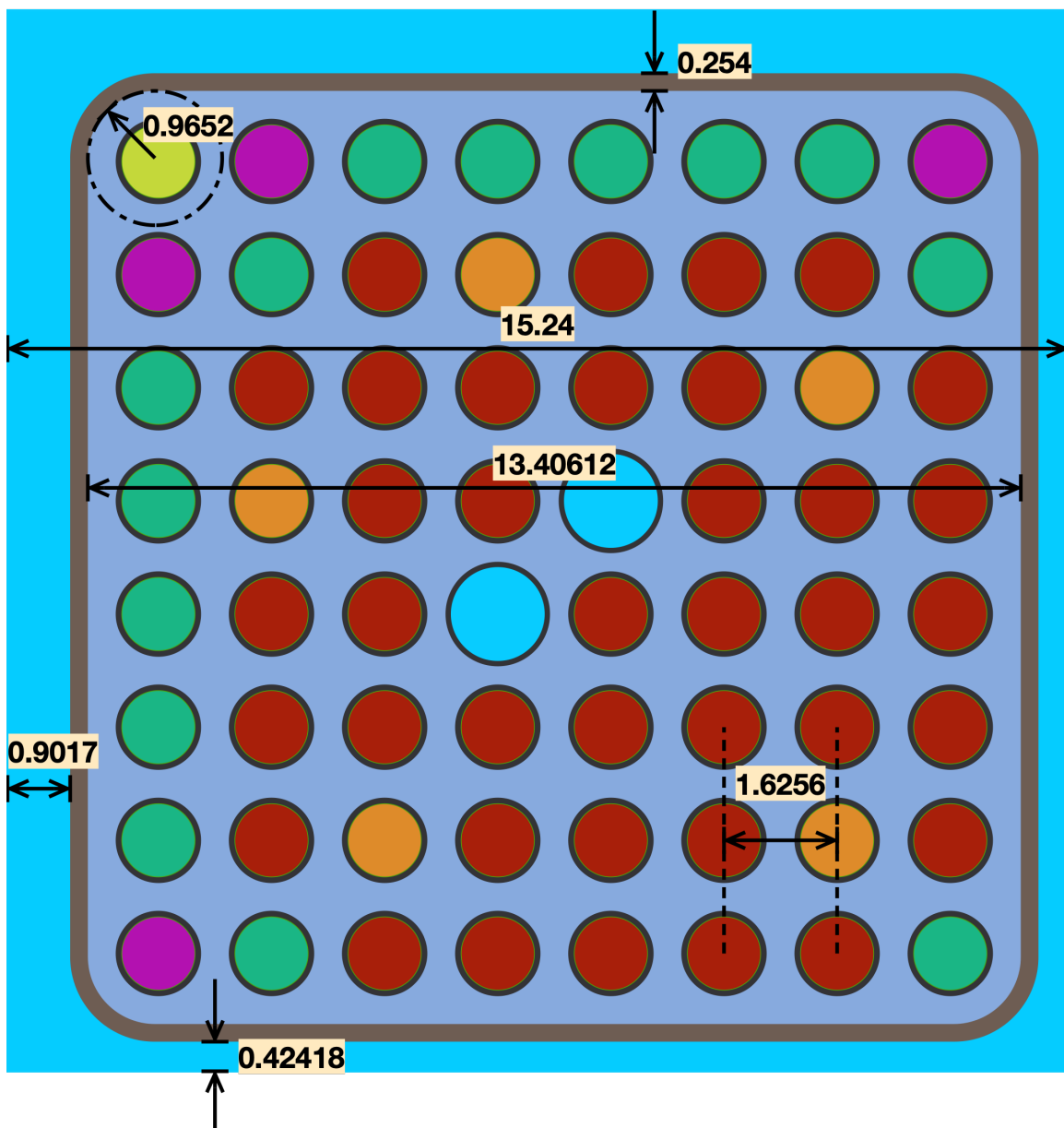


Figure 1. Dimensions for the Peach Bottom type 6 bundle design. All dimensions are in centimeters.

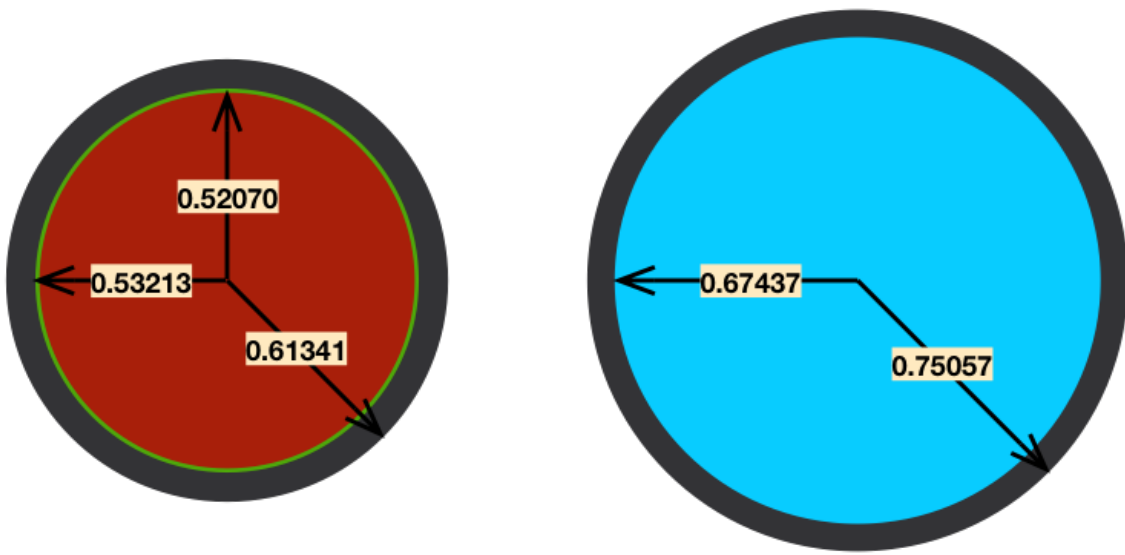


Figure 2. Dimensions for the Peach Bottom type 6 bundle fuel pin (left) and water rod (right). Dimensions are in centimeters and are not to scale.

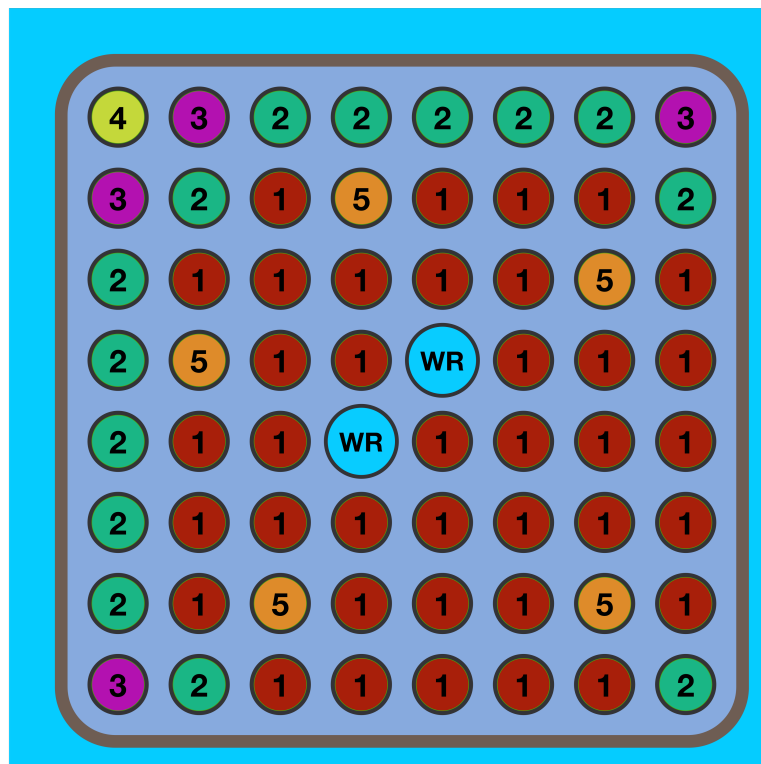


Figure 3. Fuel layout for the Peach Bottom type 6 bundle

Table 3. Fuel descriptions for Peach Bottom bundle type 6

Rod Label	U-235 Enrichment [%]	Gadolinium Loading [%]	Stack Density [g/cc]
1	3.01	0.0	10.32
2	2.22	0.0	10.32
3	1.87	0.0	10.32
4	1.45	0.0	10.32
5	3.01	2.0	10.23

Table 4. Input parameters for the Peach Bottom type 6 lattice.

Moderator Temp. [K]	600
Fuel Temp. [K]	900
Pressure [psia]	1040
Void [%]	0, 40, 80
Assembly Pitch [cm]	15.24
Height [cm]	1.0
Boundary Condition (all)	reflecting
Pin Pitch [cm]	1.6256
Gap (Wide/Narrow) [cm]	0.9017 / 0.42418
Channel Box Thickness [cm]	0.254
Channel Box Corner Radius [cm]	0.9652
Fuel Pellet Outer Radius [cm]	0.5207
Fuel Clad Inner Radius [cm]	0.53213
Fuel Clad Outer Radius [cm]	0.61341
Water Rod Inner Radius [cm]	0.67437
Water Rod Outer Radius [cm]	0.75057
Channel Box Material (name / density [g/cc])	Zircaloy-4 / 6.5514
Cladding Material (name / density [g/cc])	Zircaloy-2 / 6.5514

2.2 GE-9 Lattice

A second 8×8 BWR lattice based on the GE-9 bundle is considered for the progression problems. The geometry of the GE-9 lattice was obtained from [7]. This is also the source of the fuel layout and compositions. The GE-9 bundle contains a single large water rod in the center of the bundle and 8 gadolinium bearing fuel pins.

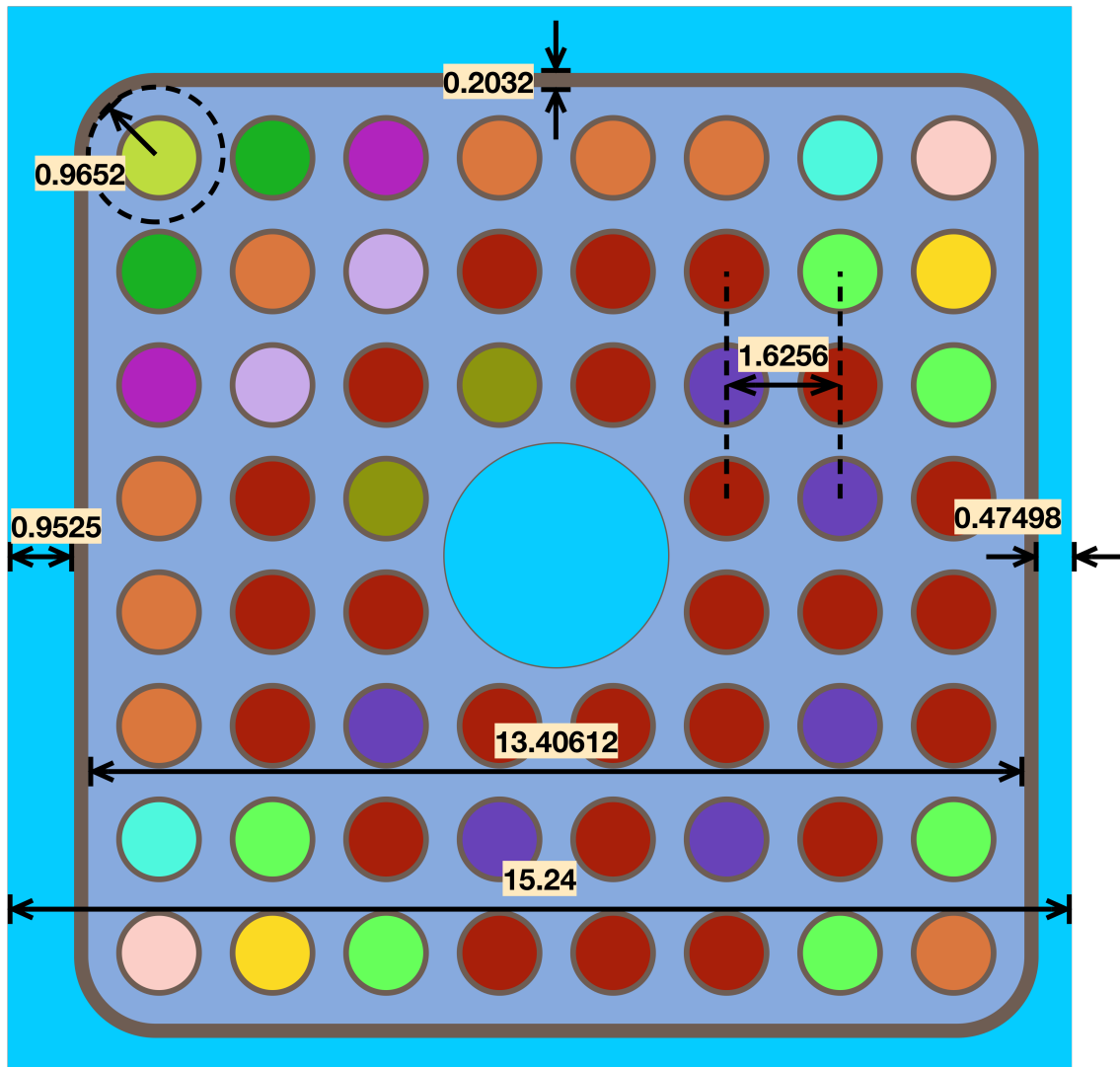


Figure 4. Dimensions for the GE-9 lattice. All dimensions are in centimeters.

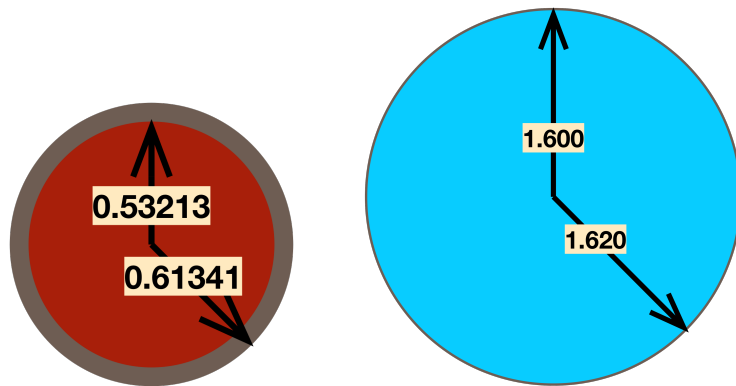


Figure 5. Dimensions for the GE-9 fuel pin (left) and water rod (right). These two figures are not to scale. All dimensions are in centimeters.

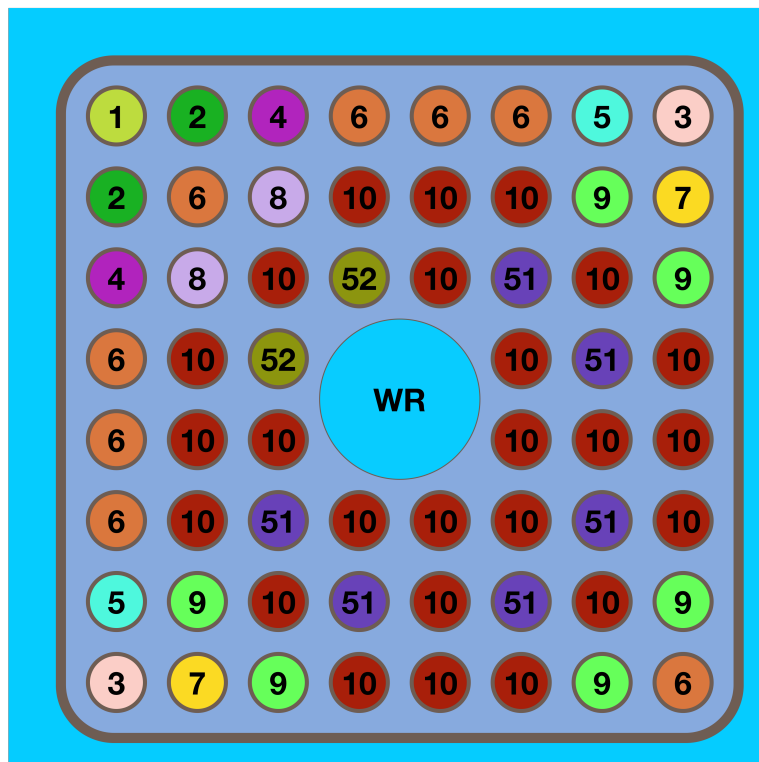


Figure 6. Fuel layout for the GE-9 bundle

Table 5. Fuel descriptions for the GE-9 lattice

Rod Label	U-235 Enrichment [%]	Gadolinium Loading [%]	Stack Density [g/cc]
1	1.60	0.0	10.0642
2	2.00	0.0	10.0642
3	2.20	0.0	10.0642
4	2.40	0.0	10.0642
5	2.60	0.0	10.0642
6	2.80	0.0	10.0642
7	3.00	0.0	10.0642
8	3.60	0.0	10.0642
9	3.80	0.0	10.0642
10	3.95	0.0	10.0642
51	3.95	4.0	9.9390
52	3.60	4.0	9.9390

The rod labels in Figure 6 and Table 5 are consistent. The oversized water rod is located in the center of the lattice and is labeled with “WR” in Figure 6. In MPACT, the oversized water rods must fit within 2 pin cells. For this reason, the dimensions of the water rod have been shaved down slightly from the original dimensions in [7]. Important input parameters are provided for the GE-9 lattice in Table 6. For the GE-9 lattice, the helium in the gap and the fuel pellet are smeared together into the fuel rod meaning there is not a separate value for the fuel pellet outer radius and clad inner radius. The densities for Zircaloy shown in Table 6 were found in [10].

Table 6. Input parameters for the GE-9 lattice.

Moderator Temp. [K]	600
Fuel Temp. [K]	900
Pressure [psia]	1040
Void [%]	0, 40, 80
Assembly Pitch [cm]	15.24
Height [cm]	1.0
Boundary Condition (all)	reflecting
Pin Pitch [cm]	1.6256
Gap (Wide/Narrow) [cm]	0.9525 / 0.47498
Channel Box Thickness [cm]	0.2032
Channel Box Corner Radius [cm]	0.9652
Fuel Clad Inner Radius [cm]	0.53213
Fuel Clad Outer Radius [cm]	0.61341
Water Rod Inner Radius [cm]	1.60000
Water Rod Outer Radius [cm]	1.62000
Channel Box Material (name / density [g/cc])	6.56
Cladding Material (name / density [g/cc])	6.56

2.3 Representative GE-14 Lattice

A representative 10×10 GE-14 bundle has been developed using data from several public sources. Much of the geometry is defined based on Table A-3 in [2]. The GE-14 dimensions are depicted in Figure 7. Radii for the fuel pins and water rods are shown in Figure 8. The fuel layout is described in Figure 9 and the corresponding compositions are listed in Table 7.

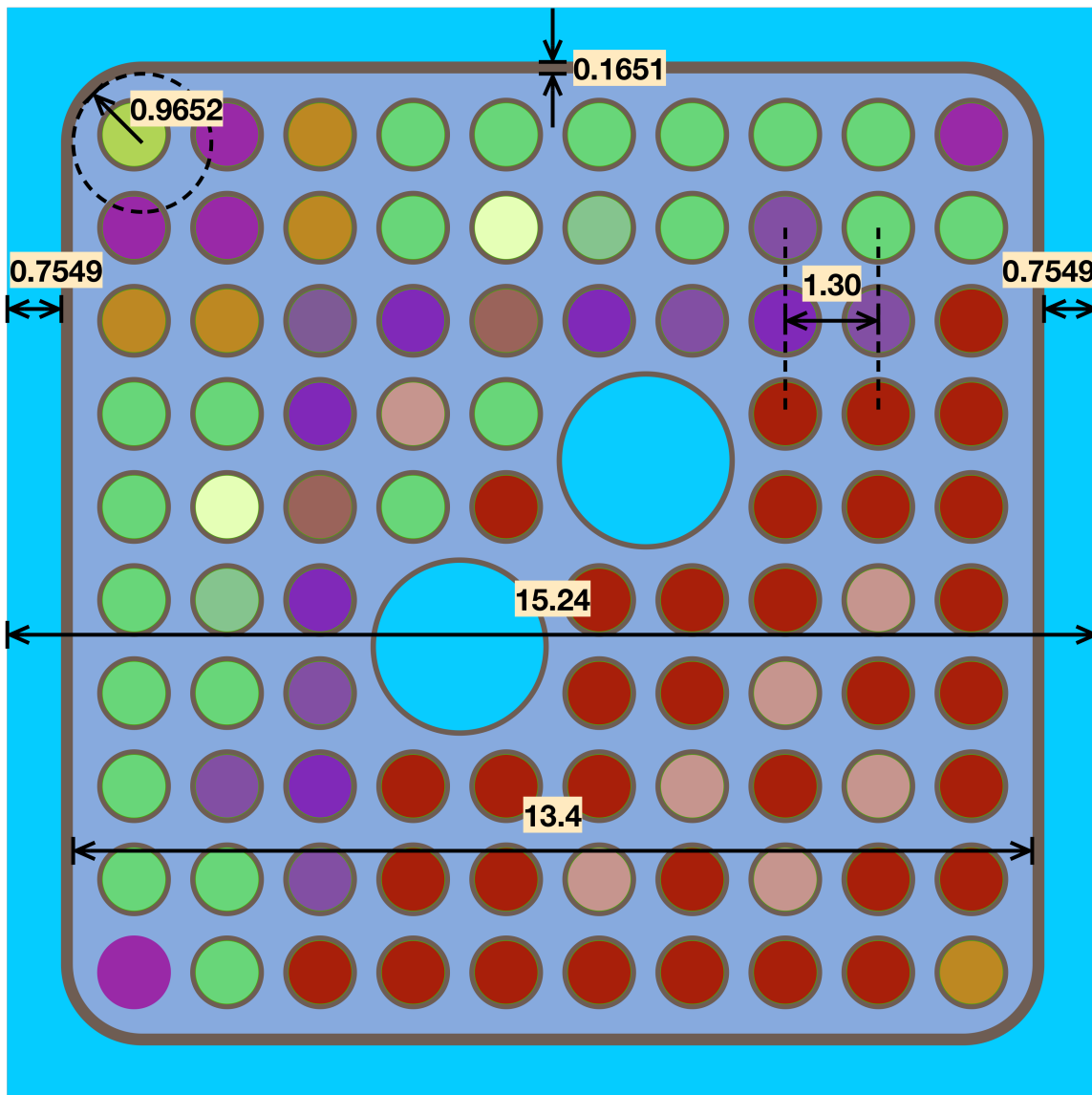


Figure 7. Dimensions for the GE-14 bundle design. All dimensions are in centimeters.

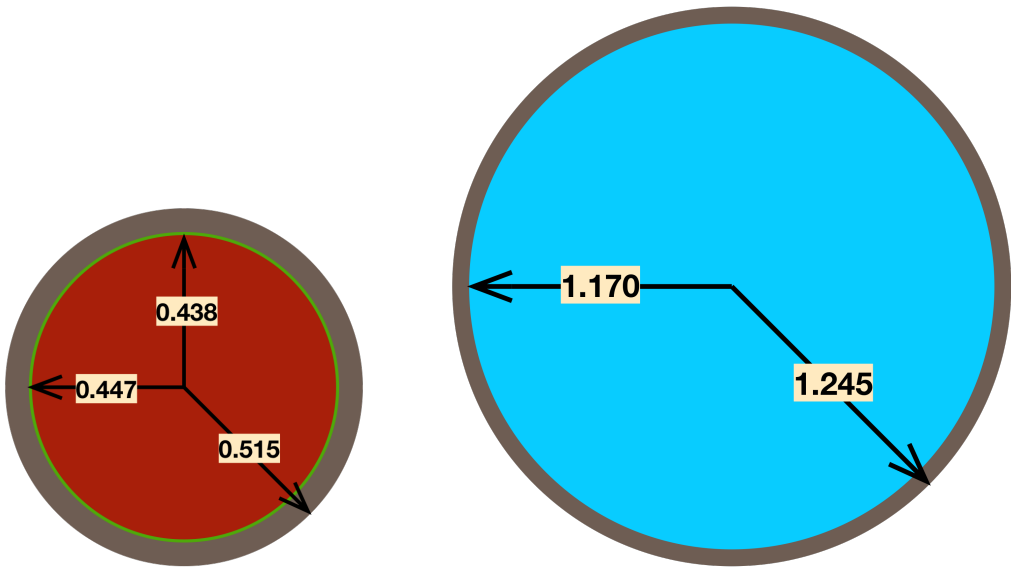


Figure 8. Dimensions for the GE-14 bundle fuel pin (left) and water rod (right). These two figures are not to scale. All dimensions are in centimeters.

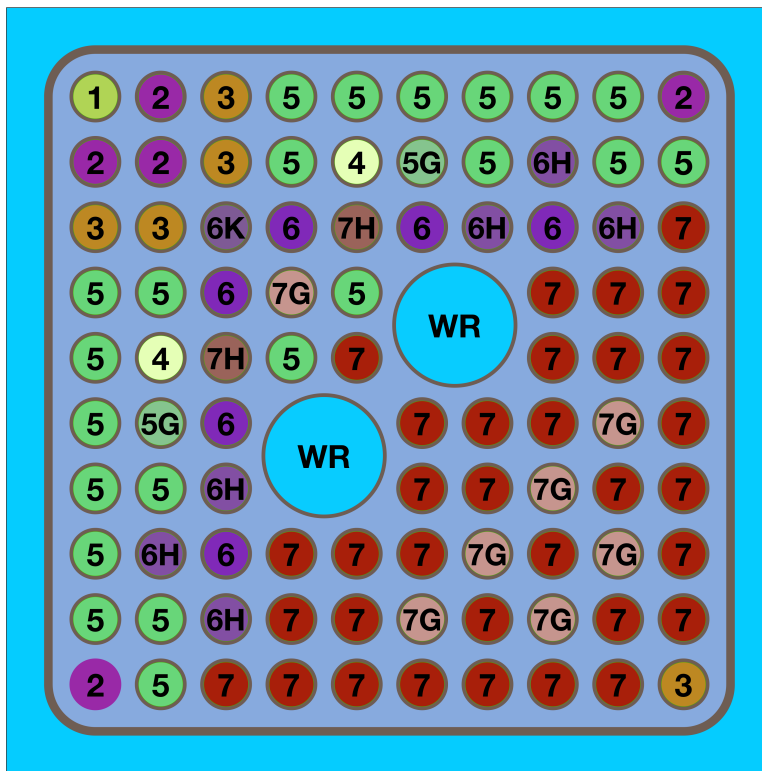


Figure 9. Fuel layout for the GE-14 bundle

Table 7. Fuel descriptions for the GE-14 lattice

Rod Label	U-235 Enrichment [%]	Gadolinium Loading [%]	Stack Density [g/cc]
1	1.60	0.0	10.40
2	2.80	0.0	10.40
3	3.20	0.0	10.40
4	3.60	0.0	10.40
5	3.95	0.0	10.40
5G	3.95	8.0	10.19
6	4.40	0.0	10.40
6H	4.40	6.0	10.19
6K	4.40	3.0	10.19
7	4.90	0.0	10.40
7G	4.90	8.0	10.19
7H	4.90	6.0	10.19
N	0.71	0.0	10.40

The rod labels in Figure 9 and Table 7 are consistent. The two oversized water rods are labeled with “WR” in Figure 9. The fuel layout and fuel specifications were found in [4]. The densities for fuel rods without gadolinium were obtained from [2], however, for gadolinium bearing fuels, the density is estimated using data from [11]. A more concise description of the problem dimensions is provided in Table 8. The densities for Zircaloy were obtained from [10].

Table 8. Input parameters for the GE-14 lattice.

Moderator Temp. [K]	600
Fuel Temp. [K]	900
Pressure [psia]	1040
Void [%]	0, 40, 80
Assembly Pitch [cm]	15.24
Height [cm]	1.0
Boundary Condition (all)	reflecting
Pin Pitch [cm]	1.3
Gap (Wide/Narrow) [cm]	0.7549 / 0.7549
Channel Box Thickness [cm]	0.1651
Channel Box Corner Radius [cm]	0.9652
Fuel Pellet Outer Radius [cm]	0.438
Fuel Clad Inner Radius [cm]	0.447
Fuel Clad Outer Radius [cm]	0.515
Water Rod Inner Radius [cm]	1.170
Water Rod Outer Radius [cm]	1.245
Channel Box Material (name / density [g/cc])	Zircaloy-4 / 6.56
Cladding Material (name / density [g/cc])	Zircaloy-2 / 6.56

2.4 GE-14 Lattice with Vanished Rods

The GE-14 bundle with vanished rods is geometrically identical to the GE-14 bundle in section 2.3 with the exception of 14 fuel pins which have been removed. The fuel layout is slightly different for the vanished rod case and is depicted in Figure 10. This fuel layout was gathered from [4].

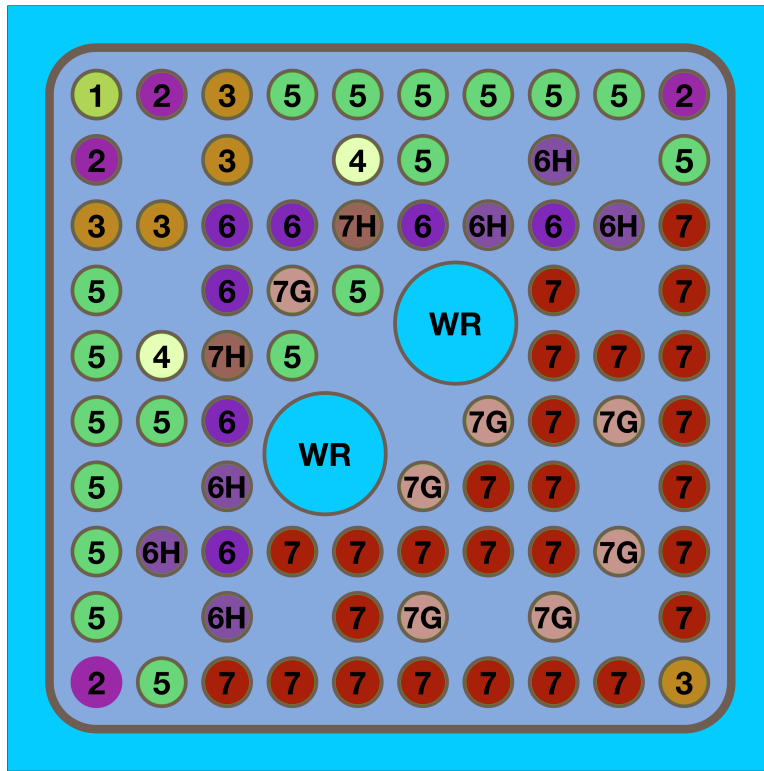


Figure 10. Fuel layout for the GE-14 lattice with vanished rods.

The fuel descriptions corresponding to the fuel labels in Figure 10 are shown in Table 7. Though the fuel layout for the remaining rods in Figure 10 is similar to that in the previous GE-14 lattice in Figure 9, they are not identical. The dimensions for the GE-14 lattice with vanished rods are those shown in Figure 7 and Figure 8. The information in Table 8 are also applicable to the GE-14 vanished rod lattice.

2.5 Mini-core

The mini-core test case consists of 16 GE-14 bundles all with the fuel layout from Figure 9 and dimensions from Figure 7 and Figure 8. Both controlled and uncontrolled configurations are tested with problem averaged voids of 0%, 20%, and 60%. The specific assembly void distributions are shown in Figure 12 and Figure 13. The controlled problem is shown in Figure 11, which demonstrates the bundle orientations for each location. The uncontrolled problem geometry is identical to the controlled problem except that the control blade in the north west corner of the problem is removed. All boundary conditions are taken to be reflective, making this problem slightly different from typical mini-core problems.

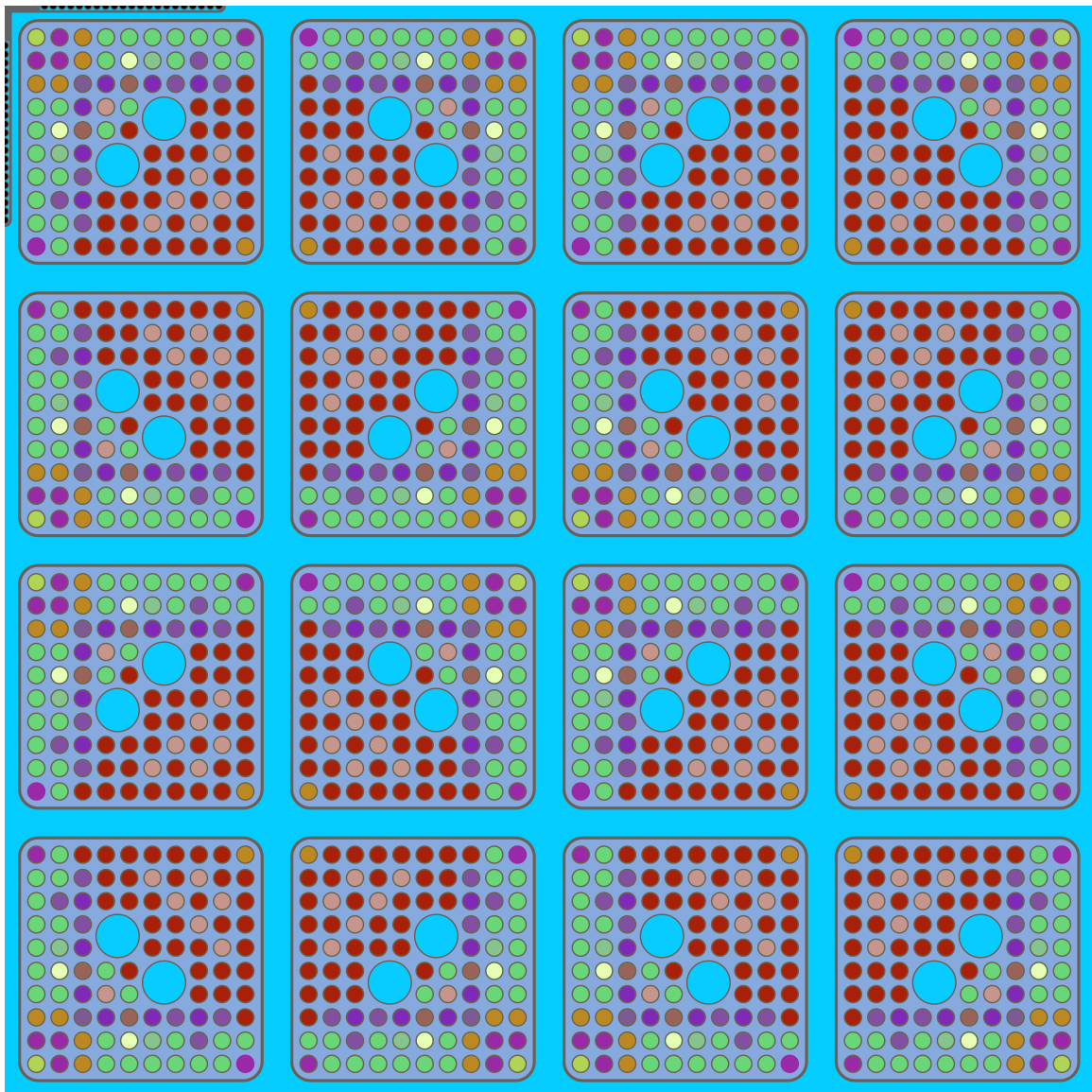


Figure 11. Geometry of the mini-core progression problem with the control blade inserted in the north west corner.

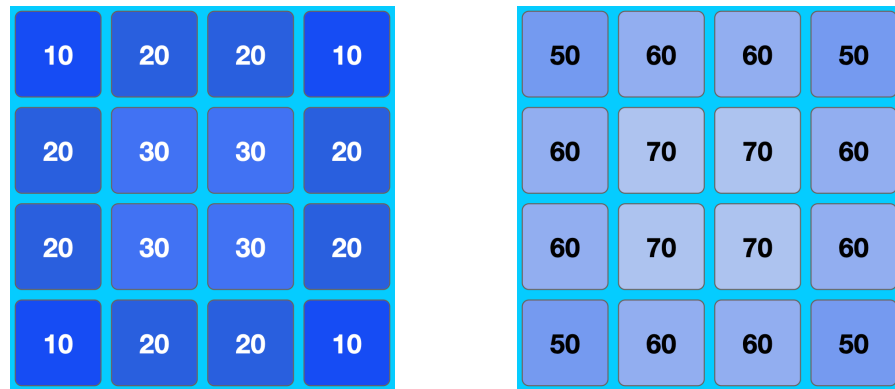


Figure 12. Void distribution for the uncontrolled multi-bundle case at 20% (left) and 60% (right) system averaged void.

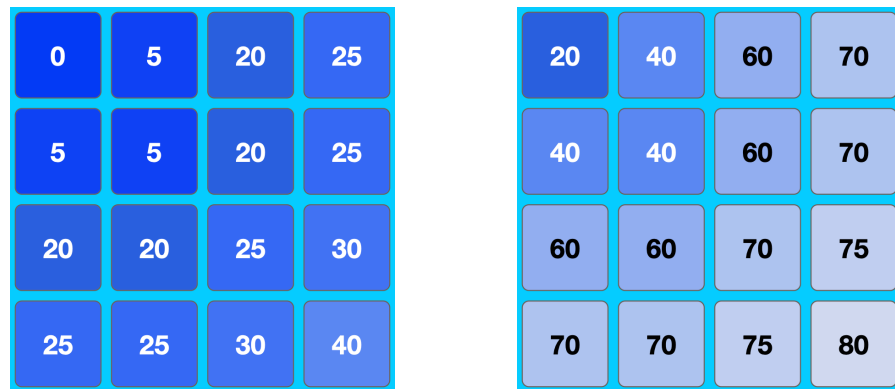


Figure 13. Void distribution for the controlled multi-bundle case at 20% (left) and 60% (right) system averaged void.

2.6 Control Blade Description

The geometry and material composition of the original equipment manufacturer (OEM) control blade is described in Figure 14. This control blade is used in all 2D controlled cases for each lattice type and is always placed in the wide-wide gap in the north west corner of the lattice. The dimensions and control blade material data were obtained from [11]. The dimensions of the control blade are shown in Figure 14 and the input parameters corresponding to these dimensions are listed in Table 9. The blade is made up of stainless steel 304 structures and B₄C granules. The density for the steel is shown in Table 9 and was obtained from [10]. The density of the B₄C is taken to be 70% of the theoretical density as stated in [11] and a theoretical density of 2.504 g/cc was obtained from [12].

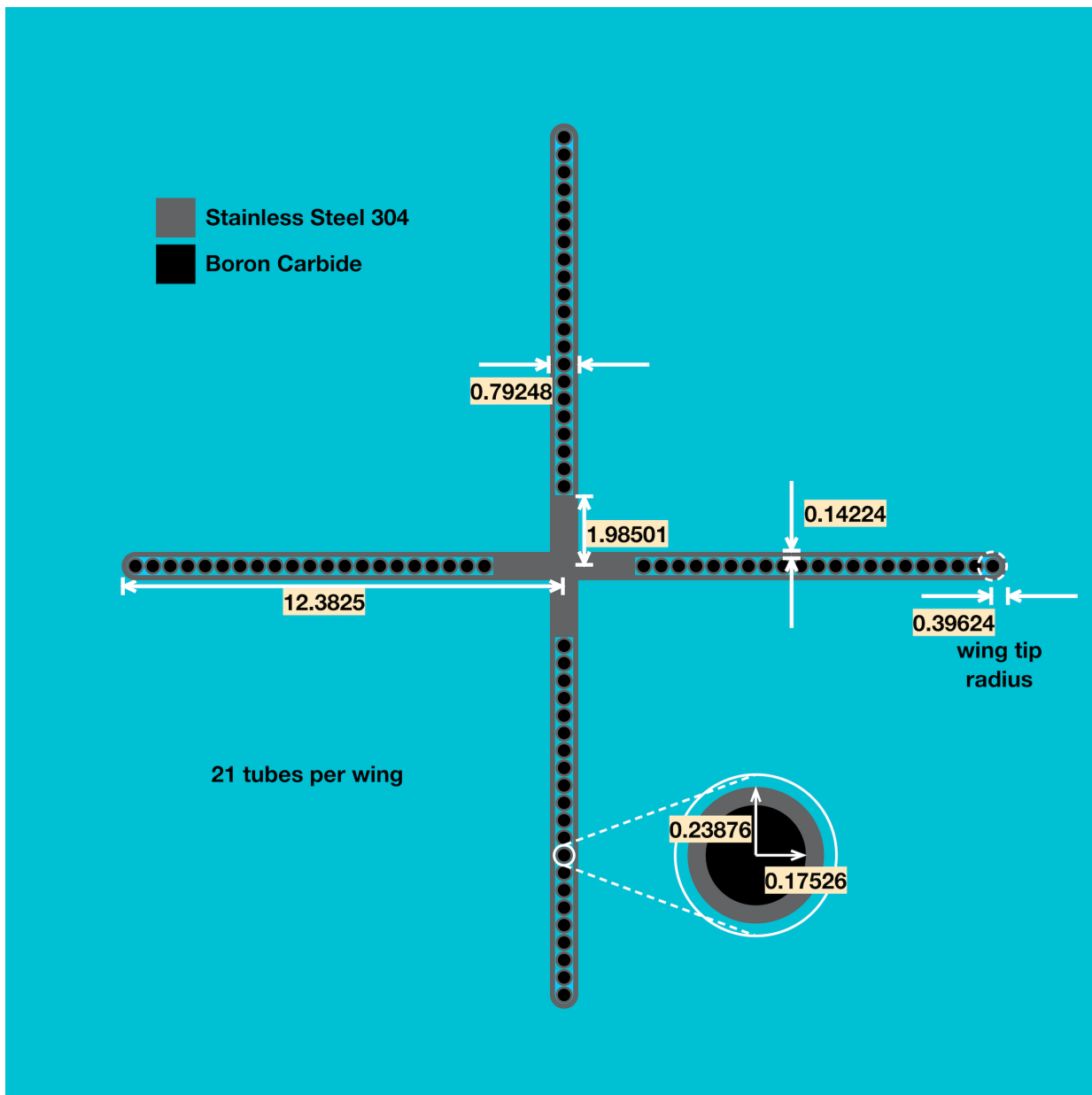


Figure 14. Dimensions for the OEM control blade. All dimensions are in centimeters.

Table 9. Input parameters for the GE OEM control blade.

Blade Half-Span [cm]	12.3825
Blade Thickness [cm]	0.79248
Number of Tubes Per Wing	21
Tip Radius [cm]	0.39624
Central Structure Half-Span [cm]	1.98501
Sheath Thickness [cm]	0.14224
Absorber Tube Inner Radius [cm]	0.17526
Absorber Tube Outer Radius [cm]	0.23876
Absorber Material (name / density [g/cc])	B ₄ C / 1.7528
Structure Material (name / density [g/cc])	Stainless Steel 304 / 8.0

3. 3D BWR PROGRESSION PROBLEMS

Currently, two 3D cases are considered. Both of these cases are based on the GE-14 bundle. The first is a hot zero power (HZP) case where the coolant has zero void and all temperatures are estimated to be 600 K. The second case is a hot full power (HFP) case with a uniform 40% void in the coolant of the bundle and the fuel temperature estimated at 900 K with everything else remaining at 600 K. The bundle is 409.3096 cm tall with the axial breakdown described in Table 10. The axial description of the fuel was obtained from [4]. A 25.4 cm plenum is added to the top of the bundle based on the information in [1]. The dimensions of the bundle are the same as those shown for the GE-14 lattice in Figure 7 and Figure 8. Additionally, all fuels match those described in Table 7. In plenum rods or empty rods, only the cladding exists and is filled with helium. In vanished rods, no pin exists and the full pin cell is filled with coolant alone. The radial boundary conditions are reflective, while the top and bottom boundary conditions are a vacuum.

Table 10. Axial Description of the GE-14 Bundle.

Region Label	Height at Base of Region [cm]	Height at top of Region [cm]
Top Nozzle	400.3096	409.3096
PLEN	374.9096	400.3096
NT	359.6696	374.9096
NV	344.4296	359.6696
VAN	249.8400	344.4296
PLE	219.3600	249.8400
DOM	143.1600	219.3600
PSZ	21.2400	143.1600
NAT	6.0000	21.2400
Bottom Nozzle	0.0000	6.0000

Data for the nozzles and grids are all approximated and are provided in Table 11. The nozzles sit within the channel box in the axial positions shown in Table 10. Eight spacer grids are used in the 3D GE-14 model [3]. The midpoints of the 8 spacer grids are listed in Table 12. The two “END” grids are placed such that their top and bottom edges are aligned with the top and bottom of the standard length fuel rods. The remaining six grids are spaced across the bundle as shown in Table 12. The grids were spaced approximately every 60 cm starting from the bottom of the bundle. In cases where the edge of a grid was close to the top or bottom of one of the regions in Table 10, the grid height was adjusted so the edge of the grid aligned with the edge of the material boundary.

Table 11. Description of Grids and Nozzles for the GE-14 Bundle.

	Material	height [cm]	Mass [g]
Top Nozzle	Stainless Steel 304	9.0	1500
Bottom Nozzle	Stainless Steel 304	6.0	1500
END Grid	Inconel	3.866	350
MID Grid	zircaloy-4	3.810	300

Table 12. Axial locations of spacer grids.

Grid Type	Grid Midpoint [cm]
END	398.3766
MID	368.0000
MID	308.0000
MID	247.9350
MID	188.0000
MID	128.0000
MID	68.0000
END	7.9330

The fuel layouts for each of the regions in Table 10 are shown in Figure 15 through Figure 22. All fuel rod labels are consistent with those in Table 7. In the 3D bundle the label “P” is used for plenum cells, which consist of helium inside of the fuel rod cladding and no fuel. The rods labeled “E” also represent pincells with helium inside the fuel rod cladding and no fuel pellet. The fuel pin layouts were sourced from [4].

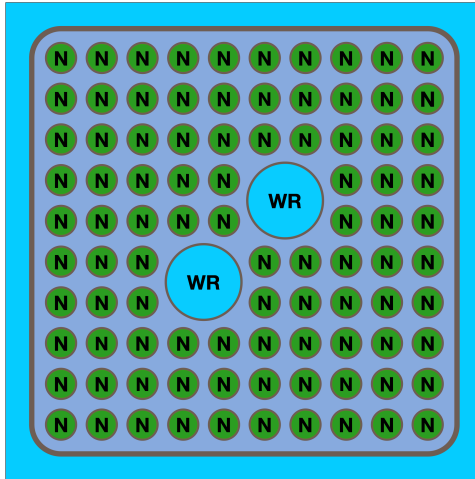


Figure 15. Fuel layout in NAT region: a natural blanket at the base of the bundle.

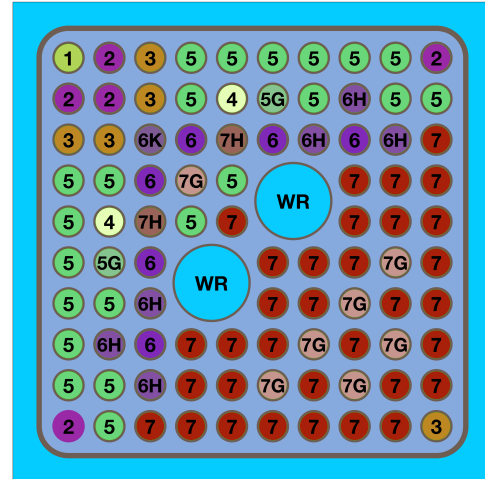


Figure 16. Fuel layout in the PSZ region (power shaping zone).

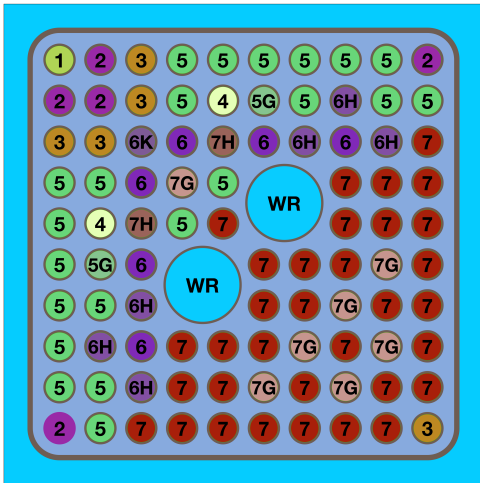


Figure 17. Fuel layout in the DOM region (dominate zone).

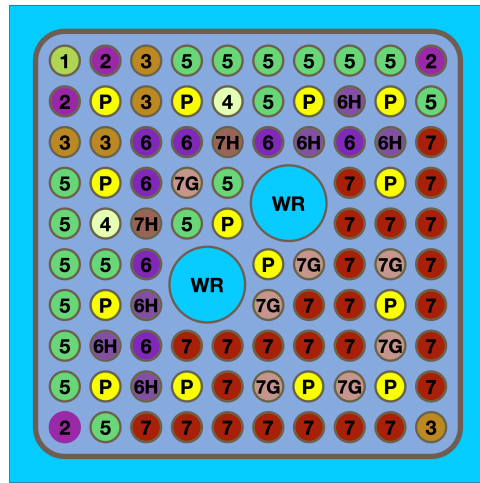


Figure 19. Fuel layout in the PLE region: the plenum region for part length rods.

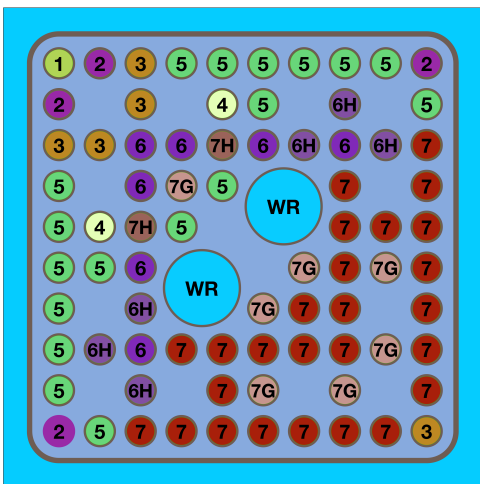


Figure 18. Fuel layout in the VAN region: the part length rods “vanish” in this region.

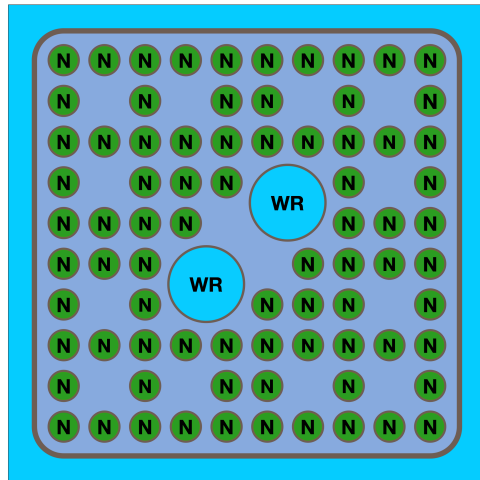


Figure 20. Fuel layout in the NV region: natural blanket in the top of the bundle where only full length rods exist.

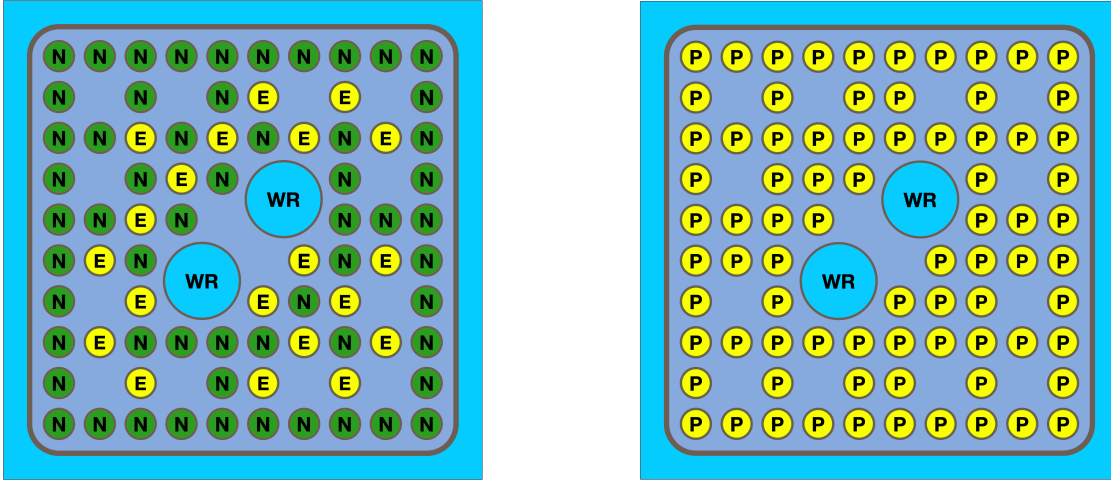


Figure 21. Fuel layout in the NT region: similar to the NV region, however, full length rods containing gadolinium at lower levels are now empty rods containing helium and no fuel inside the clad.

Figure 22. Fuel layout in the PLEN region: plenum region for the full length rods containing only helium inside the cladding.

Several useful input parameters is provided in Table 13 and Table 14 for the 3D GE-14 bundle. The Zircaloy densities were obtained from [10].

Table 13. Input parameters for the 3D HZP GE-14 bundle.

Moderator Temp. [K]	600
Fuel Temp. [K]	600
Pressure [psia]	1040
Void [%]	0
Assembly Pitch [cm]	15.24
Height [cm]	409.3096
Boundary Condition (radial)	reflecting
Boundary Condition (top/bottom)	vacuum
Pin Pitch [cm]	1.3
Gap (Wide/Narrow) [cm]	0.7549 / 0.7549
Channel Box Thickness [cm]	0.1651
Channel Box Corner Radius [cm]	0.9652
Fuel Pellet Outer Radius [cm]	0.438
Fuel Clad Inner Radius [cm]	0.447
Fuel Clad Outer Radius [cm]	0.515
Water Rod Inner Radius [cm]	1.170
Water Rod Outer Radius [cm]	1.245
Channel Box Material (name / density [g/cc])	Zircaloy-4 / 6.56
Cladding Material (name / density [g/cc])	Zircaloy-2 / 6.56

Table 14. Input parameters for the 3D HFP GE-14 bundle.

Moderator Temp. [K]	600
Fuel Temp. [K]	900
Pressure [psia]	1040
Void [%]	40
Assembly Pitch [cm]	15.24
Height [cm]	409.3096
Boundary Condition (radial)	reflecting
Boundary Condition (top/bottom)	vacuum
Pin Pitch [cm]	1.3
Gap (Wide/Narrow) [cm]	0.7549 / 0.7549
Channel Box Thickness [cm]	0.1651
Channel Box Corner Radius [cm]	0.9652
Fuel Pellet Outer Radius [cm]	0.438
Fuel Clad Inner Radius [cm]	0.447
Fuel Clad Outer Radius [cm]	0.515
Water Rod Inner Radius [cm]	1.170
Water Rod Outer Radius [cm]	1.245
Channel Box Material (name / density [g/cc])	Zircaloy-4 / 6.56
Cladding Material (name / density [g/cc])	Zircaloy-2 / 6.56

4. RESULTS

Reference solutions are provided for the VERA BWR progression problems where possible using continuous energy Monte Carlo calculations. Results are provided from both Serpent 2 [8] and MCNP6.2 [9]. For the 2D problems, solutions from MPACT are compared to the Monte Carlo results. When comparing normalized fission rates, all differences are always calculated as:

$$\Delta p_{i,j} = \left(p_{i,j}^{\text{MPACT}} - p_{i,j}^{\text{MC}} \right) \times 100 \quad (1)$$

where $p_{i,j}^{\text{MPACT}}$ is the normalized fission rate from MPACT in pin (i, j) and MC will either be MCNP or Serpent. Additionally, the differences in eigenvalues are determined using the formula:

$$\Delta k = \left(k^{\text{MPACT}} - k^{\text{MC}} \right) \times 10^5 \text{ pcm} \quad (2)$$

4.1 Peach Bottom 6

The eigenvalues calculated with MCNP and Serpent for the Peach Bottom lattice described in section 2.1 are shown in Table 15. MCNP calculations for the peach bottom lattice used 360 million active particles, while the Serpent calculations used 1.32 billion active particles. The standard deviations in the eigenvalues for the MCNP calculations are all 4 pcm or less and are 2 pcm or less for the Serpent calculations.

Table 15. Eigenvalues from MCNP, Serpent, and MPACT for the Peach Bottom lattice 6.

Uncontrolled					
Void [%]	MCNP	Serpent	MPACT	MPACT-MCNP [pcm]	MPACT-Serpent [pcm]
0	1.10511	1.10522	1.105519	40.9	29.9
40	1.08356	1.08362	1.084152	59.2	53.2
80	1.04265	1.04260	1.041948	-70.2	-65.2
Controlled					
Void [%]	MCNP	Serpent	MPACT	MPACT-MCNP [pcm]	MPACT-Serpent [pcm]
0	0.88079	0.880892	0.881147	35.7	25.5
40	0.81752	0.817562	0.818517	99.7	95.5
80	0.72128	0.721281	0.722145	86.5	86.4

4.1.1 Normalized Fission Rate Monte Carlo Results

A summary of the differences in normalized fission rates between MPACT and MCNP or Serpent is presented in Table 16. For all Peach Bottom type 6 lattice calculations, the maximum relative standard deviation in the fission rates was 0.04% for the MCNP results and 0.03% for the Serpent results. In Figure 23 through Figure 28 more detailed descriptions of the differences in normalized fission rates between MPACT and Monte Carlo results are provided on a case by case basis.

Table 16. Summary of maximum and minimum differences in normalized fission rates between MPACT and Monte Carlo results for the Peach Bottom 6 lattice.

Uncontrolled						
Void [%]	MPACT - MCNP			MPACT - Serpent		
	Max [%]	Min [%]	RMS [%]	Max [%]	Min [%]	RMS [%]
0	0.87	-1.25	0.53	0.86	-1.35	0.53
40	0.42	-0.95	0.35	0.45	-0.99	0.35
80	0.89	-0.68	0.30	0.92	-0.66	0.30
Controlled						
Void [%]	MPACT - MCNP			MPACT - Serpent		
	Max [%]	Min [%]	RMS [%]	Max [%]	Min [%]	RMS [%]
0	0.51	-1.16	0.36	0.52	-1.16	0.36
40	0.32	-0.77	0.23	0.33	-0.77	0.23
80	0.97	-0.54	0.24	0.93	-0.50	0.23

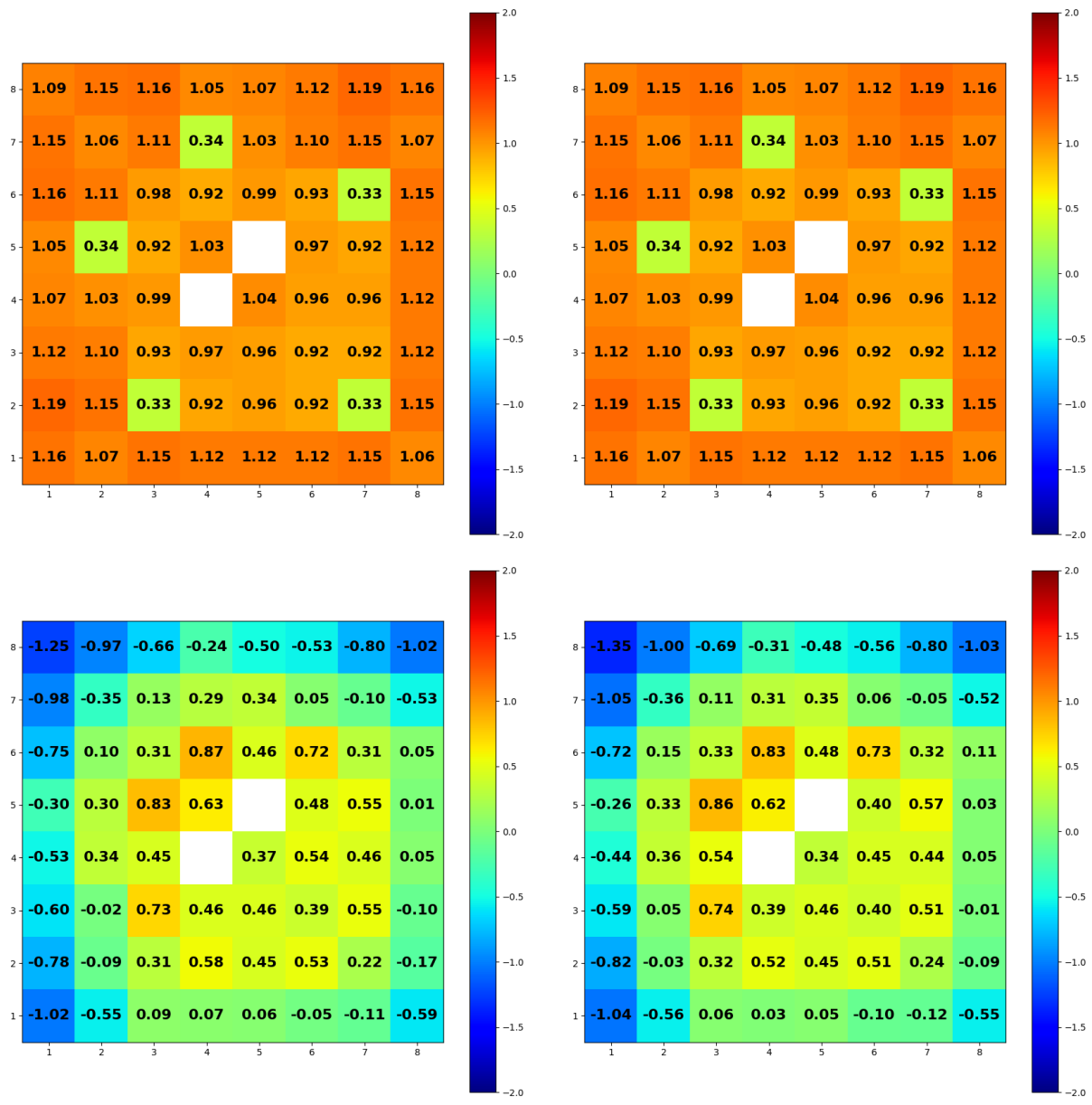


Figure 23. Normalized fission rates from MCNP (top left), Serpent (top right), differences between MPACT and MCNP (bottom left), and differences between MPACT and Serpent (bottom right) for the Peach Bottom 6 Uncontrolled case at 0% Void

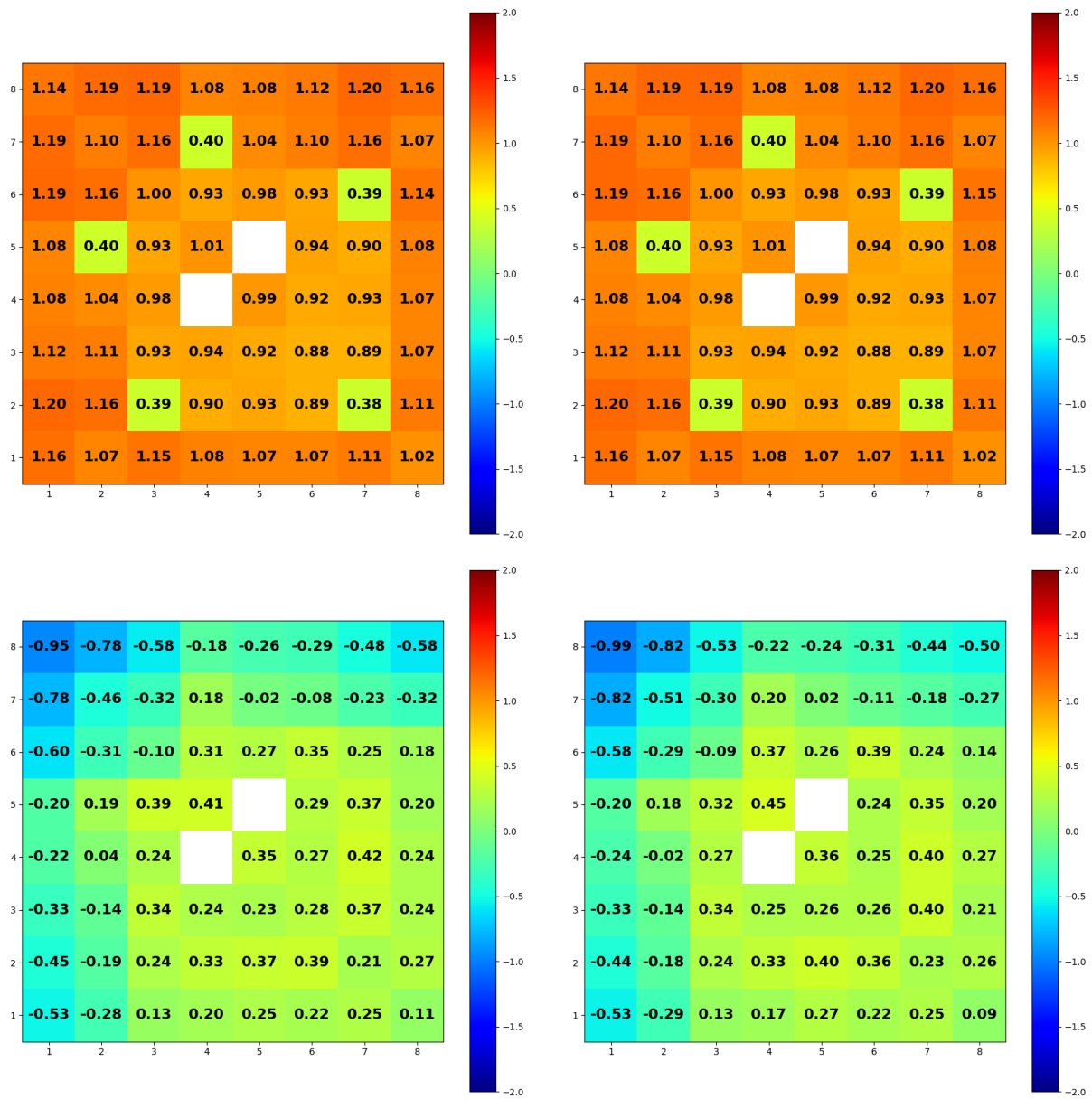


Figure 24. Normalized fission rates from MCNP (top left), Serpent (top right), differences between MPACT and MCNP (bottom left), and differences between MPACT and Serpent (bottom right) for the Peach Bottom 6 Uncontrolled case at 40% Void

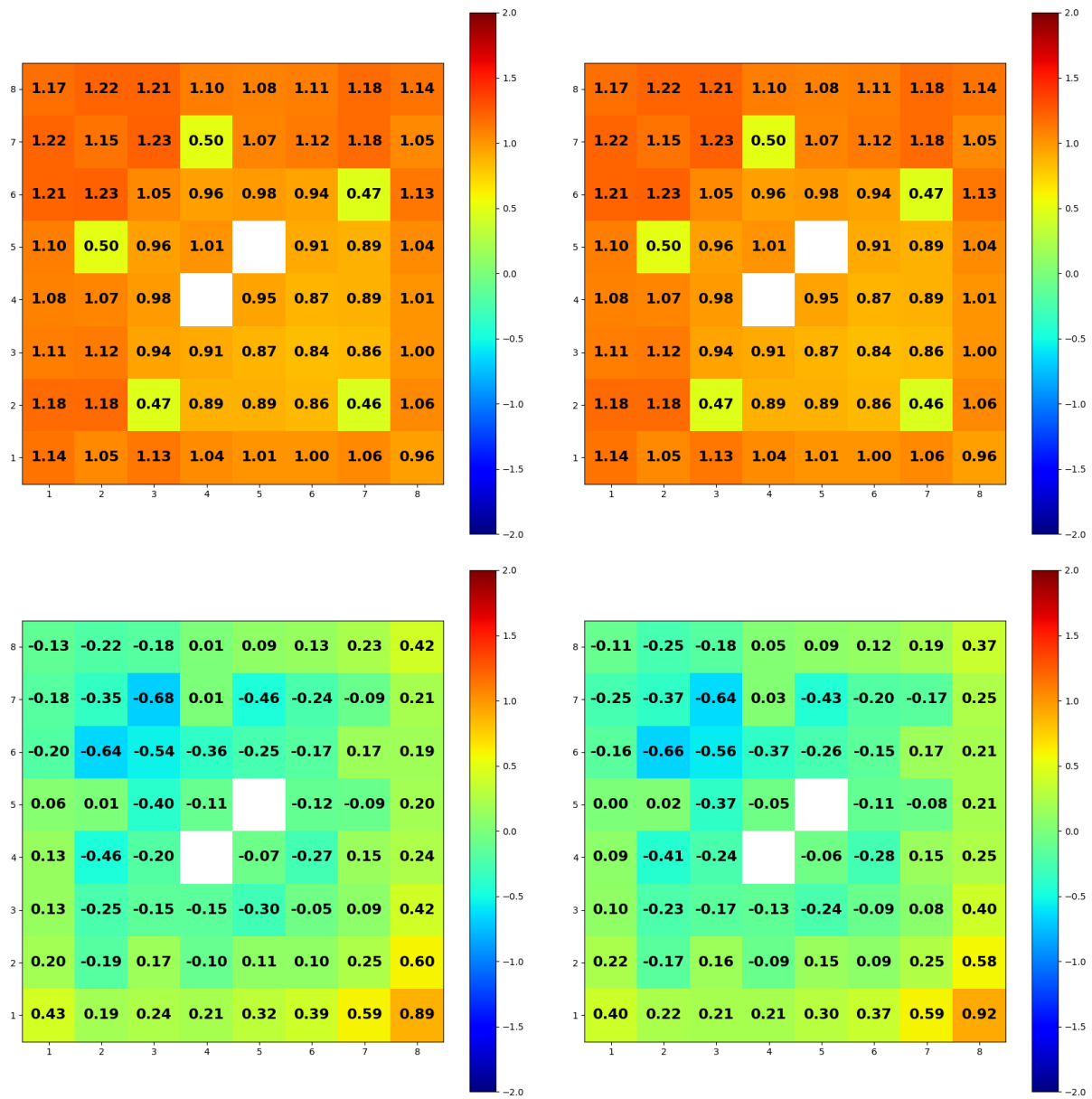


Figure 25. Normalized fission rates from MCNP (top left), Serpent (top right), differences between MPACT and MCNP (bottom left), and differences between MPACT and Serpent (bottom right) for the Peach Bottom 6 Uncontrolled case at 80% Void

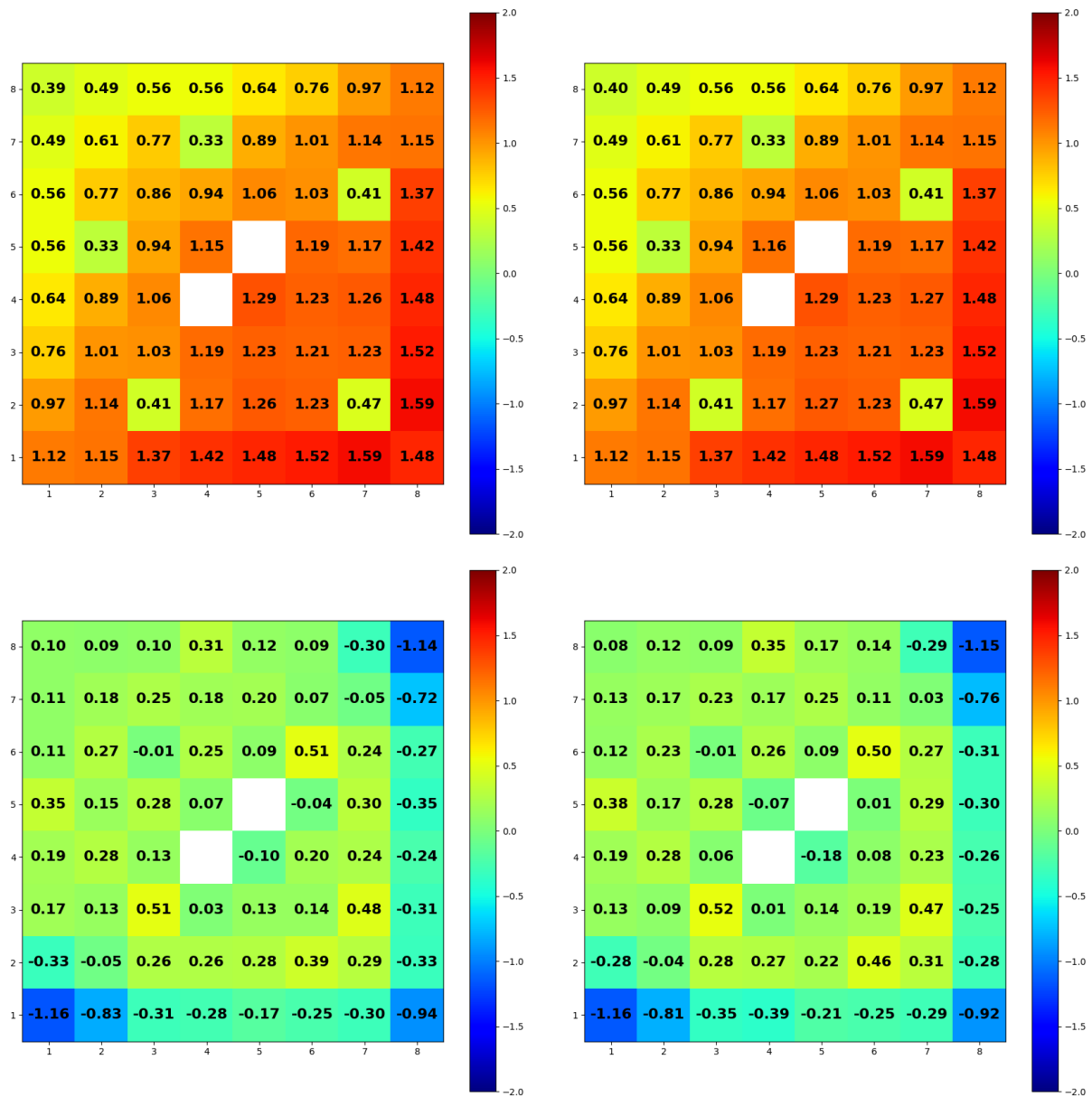


Figure 26. Normalized fission rates from MCNP (top left), Serpent (top right), differences between MPACT and MCNP (bottom left), and differences between MPACT and Serpent (bottom right) for the Peach Bottom 6 Controlled case at 0% Void

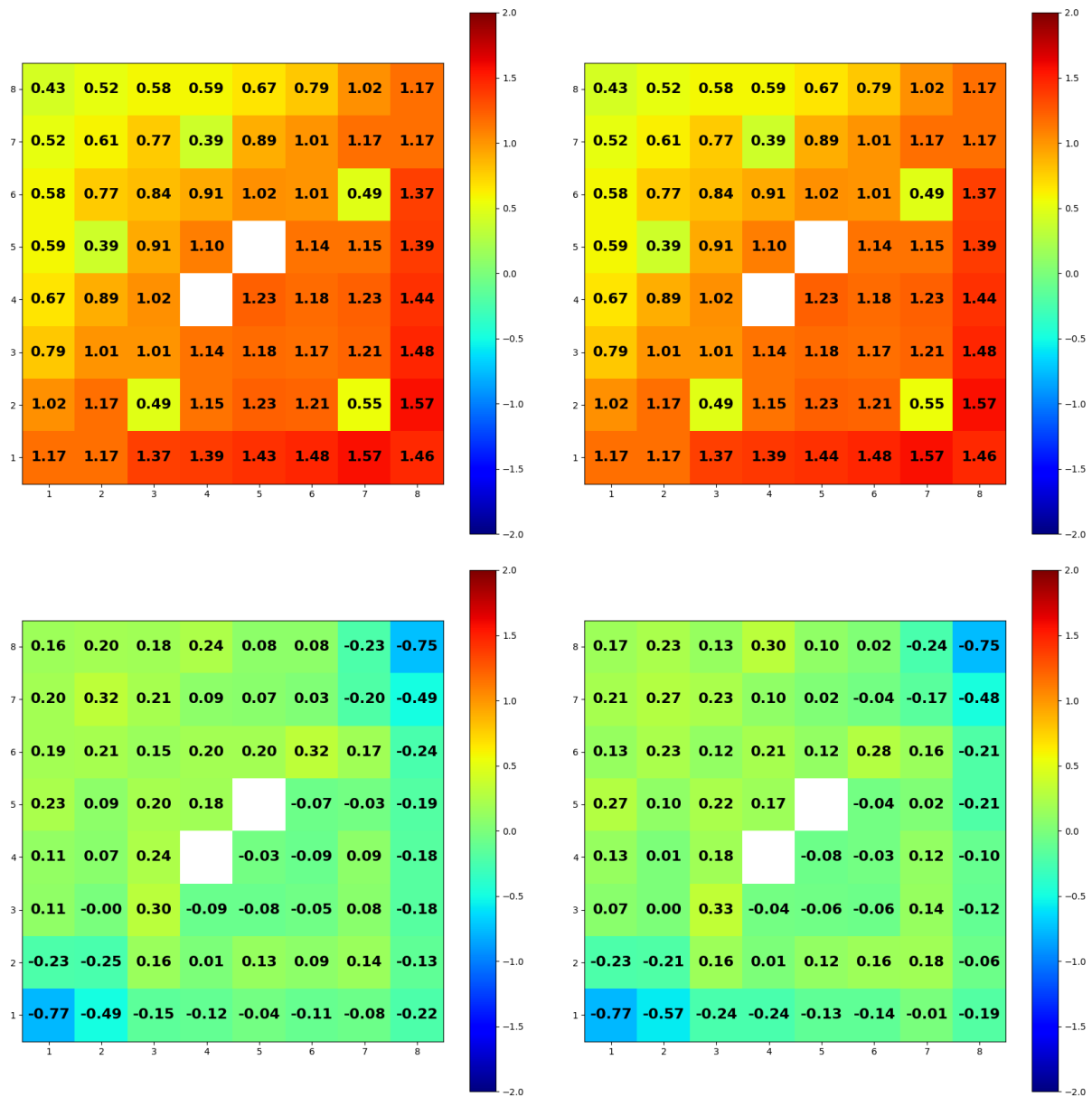


Figure 27. Normalized fission rates from MCNP (top left), Serpent (top right), differences between MPACT and MCNP (bottom left), and differences between MPACT and Serpent (bottom right) for the Peach Bottom 6 Controlled case at 40% Void

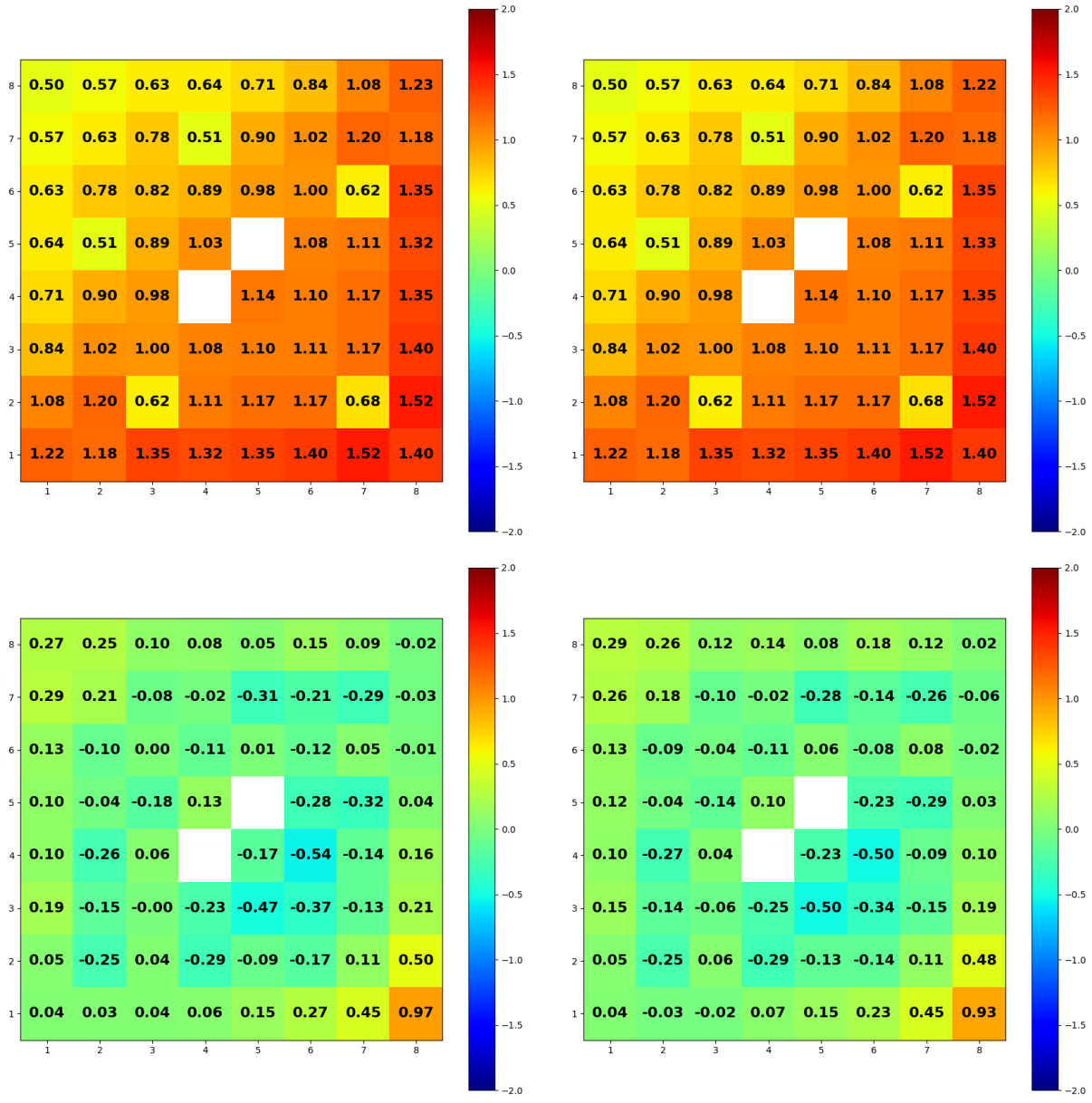


Figure 28. Normalized fission rates from MCNP (top left), Serpent (top right), differences between MPACT and MCNP (bottom left), and differences between MPACT and Serpent (bottom right) for the Peach Bottom 6 Controlled case at 80% Void

4.2 GE-9

Table 17 shows the eigenvalues from MCNP and Serpent for the GE-9 bundle described in section 2.2. MCNP calculations for the GE-9 lattice used 360 million active particles, while the Serpent calculations used 1.32 billion active particles. All MCNP eigenvalues have an estimated standard deviation of 4 pcm or less while for the Serpent cases the estimated standard deviation was 2 pcm or less.

Table 17. Eigenvalues from MCNP, Serpent, and MPACT for the GE-9 lattice.

Uncontrolled					
Void [%]	MCNP	Serpent	MPACT	MPACT-MCNP [pcm]	MPACT-Serpent [pcm]
0	1.08613	1.08623	1.086086	-4.4	-14.4
40	1.06902	1.06903	1.069418	39.8	38.8
80	1.03630	1.03635	1.036668	36.8	31.8
Controlled					
Void [%]	MCNP	Serpent	MPACT	MPACT-MCNP [pcm]	MPACT-Serpent [pcm]
0	0.84432	0.844339	0.844863	54.3	52.4
40	0.79664	0.796580	0.797827	118.7	124.7
80	0.73008	0.730167	0.731365	128.5	119.8

4.2.1 Normalized Fission Rate Monte Carlo Results

A summary of the differences in normalized fission rates between MPACT and MCNP or Serpent is presented in Table 18. For all GE-9 lattice calculations, the maximum relative standard deviation in the fission rates was 0.04% for the MCNP results and 0.03% for the Serpent results. In Figure 29 through Figure 34 more detailed descriptions of the differences in normalized fission rates between MPACT and Monte Carlo results are provided on a case by case basis.

Table 18. Summary of maximum and minimum differences in normalized fission rates between MPACT and Monte Carlo results for the GE-9 lattice.

Uncontrolled						
	MPACT - MCNP			MPACT - Serpent		
Void [%]	Max [%]	Min [%]	RMS [%]	Max [%]	Min [%]	RMS [%]
0	1.15	-1.33	0.57	1.15	-1.40	0.57
40	0.83	-0.90	0.41	0.84	-0.95	0.42
80	1.08	-0.84	0.39	1.06	-0.88	0.39
Controlled						
	MPACT - MCNP			MPACT - Serpent		
Void [%]	Max [%]	Min [%]	RMS [%]	Max [%]	Min [%]	RMS [%]
0	0.91	-1.29	0.45	0.94	-1.32	0.46
40	0.74	-0.88	0.29	0.75	-0.88	0.29
80	1.19	-0.59	0.31	1.25	-0.56	0.30

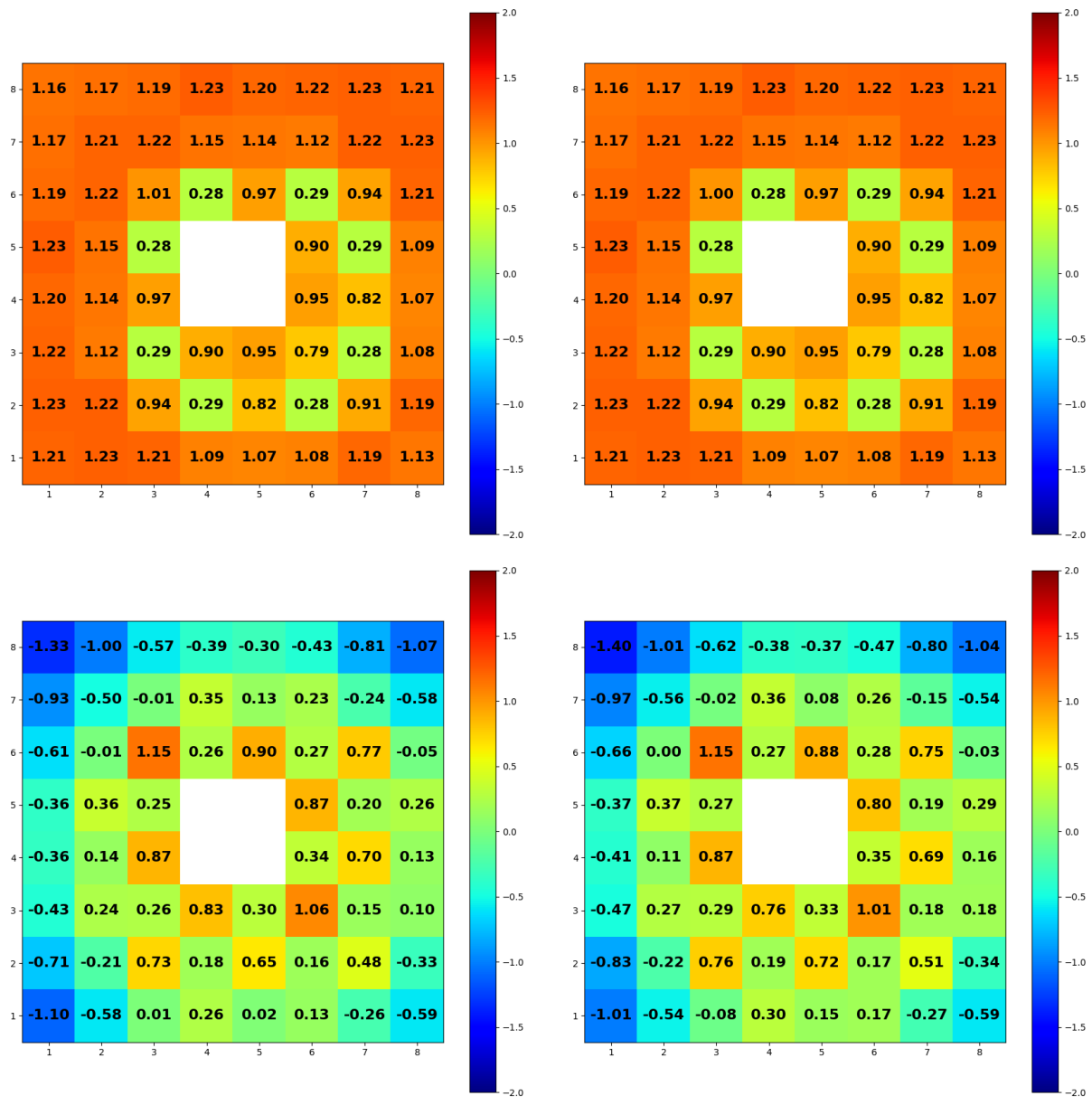


Figure 29. Normalized fission rates from MCNP (top left), Serpent (top right), differences between MPACT and MCNP (bottom left), and differences between MPACT and Serpent (bottom right) for the GE-9 Uncontrolled case at 0% Void

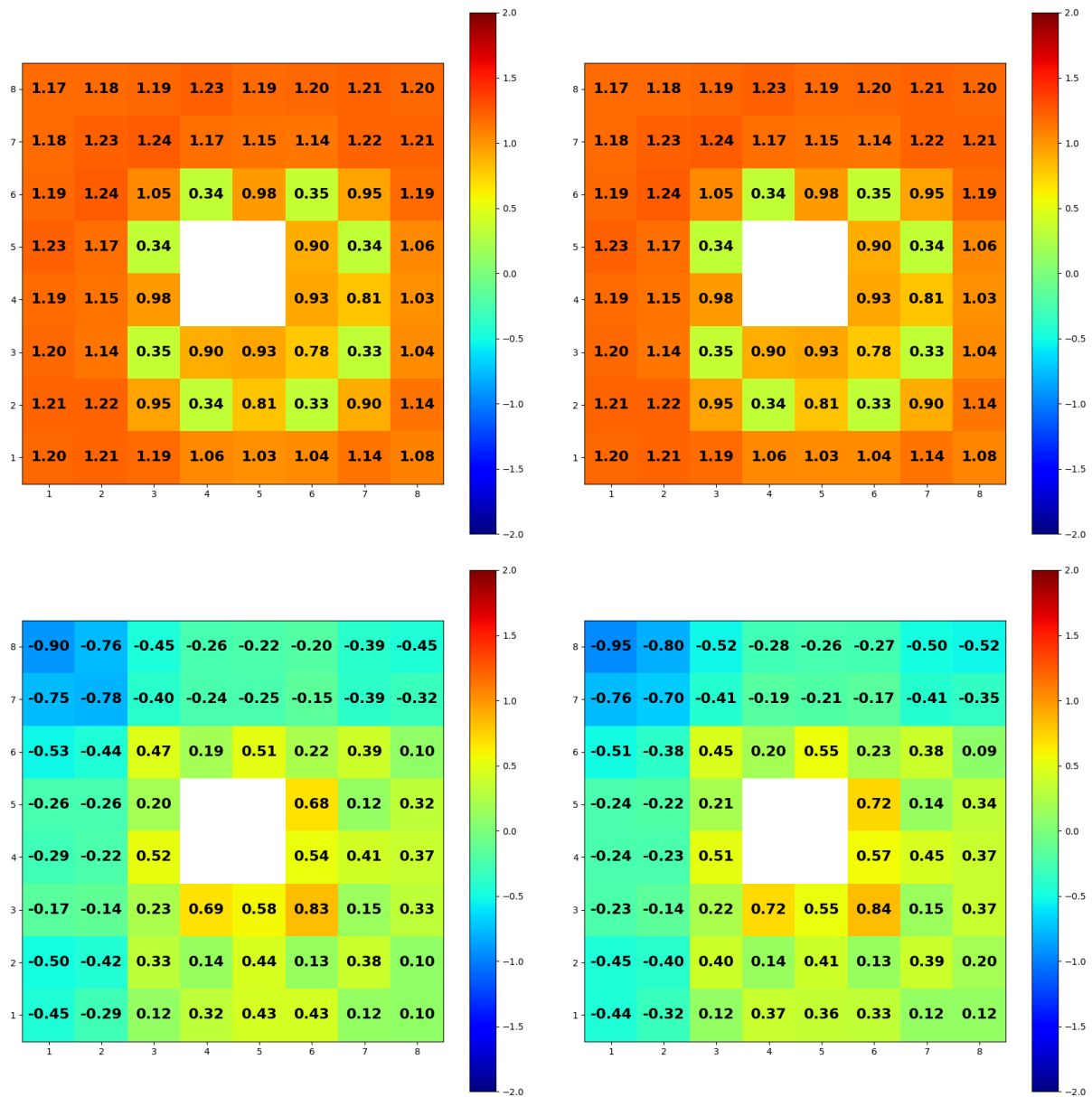


Figure 30. Normalized fission rates from MCNP (top left), Serpent (top right), differences between MPACT and MCNP (bottom left), and differences between MPACT and Serpent (bottom right) for the GE-9 Uncontrolled case at 40% Void

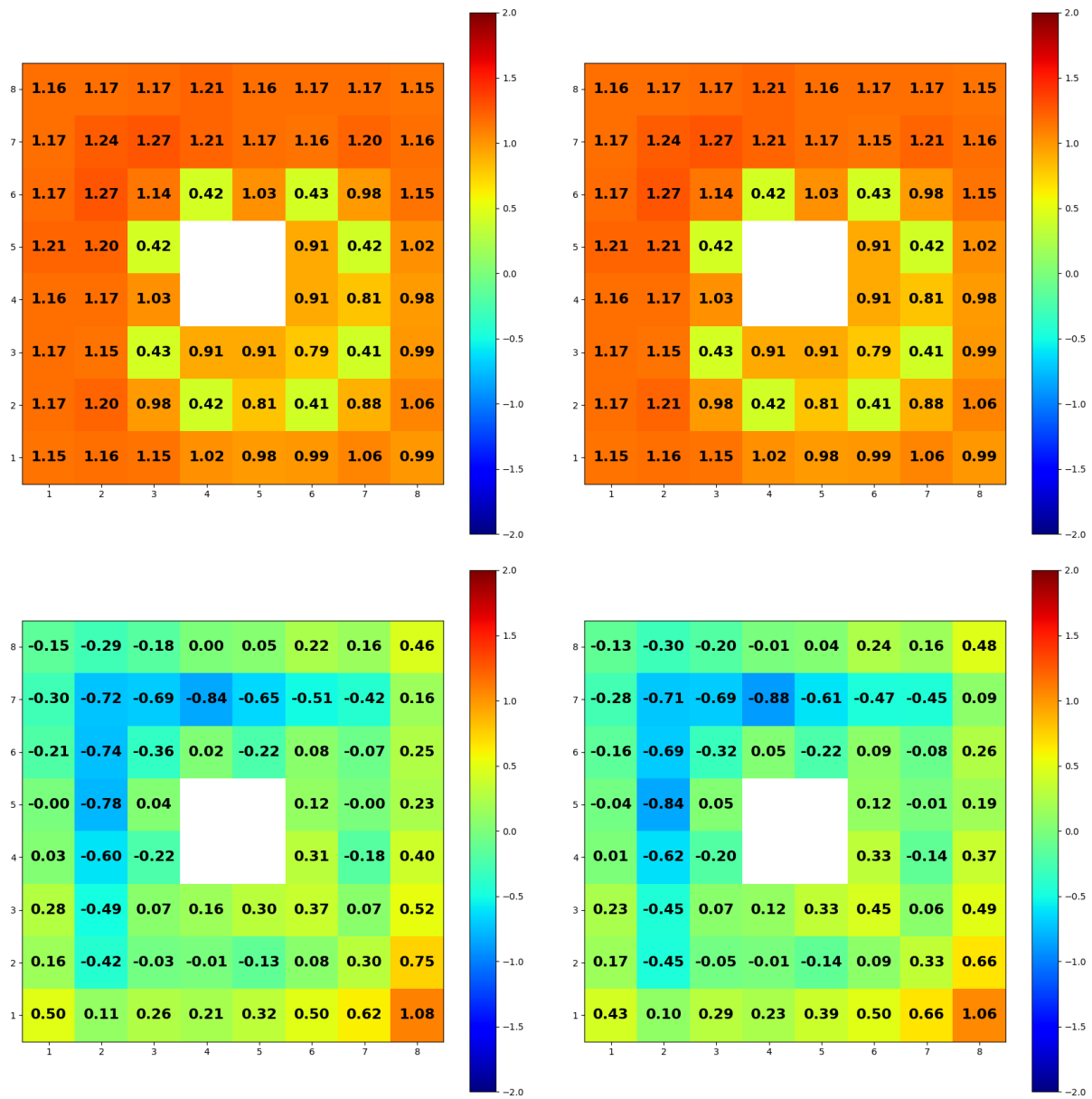


Figure 31. Normalized fission rates from MCNP (top left), Serpent (top right), differences between MPACT and MCNP (bottom left), and differences between MPACT and Serpent (bottom right) for the GE-9 Uncontrolled case at 80% Void

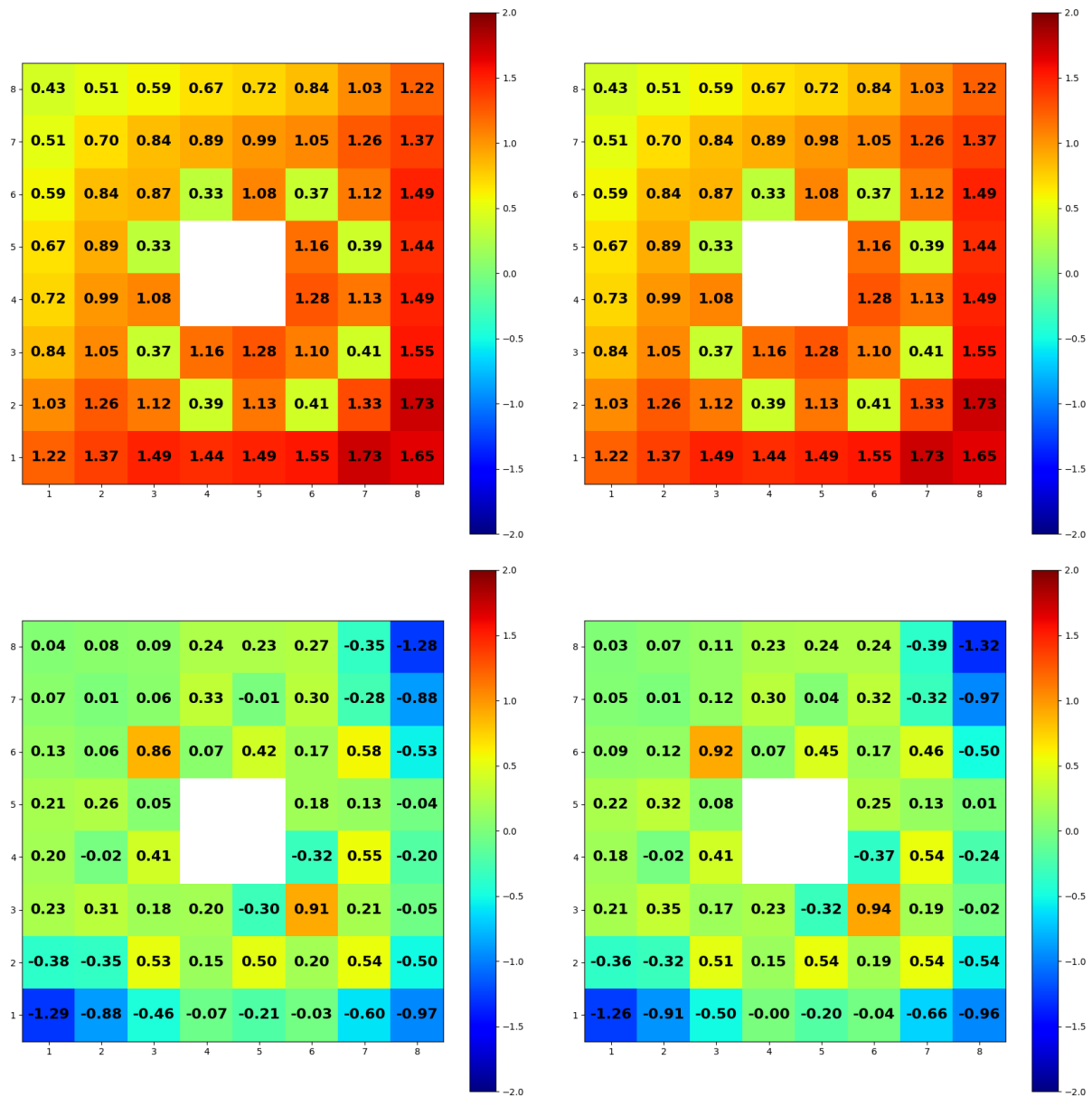


Figure 32. Normalized fission rates from MCNP (top left), Serpent (top right), differences between MPACT and MCNP (bottom left), and differences between MPACT and Serpent (bottom right) for the GE-9 Controlled case at 0% Void

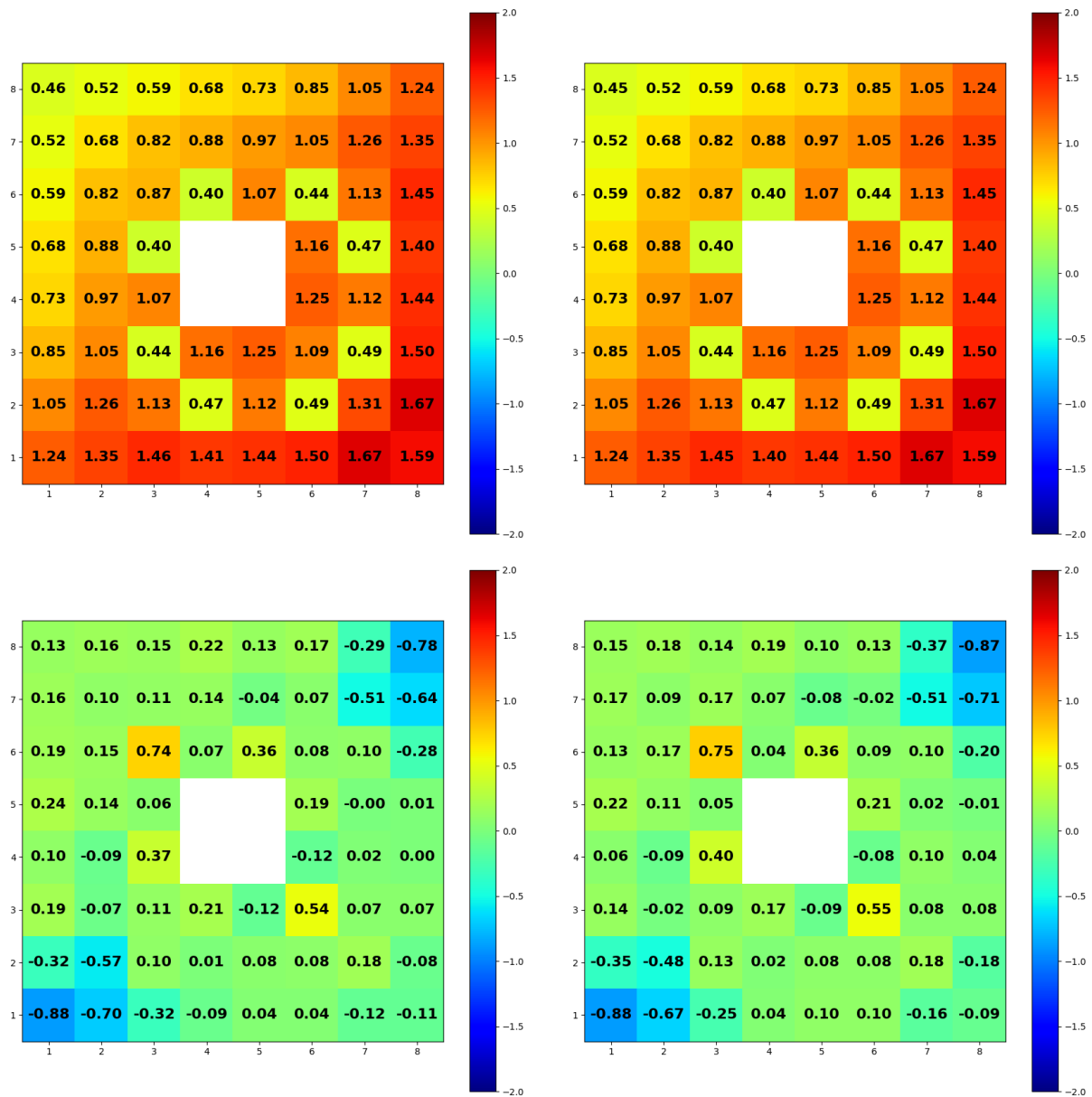


Figure 33. Normalized fission rates from MCNP (top left), Serpent (top right), differences between MPACT and MCNP (bottom left), and differences between MPACT and Serpent (bottom right) for the GE-9 Controlled case at 40% Void

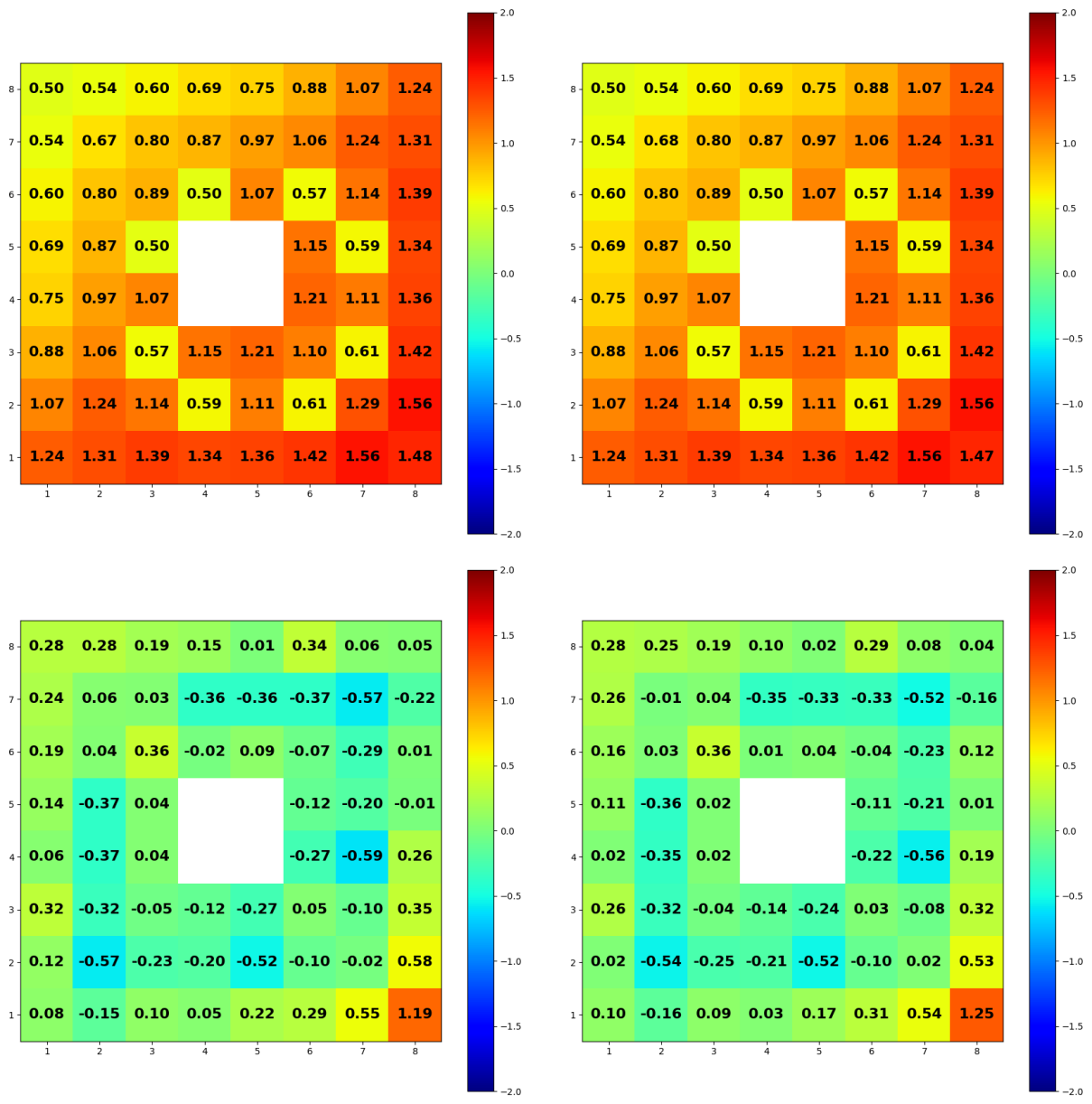


Figure 34. Normalized fission rates from MCNP (top left), Serpent (top right), differences between MPACT and MCNP (bottom left), and differences between MPACT and Serpent (bottom right) for the GE-9 Controlled case at 80% Void

4.3 GE-14

Table 19 shows the eigenvalues from MCNP and Serpent for the GE-14 bundle described in section 2.3. MCNP calculations for the GE-14 lattice used 360 million active particles, while the Serpent calculations used 1.32 billion active particles. All MCNP eigenvalues have an estimated standard deviation of 4 pcm or less while for the Serpent cases the estimated standard deviation was 2 pcm or less.

Table 19. Eigenvalues from MCNP, Serpent, and MPACT for the GE-14 lattice.

Uncontrolled					
Void [%]	MCNP	Serpent	MPACT	MPACT-MCNP [pcm]	MPACT-Serpent [pcm]
0	0.98915	0.989207	0.991415	226.5	220.8
40	0.97138	0.971401	0.974220	284.0	281.9
80	0.94739	0.947437	0.949807	241.7	237.0
Controlled					
Void [%]	MCNP	Serpent	MPACT	MPACT-MCNP [pcm]	MPACT-Serpent [pcm]
0	0.81694	0.816986	0.819267	232.7	228.1
40	0.78501	0.785002	0.787691	268.1	268.9
80	0.74837	0.748449	0.750701	233.1	225.2

4.3.1 Normalized Fission Rate Monte Carlo Results

A summary of the differences in normalized fission rates between MPACT and MCNP or Serpent is presented in Table 20. For all GE-14 lattice calculations, the maximum relative standard deviation in the fission rates was 0.05% for the MCNP results and 0.04% for the Serpent results. In Figure 35 through Figure 40 more detailed descriptions of the differences in normalized fission rates between MPACT and Monte Carlo results are provided on a case by case basis.

Table 20. Summary of maximum and minimum differences in normalized fission rates between MPACT and Monte Carlo results for the GE-14 lattice.

Uncontrolled						
	MPACT - MCNP			MPACT - Serpent		
Void [%]	Max [%]	Min [%]	RMS [%]	Max [%]	Min [%]	RMS [%]
0	1.22	-1.08	0.53	1.24	-1.17	0.55
40	0.79	-0.74	0.32	0.76	-0.80	0.33
80	1.33	-0.80	0.39	1.28	-0.80	0.38
Controlled						
	MPACT - MCNP			MPACT - Serpent		
Void [%]	Max [%]	Min [%]	RMS [%]	Max [%]	Min [%]	RMS [%]
0	1.33	-1.36	0.53	1.47	-1.45	0.55
40	0.68	-0.76	0.32	0.72	-0.83	0.33
80	1.67	-1.17	0.42	1.60	-1.14	0.41

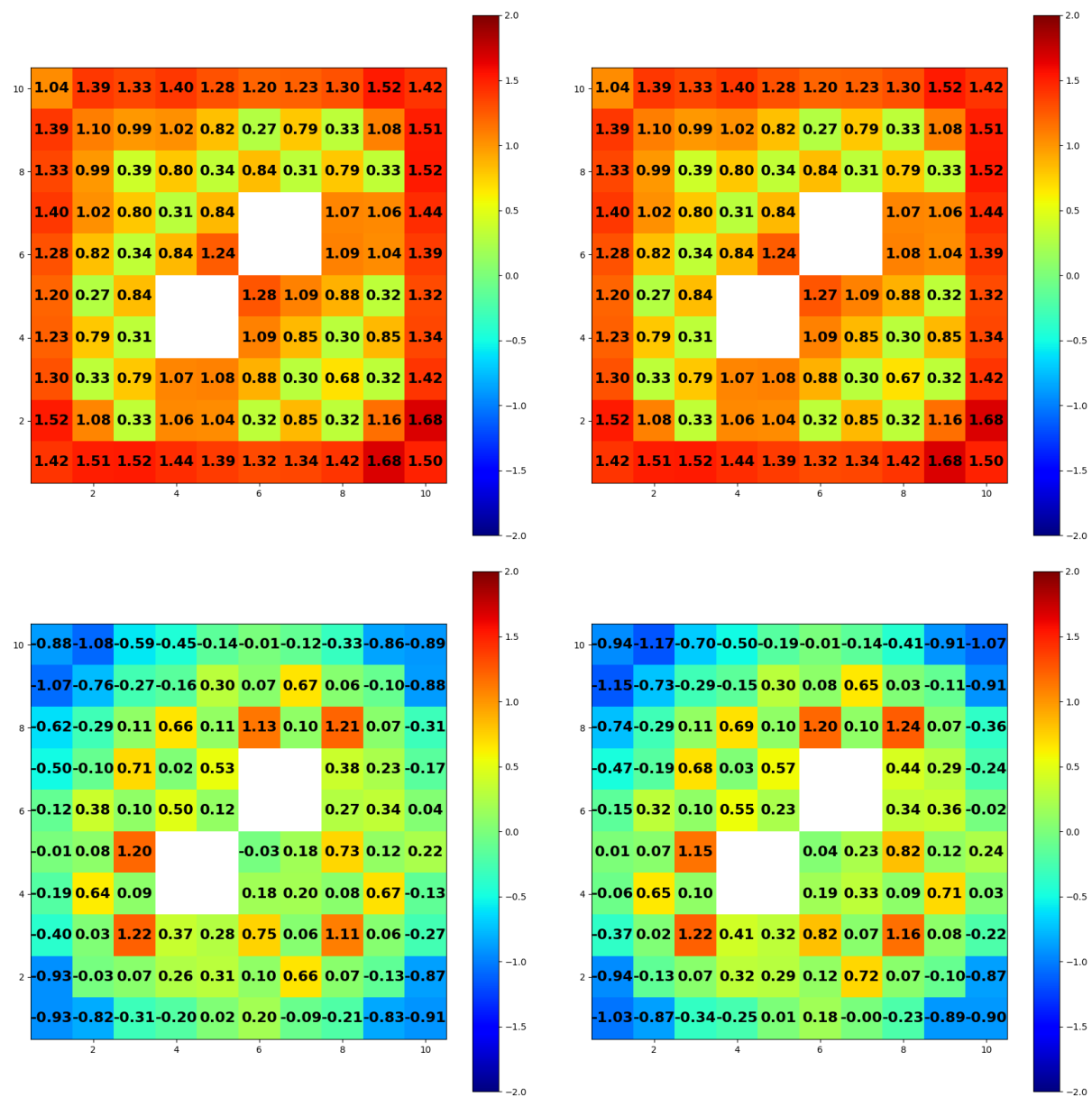


Figure 35. Normalized fission rates from MCNP (top left), Serpent (top right), differences between MPACT and MCNP (bottom left), and differences between MPACT and Serpent (bottom right) for the GE-14 Uncontrolled case at 0% Void

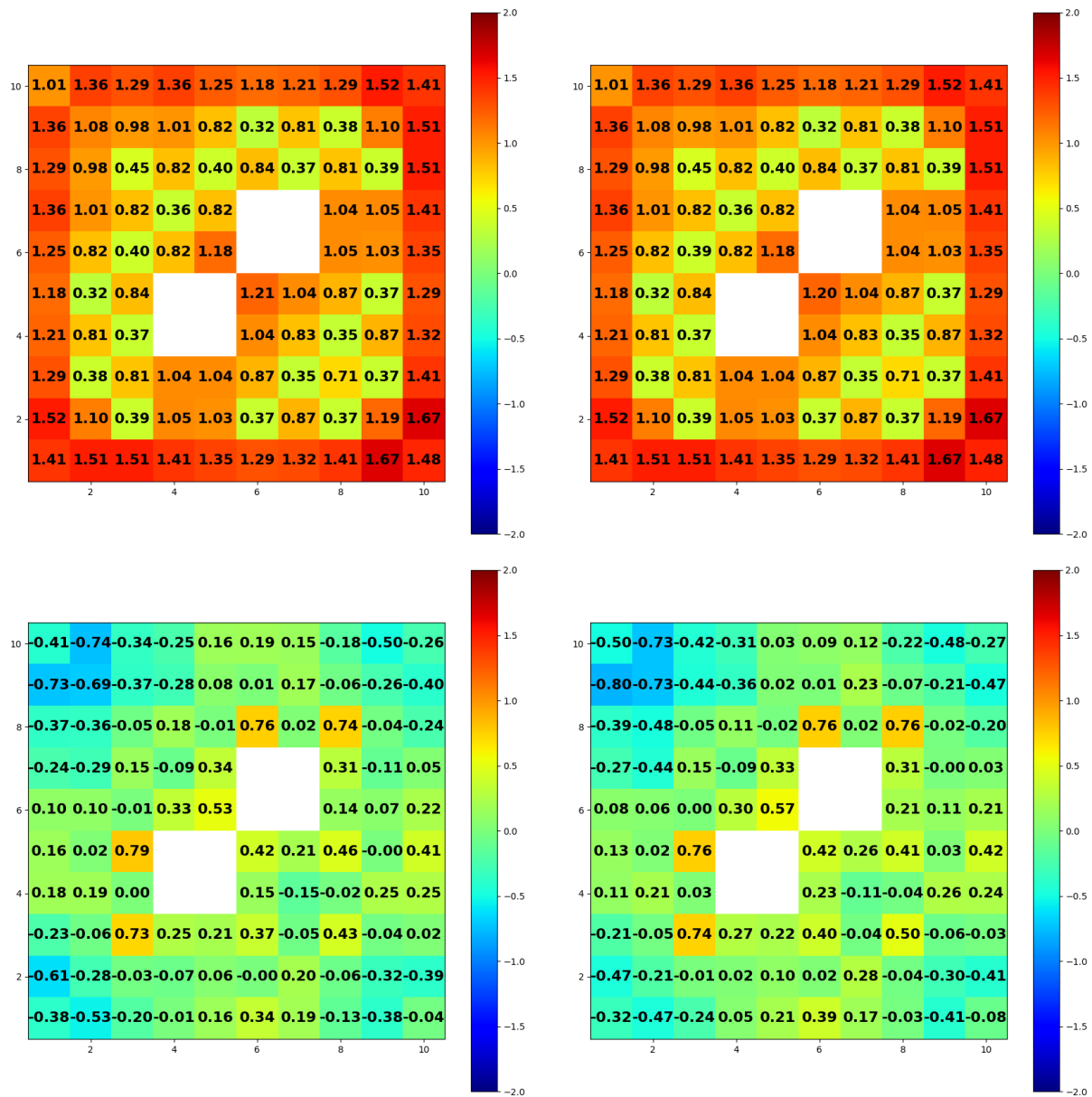


Figure 36. Normalized fission rates from MCNP (top left), Serpent (top right), differences between MPACT and MCNP (bottom left), and differences between MPACT and Serpent (bottom right) for the GE-14 Uncontrolled case at 40% Void

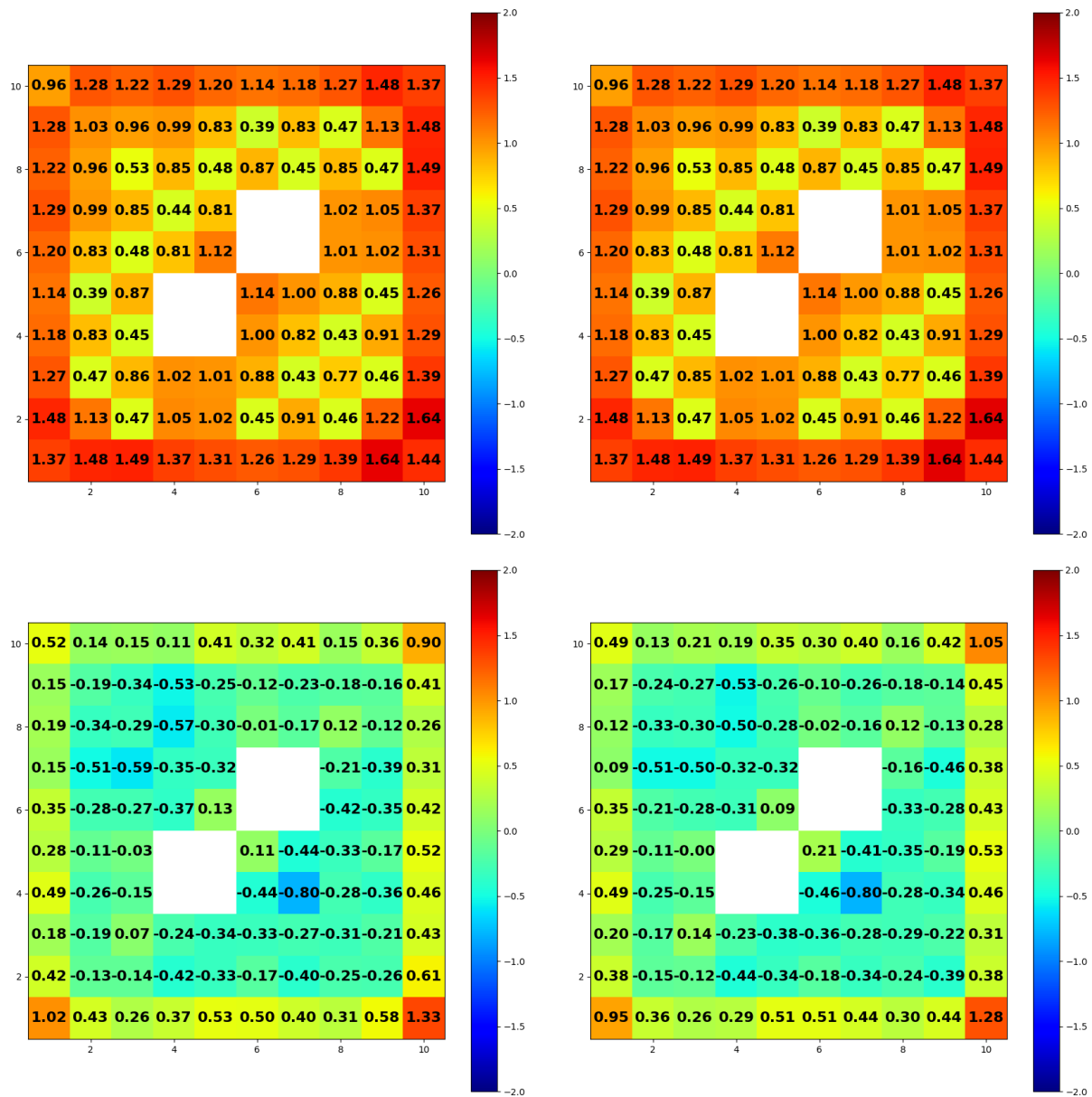


Figure 37. Normalized fission rates from MCNP (top left), Serpent (top right), differences between MPACT and MCNP (bottom left), and differences between MPACT and Serpent (bottom right) for the GE-14 Uncontrolled case at 80% Void

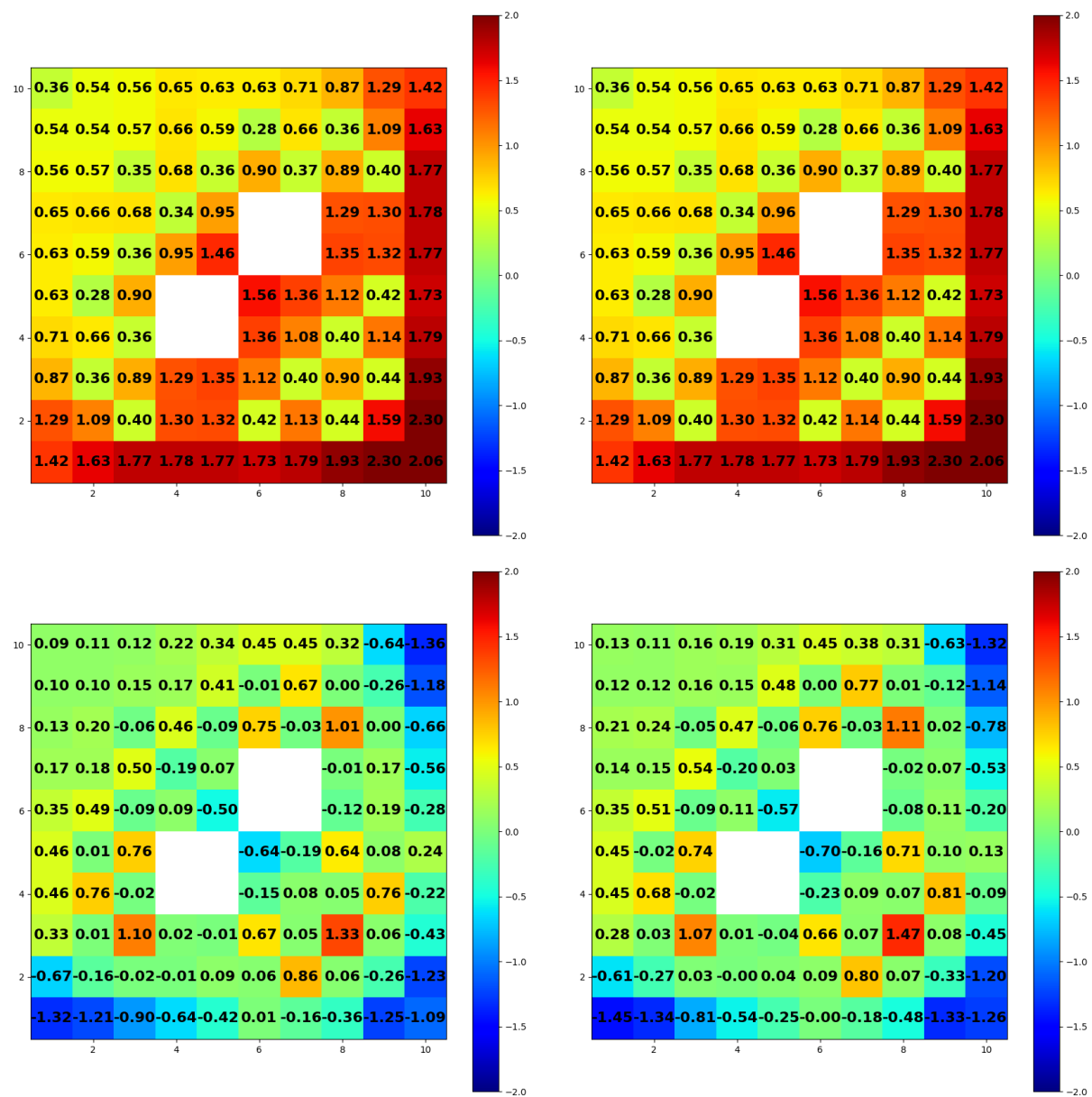


Figure 38. Normalized fission rates from MCNP (top left), Serpent (top right), differences between MPACT and MCNP (bottom left), and differences between MPACT and Serpent (bottom right) for the GE-14 Controlled case at 0% Void

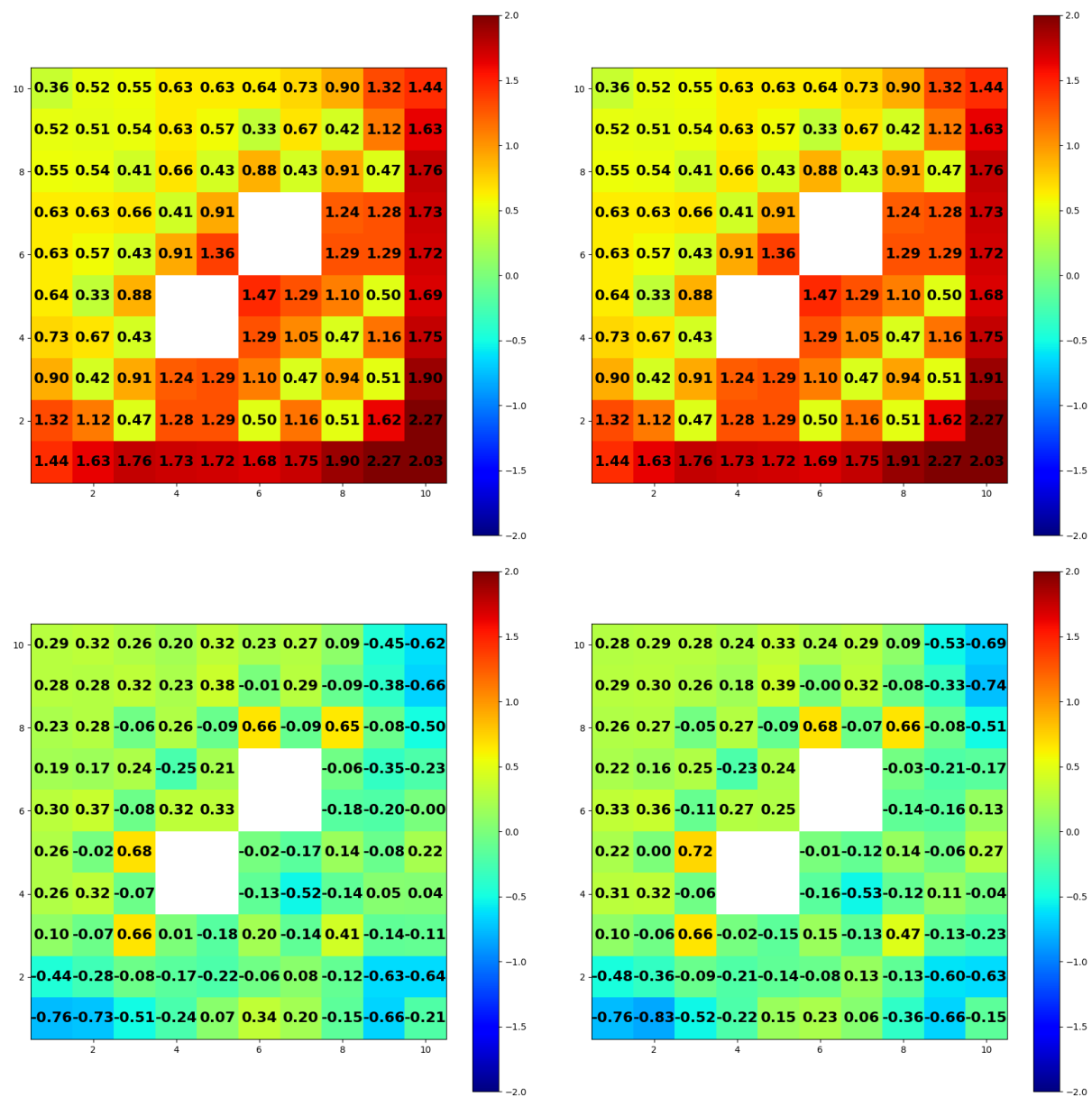


Figure 39. Normalized fission rates from MCNP (top left), Serpent (top right), differences between MPACT and MCNP (bottom left), and differences between MPACT and Serpent (bottom right) for the GE-14 Controlled case at 40% Void

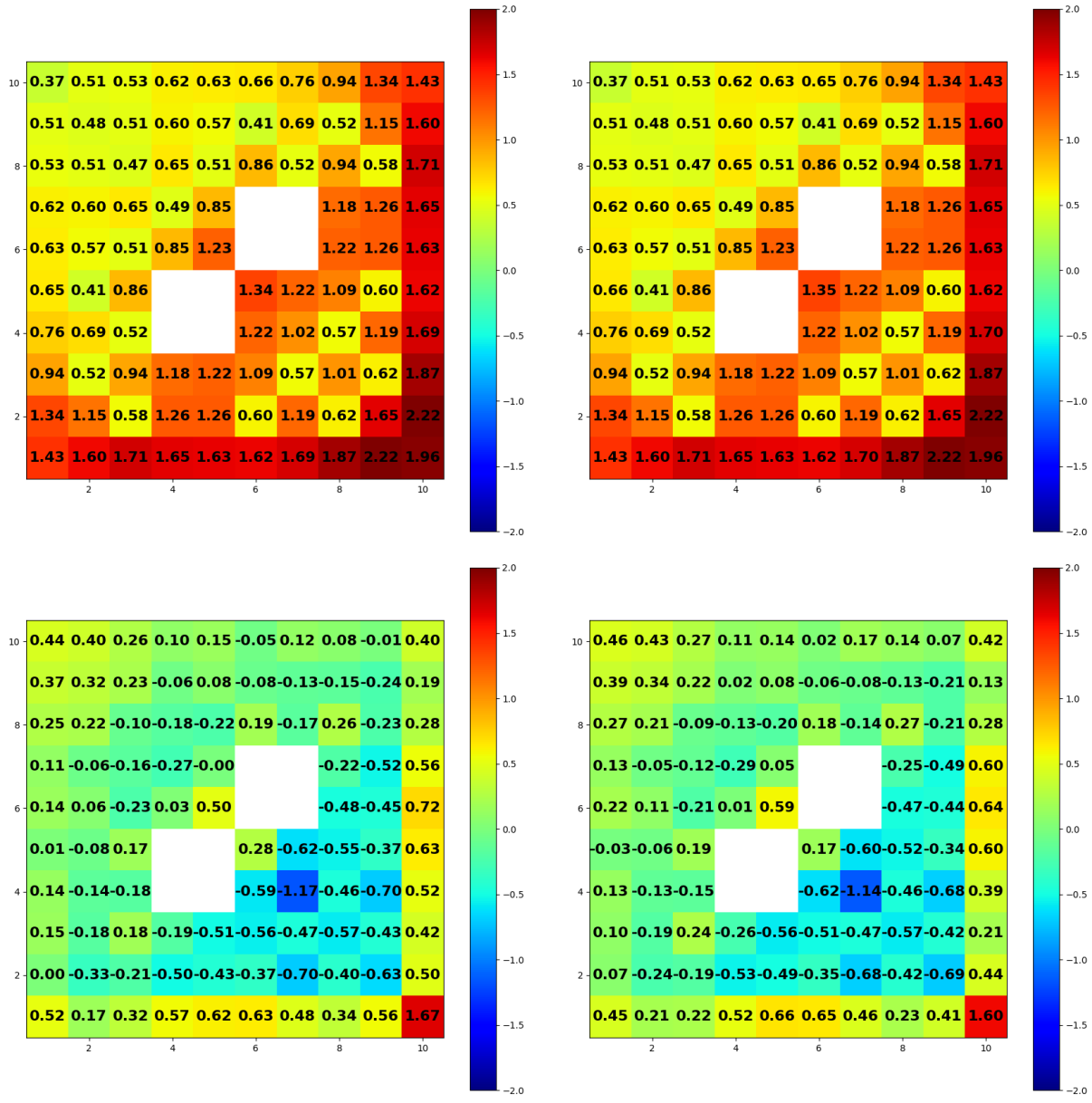


Figure 40. Normalized fission rates from MCNP (top left), Serpent (top right), differences between MPACT and MCNP (bottom left), and differences between MPACT and Serpent (bottom right) for the GE-14 Controlled case at 80% Void

4.4 GE-14 With Vanished Rods

Table 21 shows the eigenvalues from MCNP and Serpent for the GE-14 lattice with vanished rods described in section 2.4. MCNP calculations used 360 million active particles, while the Serpent calculations used 1.32 billion active particles. All MCNP eigenvalues have an estimated standard deviation of 4 pcm or less while for the Serpent cases the estimated standard deviation was 2 pcm or less.

Table 21. Eigenvalues from MCNP, Serpent, and MPACT for the GE-14 lattice with vanished rods.

Uncontrolled					
Void [%]	MCNP	Serpent	MPACT	MPACT-MCNP [pcm]	MPACT-Serpent [pcm]
0	0.98088	0.980903	0.983255	237.5	235.2
40	0.96658	0.966607	0.969702	312.2	309.5
80	0.94246	0.942449	0.945591	313.1	314.2
Controlled					
Void [%]	MCNP	Serpent	MPACT	MPACT-MCNP [pcm]	MPACT-Serpent [pcm]
0	0.78203	0.782067	0.784768	273.8	270.1
40	0.75188	0.751855	0.755028	314.8	317.3
80	0.71390	0.713857	0.716701	280.1	284.4

4.4.1 Normalized Fission Rate Monte Carlo Results

A summary of the differences in normalized fission rates between MPACT and MCNP or Serpent is presented in Table 22. For all of the vanished rod problems, the maximum relative standard deviation in the fission rates was 0.05% for the MCNP results and 0.04% for the Serpent results. In Figure 41 through Figure 46 more detailed descriptions of the differences in normalized fission rates between MPACT and Monte Carlo results are provided on a case by case basis.

Table 22. Summary of maximum and minimum differences in normalized fission rates between MPACT and Monte Carlo results for the GE-14 lattice with vanished rods.

Uncontrolled						
	MPACT - MCNP			MPACT - Serpent		
Void [%]	Max [%]	Min [%]	RMS [%]	Max [%]	Min [%]	RMS [%]
0	1.71	-1.25	0.63	1.73	-1.30	0.64
40	1.06	-0.91	0.41	1.12	-0.94	0.42
80	0.86	-0.76	0.35	0.86	-0.77	0.35
Controlled						
	MPACT - MCNP			MPACT - Serpent		
Void [%]	Max [%]	Min [%]	RMS [%]	Max [%]	Min [%]	RMS [%]
0	1.59	-1.40	0.61	1.64	-1.40	0.62
40	1.05	-1.05	0.38	1.03	-1.06	0.40
80	0.97	-1.27	0.37	1.05	-1.26	0.37

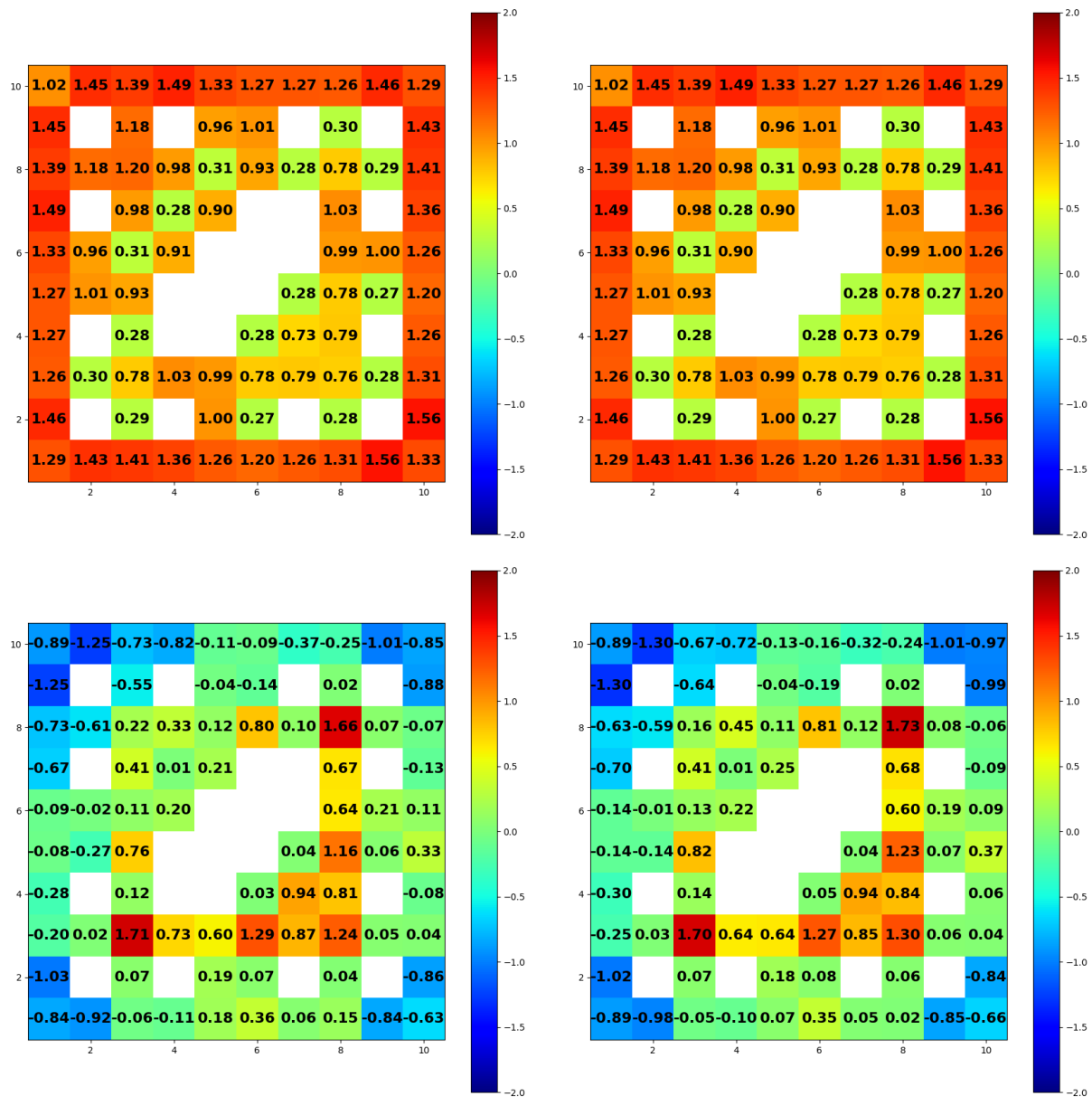


Figure 41. Normalized fission rates from MCNP (top left), Serpent (top right), differences between MPACT and MCNP (bottom left), and differences between MPACT and Serpent (bottom right) for the Uncontrolled GE-14 case with vanished rods at 0% Void

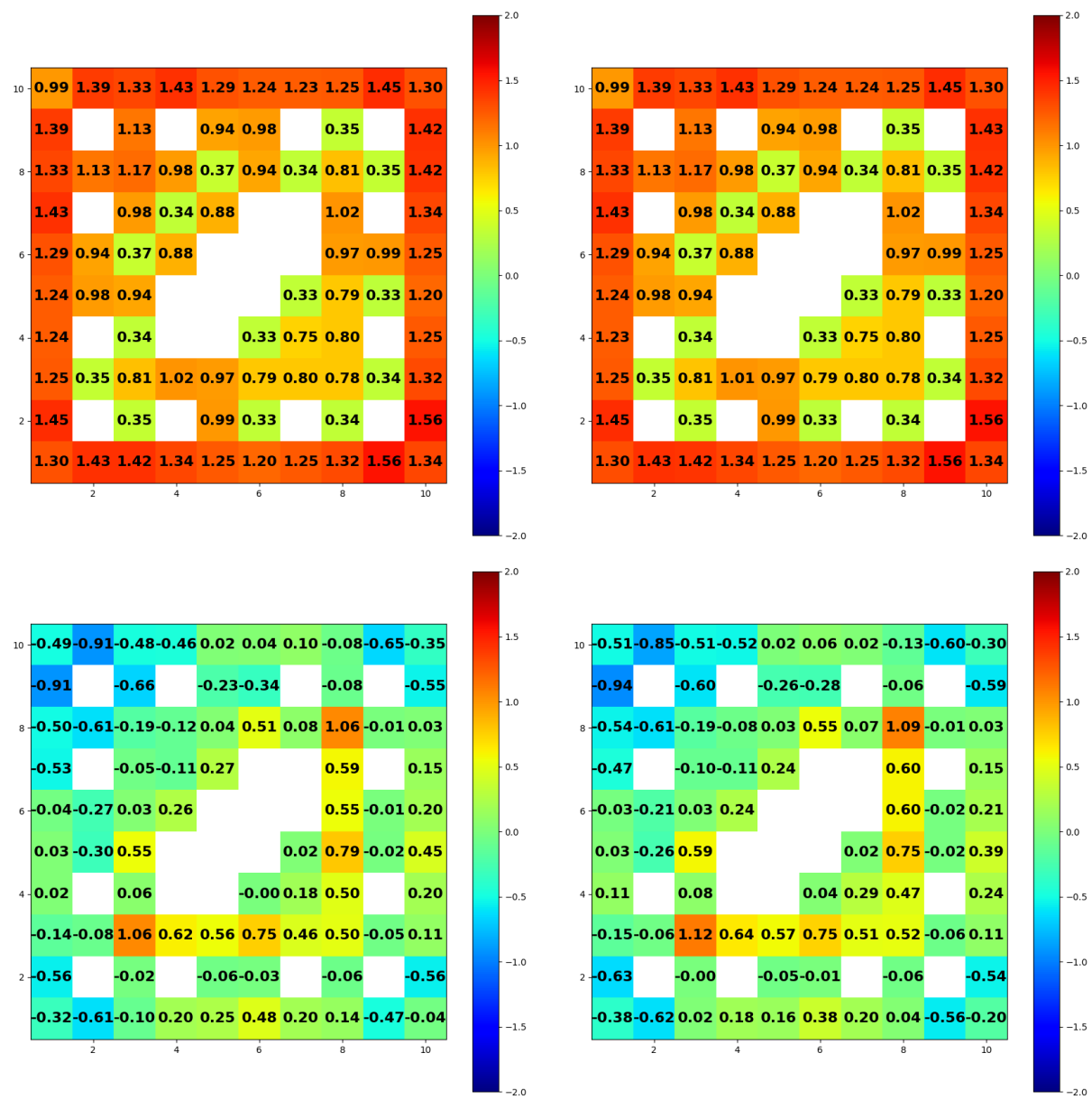


Figure 42. Normalized fission rates from MCNP (top left), Serpent (top right), differences between MPACT and MCNP (bottom left), and differences between MPACT and Serpent (bottom right) for the Uncontrolled GE-14 case with vanished rods at 40% Void

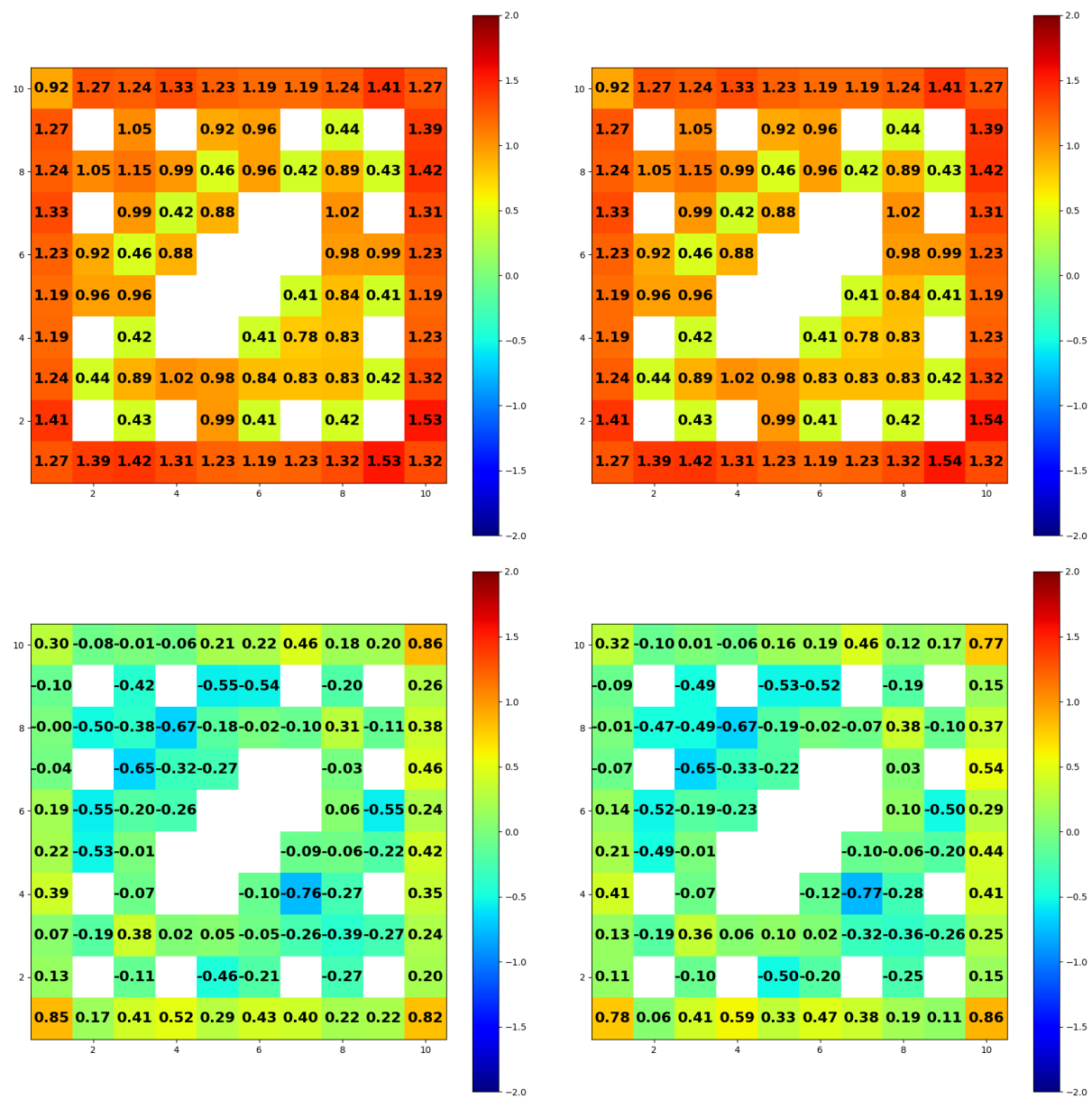


Figure 43. Normalized fission rates from MCNP (top left), Serpent (top right), differences between MPACT and MCNP (bottom left), and differences between MPACT and Serpent (bottom right) for the Uncontrolled GE-14 case with vanished rods at 80% Void

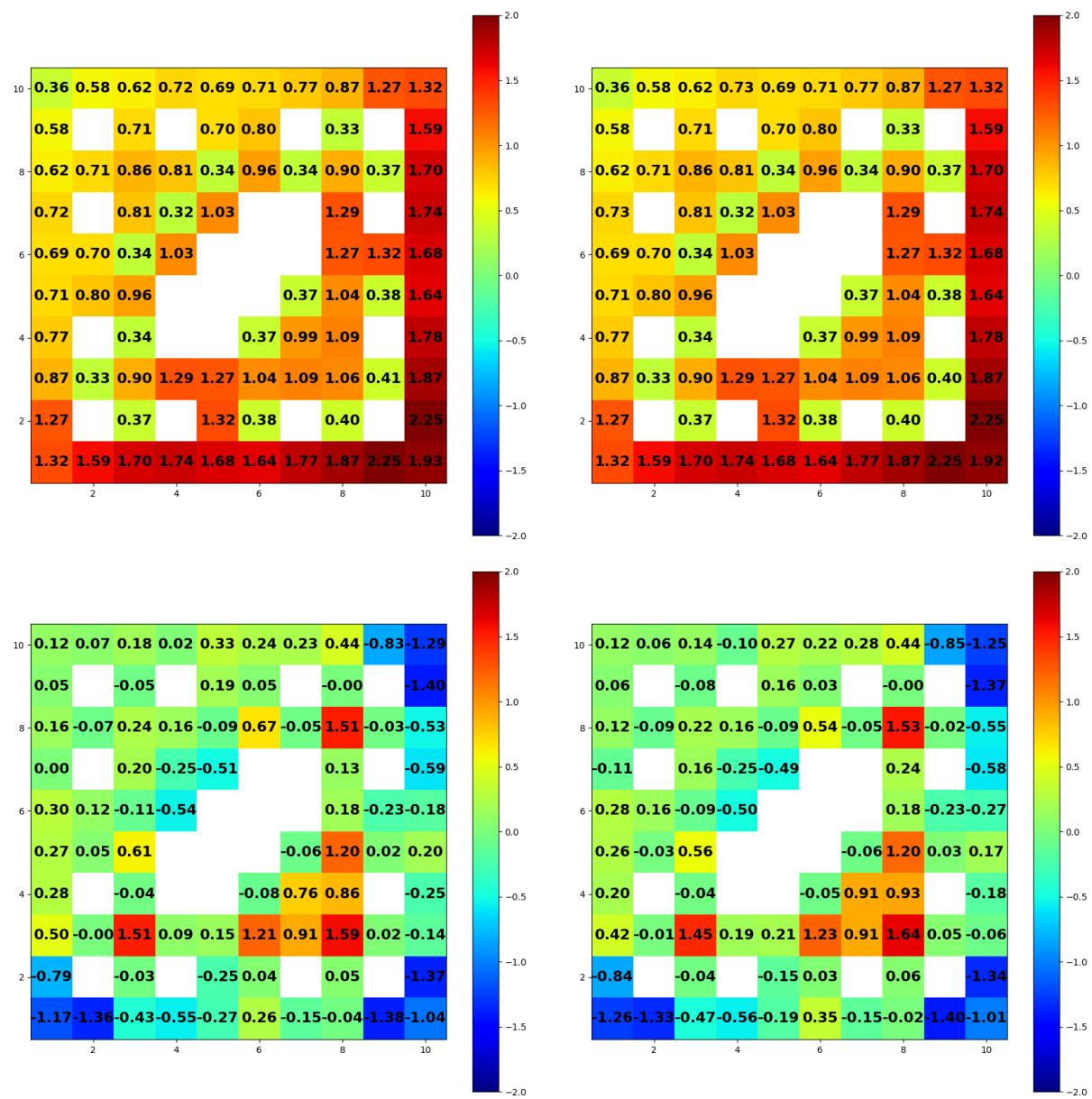


Figure 44. Normalized fission rates from MCNP (top left), Serpent (top right), differences between MPACT and MCNP (bottom left), and differences between MPACT and Serpent (bottom right) for the Controlled GE-14 case with vanished rods at 0% Void

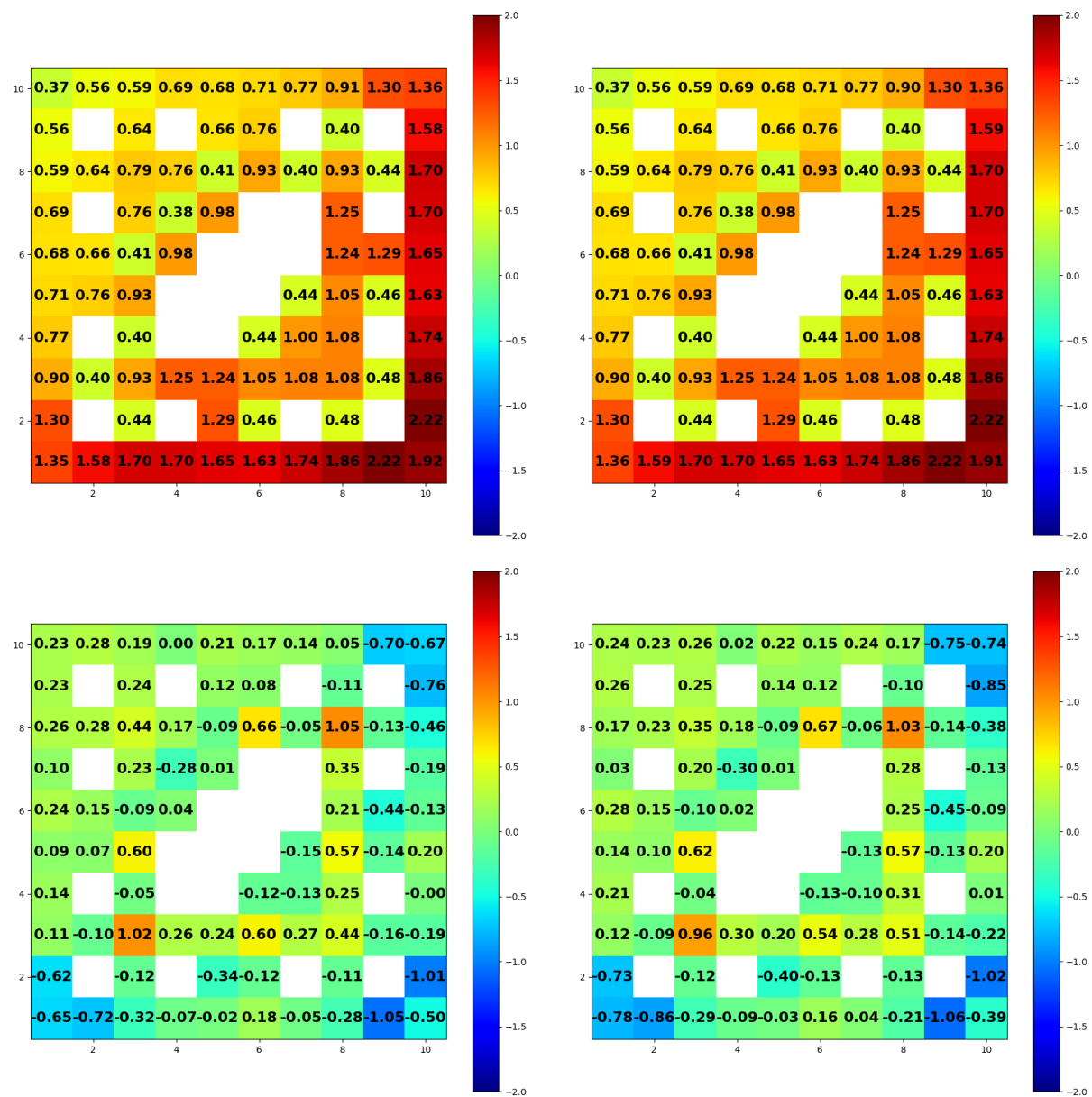


Figure 45. Normalized fission rates from MCNP (top left), Serpent (top right), differences between MPACT and MCNP (bottom left), and differences between MPACT and Serpent (bottom right) for the Controlled GE-14 case with vanished rods at 40% Void

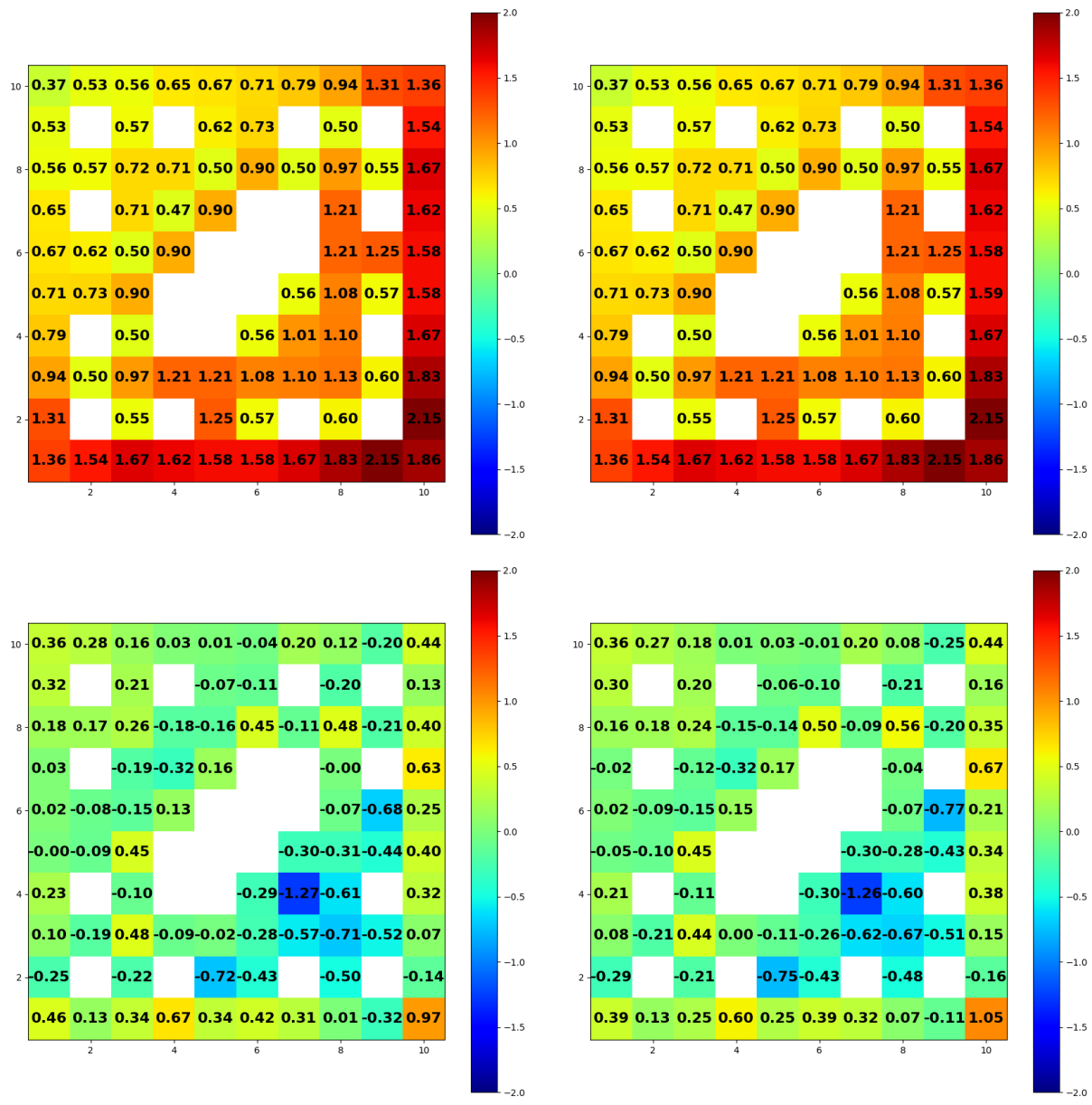


Figure 46. Normalized fission rates from MCNP (top left), Serpent (top right), differences between MPACT and MCNP (bottom left), and differences between MPACT and Serpent (bottom right) for the Controlled GE-14 case with vanished rods at 80% Void

4.5 2D Mini-Core

Eigenvalues from MCNP are provided in Table 23 and are compared with results from MPACT. The MCNP solutions were obtained using runs with 1.44 billion active particles. This resulted in standard deviations in the eigenvalue all 2 pcm or less.

Table 23. Eigenvalues from MCNP and MPACT for the 16 bundle mini-core.

Uncontrolled			
Void [%]	MCNP	MPACT	MPACT-MCNP [pcm]
0	0.98915	0.991415	226.5
20	0.98108	0.983707	262.7
60	0.96017	0.962929	275.9

Controlled			
Void [%]	MCNP	MPACT	MPACT-MCNP [pcm]
0	0.98209	0.984354	226.4
20	0.97261	0.975177	256.7
60	0.94937	0.952007	263.7

4.5.1 Normalized Fission Rate Monte Carlo Results

A summary of the differences in normalized fission rates between MPACT and MCNP is presented in Table 24. For all of the Uncontrolled 4x4 bundle test cases, the relative standard deviation in fission rates was 0.09% or less and was 0.13% or less in the Controlled cases. In these larger problems, the low flux in the controlled bundle leads to higher errors in the controlled bundle when calculating tallies in MCNP. In Figure 47 through Figure 52 more detailed descriptions of the differences in normalized fission rates between MPACT and Monte Carlo results are provided on a case by case basis.

Table 24. Summary of maximum and minimum differences in normalized fission rates between MPACT and Monte Carlo results for the 16 bundle mini-core.

Uncontrolled			
	MPACT - MCNP		
Void [%]	Max [%]	Min [%]	RMS [%]
0	1.33	-1.43	0.55
20	1.37	-1.44	0.45
60	0.79	-0.62	0.25

Controlled			
	MPACT - MCNP		
Void [%]	Max [%]	Min [%]	RMS [%]
0	1.44	-1.61	0.57
20	1.31	-1.27	0.45
60	1.29	-0.93	0.36

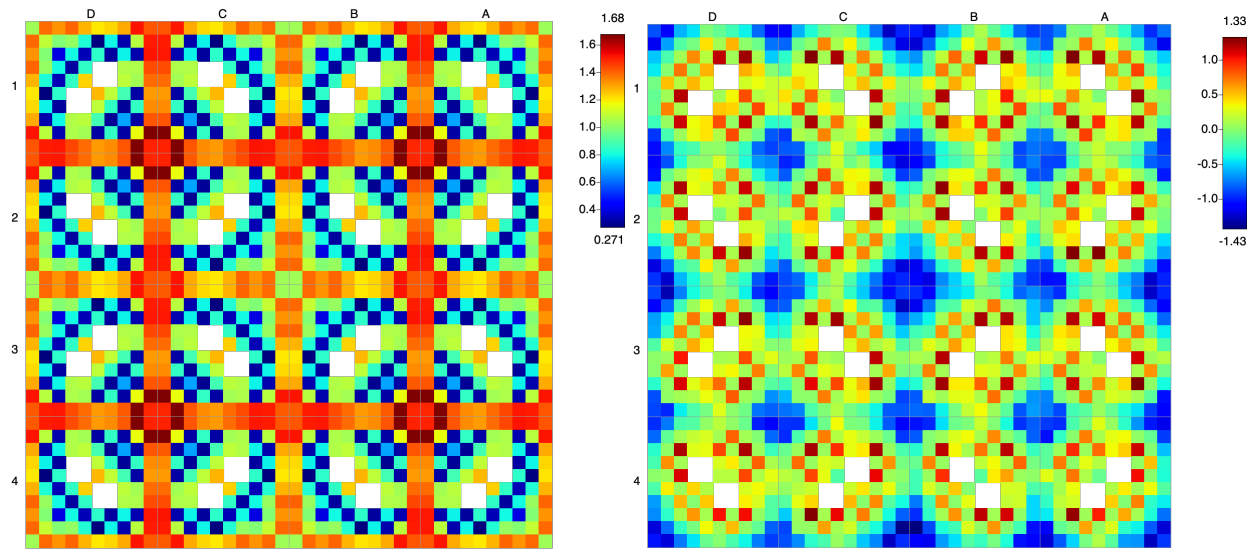


Figure 47. Normalized fission rates from MCNP (left) and differences between MPACT and MCNP (right) for the Uncontrolled mini-core at 0% system averaged void

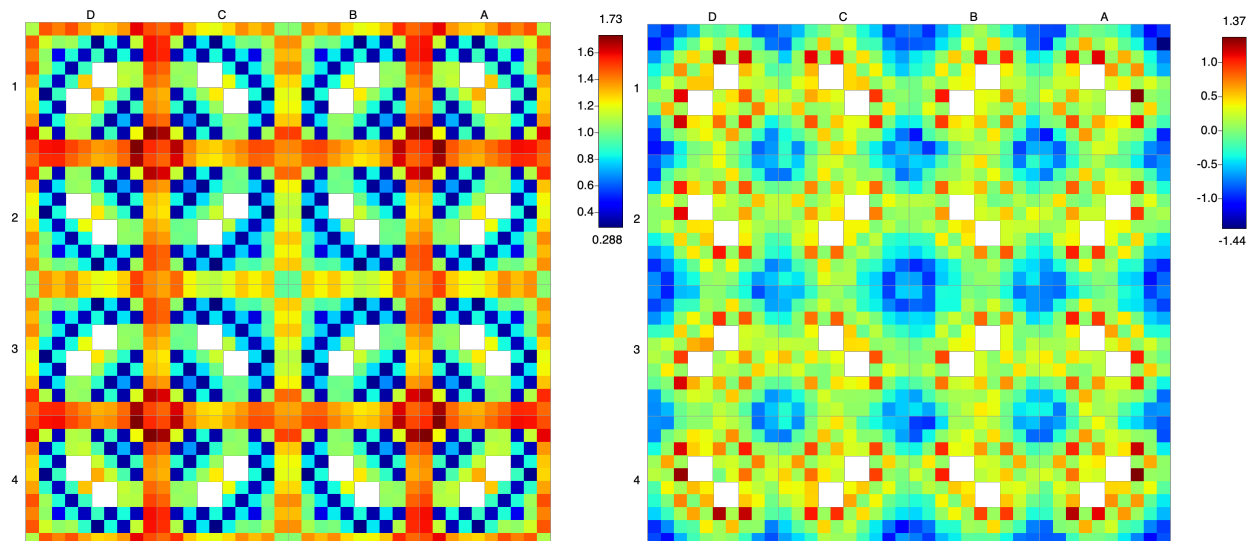


Figure 48. Normalized fission rates from MCNP (left) and differences between MPACT and MCNP (right) for the Uncontrolled mini-core at 20% system averaged void

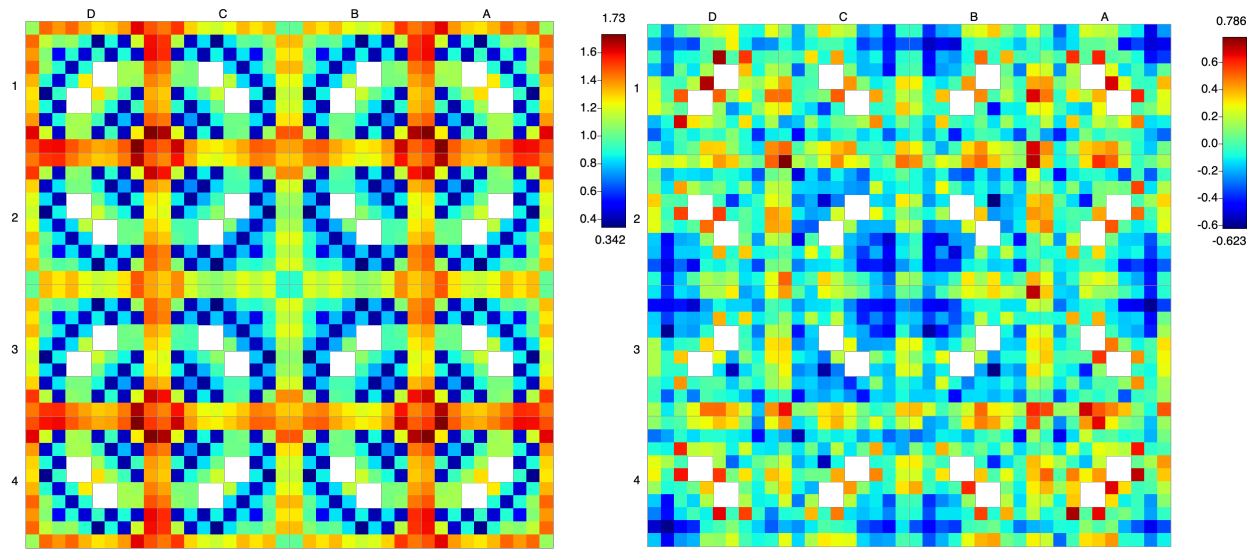


Figure 49. Normalized fission rates from MCNP (left) and differences between MPACT and MCNP (right) for the Uncontrolled mini-core at 60% system averaged void

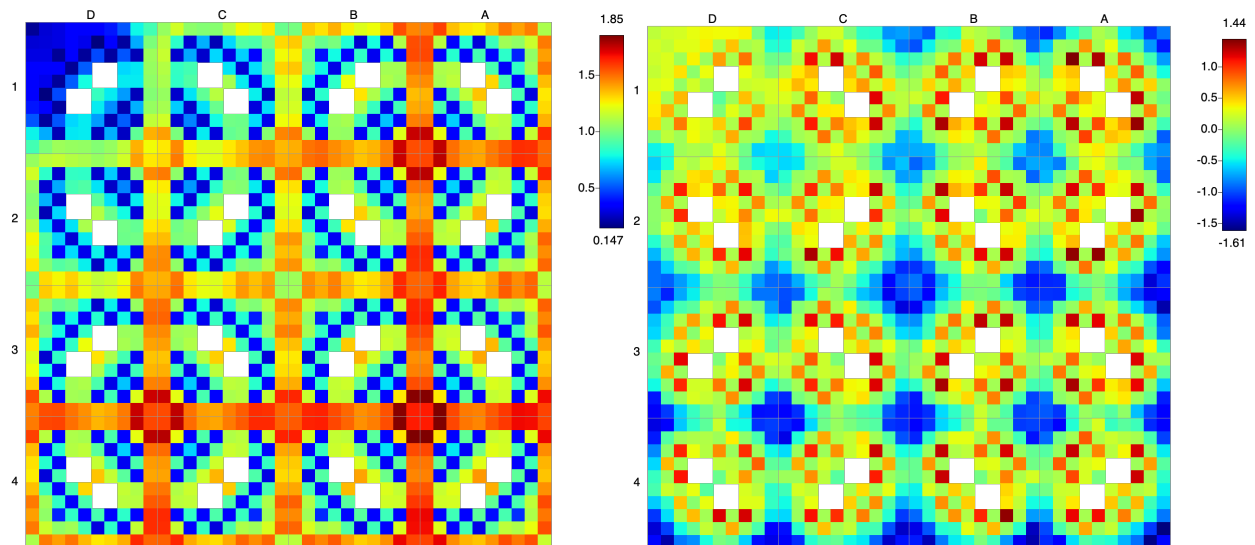


Figure 50. Normalized fission rates from MCNP (left) and differences between MPACT and MCNP (right) for the Controlled mini-core at 0% system averaged void

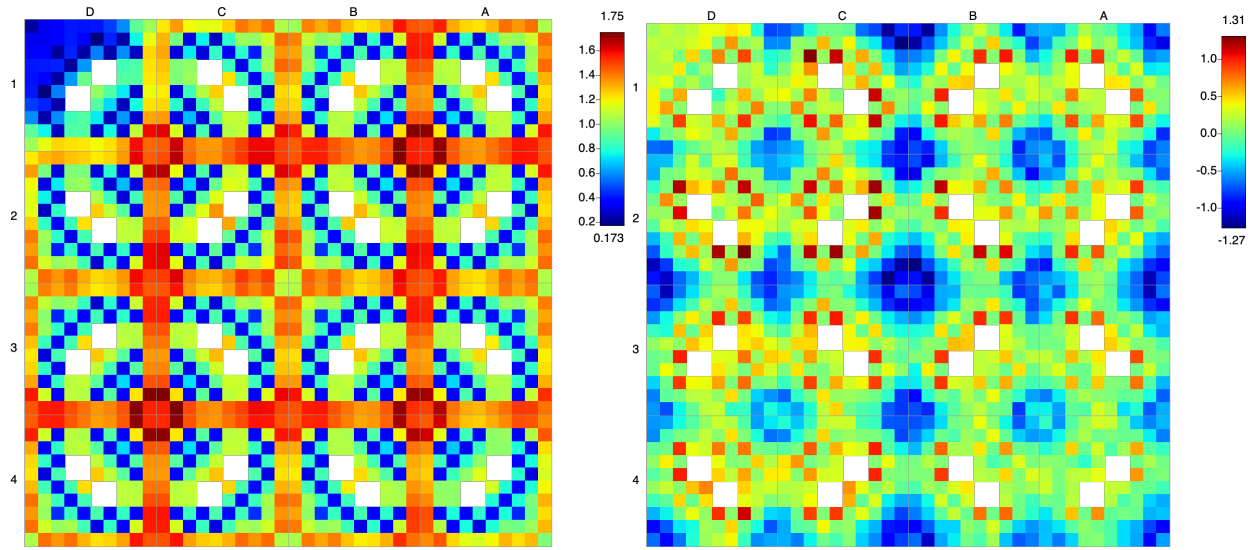


Figure 51. Normalized fission rates from MCNP (left) and differences between MPACT and MCNP (right) for the Controlled mini-core at 20% system averaged void

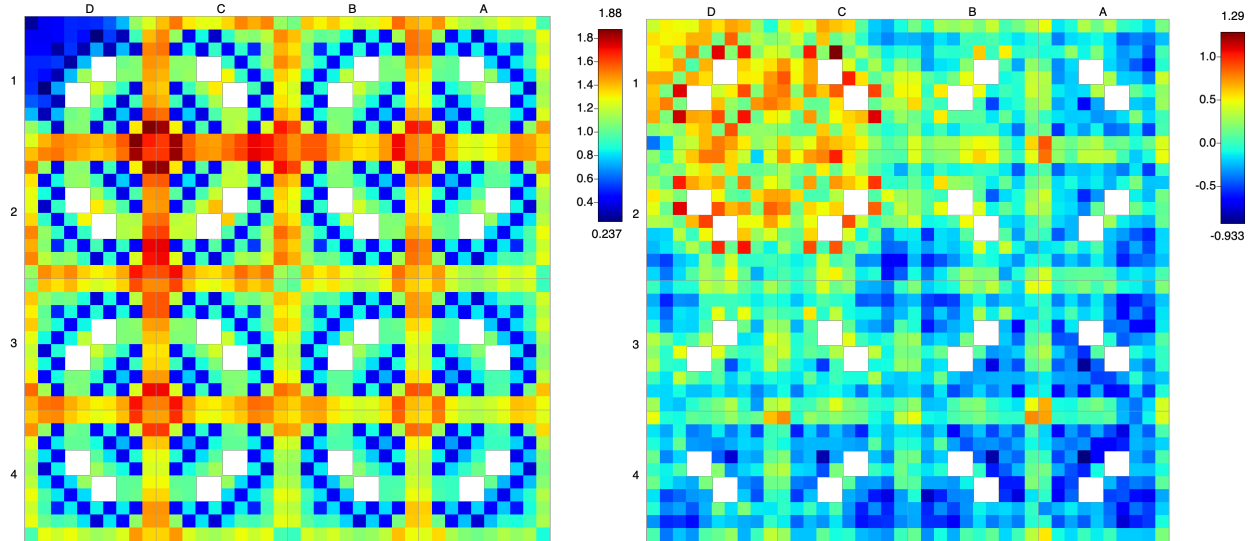


Figure 52. Normalized fission rates from MCNP (left) and differences between MPACT and MCNP (right) for the Controlled mini-core at 60% system averaged void

4.6 3D GE14 Bundle

Eigenvalues for the two single assembly 3D problems are provided in Table 25. These results were obtained with MCNP simulations using 3.6 billion active particles resulting in a standard deviation of the eigenvalue of 1 pcm for both cases. This large number of particles was necessary to drive down the error in tallies near the top or bottom of the bundle where the flux is relatively low.

Table 25. Eigenvalues from MCNP for the 3D GE14 bundle problems.

Uncontrolled		
State	Void [%]	MCNP
HZP	0	0.98753
HFP	40	0.96317

The power distribution from the HFP case with 40% void throughout the bundle can be seen in Figure 53 it was calculated with MCNP6 and was visualized using the Consortium for the Advanced Simulation of Light Water Reactors (CASL) VERAView. In Figure 53, the figure on the left has axial slices along the north and west edges of the GE14 bundle and offers a clear view of the fission rate distribution axially. The top and bottom axial blankets are very distinguishable. The left image in Figure 53 slices the bundle axially one row in from the north and west edges and shows how well the MCNP calculation captures the part length rods. Similar figures for the HZP case are shown in Figure 54. The percent relative standard deviation is plotted axially for the most limiting pin for both cases in Figure 55. For the majority of both bundles the relative standard deviation is below 0.1%. In the very top and bottom of the bundle where the fission rate drops off significantly as seen in Figure 53 and Figure 54, the errors spike to just over 0.3% in the HZP case and to 0.19% in the HFP case. Where the thermal flux and fission rates are suppressed due to spacer grids, the relative errors peak. In Figure 57 and Figure 58, the axial fission rate distribution in a part length rod and the hottest rod are shown for the two cases.

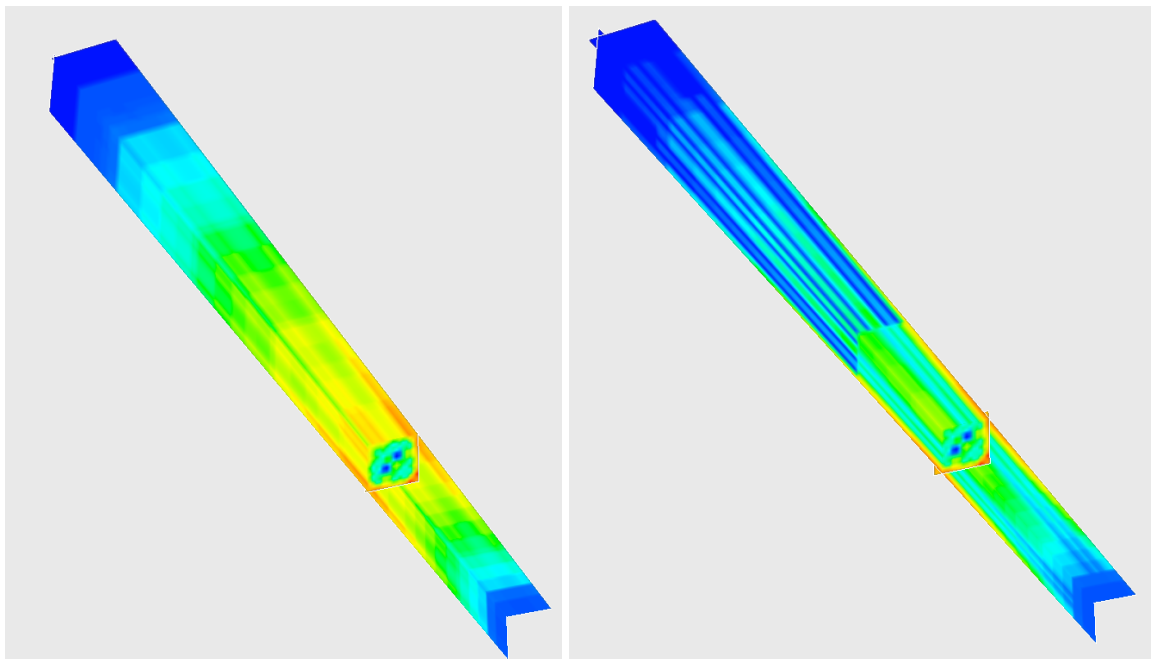


Figure 53. Normalized fission rate distribution throughout the HFP GE14 Bundle from MCNP calculations.

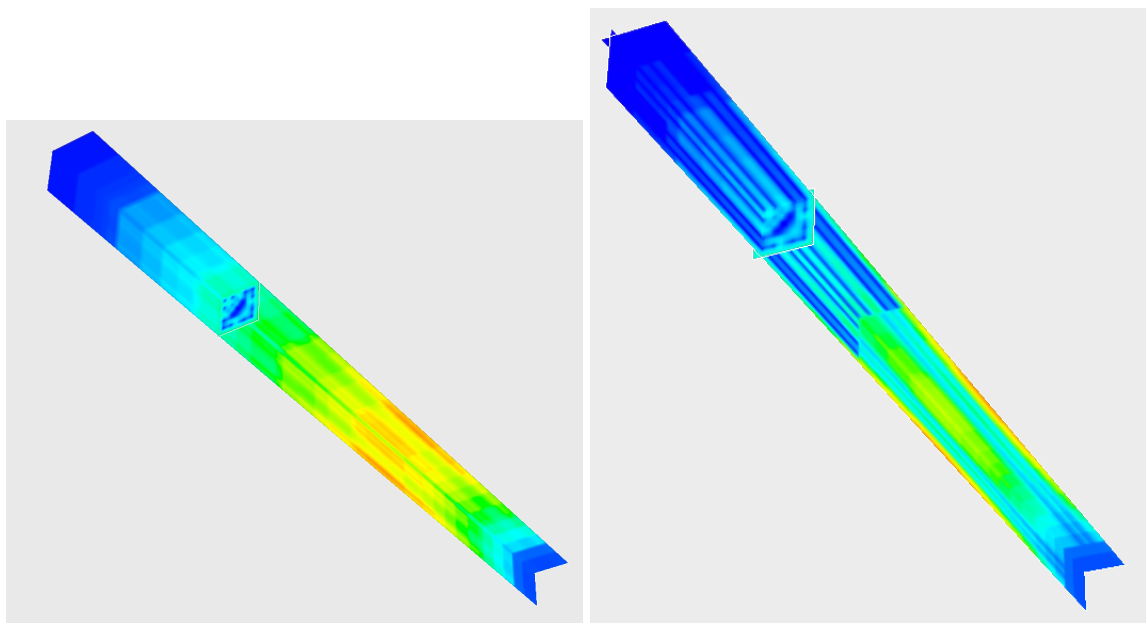


Figure 54. Normalized fission rate distribution throughout the HZP GE14 Bundle from MCNP calculations.

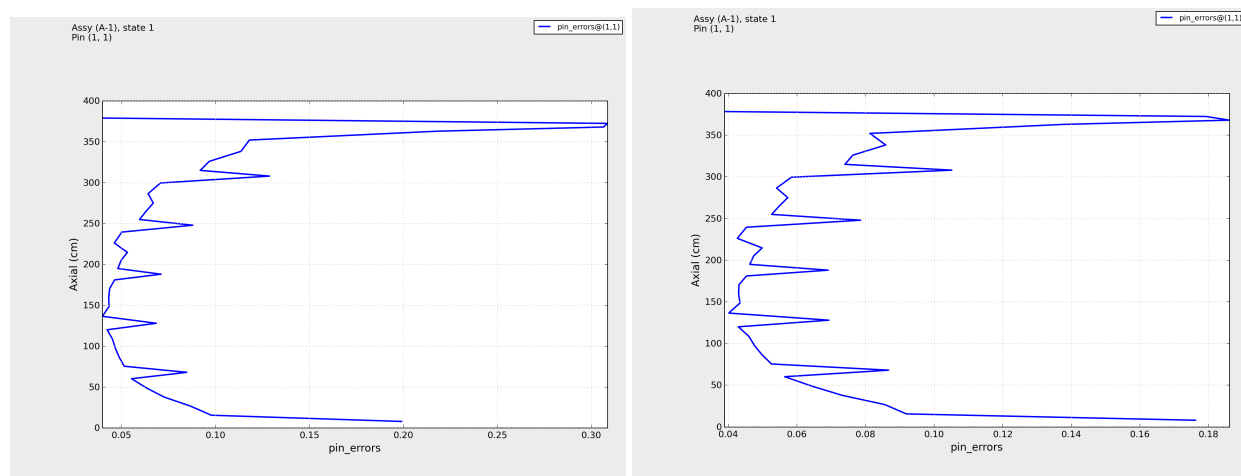


Figure 55. Relative standard deviation in the most limiting pin for the HZP (left) and HFP (right) cases. The errors are in percent.

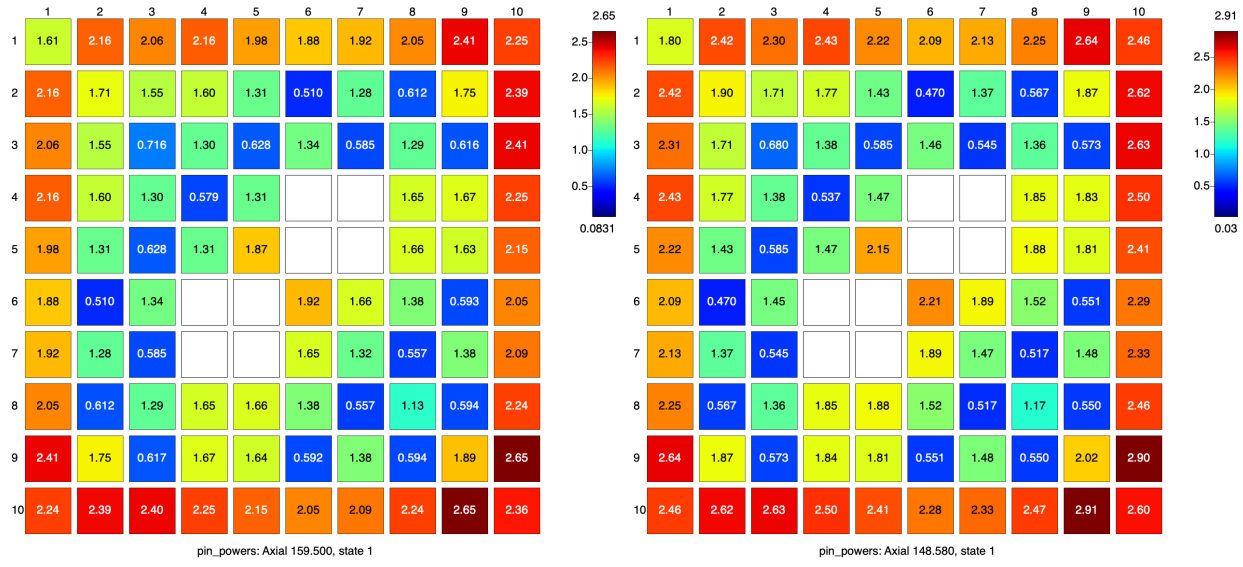


Figure 56. Radial view of normalized fission rates at the axial peak for the HFP (left) and HZP (right) cases.

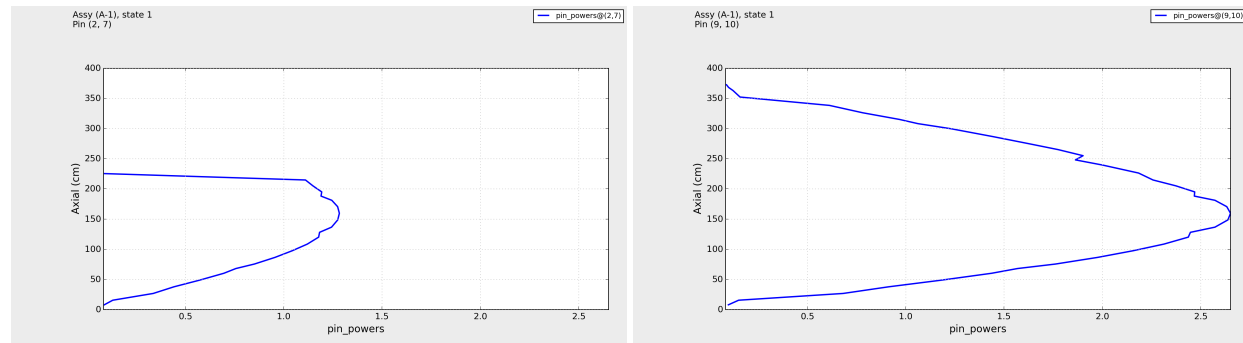


Figure 57. Axial distribution of fission rates for the HFP case in a part length rod (left) and the hottest rod (right).

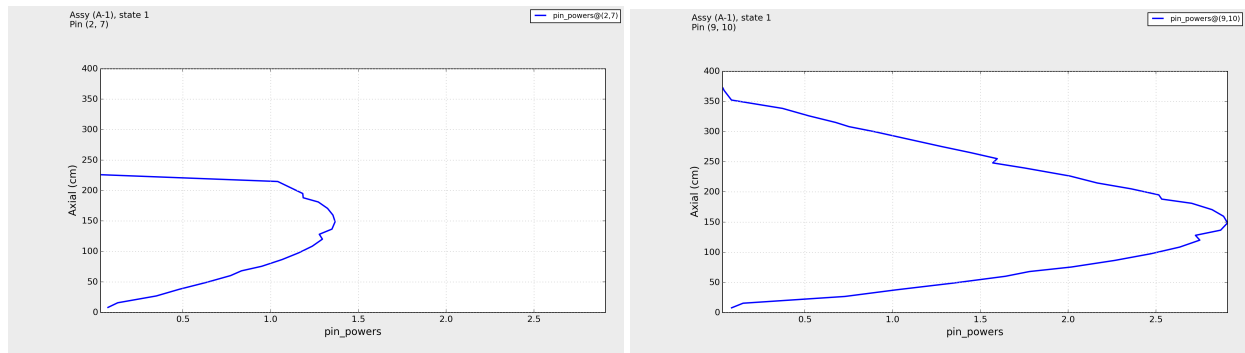


Figure 58. Axial distribution of fission rates for the HZP case in a part length rod (left) and the hottest rod (right).

5. CONCLUSION

The BWR progression problems will be used to test VERA during the development of its BWR capabilities. So far, 4 lattice problems have been developed consisting of two 8×8 bundles and two 10×10 bundles one of which has 14 vanished rods. Each lattice is tested with a void concentration of 0%, 40%, and 80% and with a controlled and uncontrolled variant, resulting in 24 lattice progression problems. Additionally, a 2D, 16 bundle mini-core problem has been developed which has controlled and uncontrolled variations with 3 different assembly void distributions.

The development of the 2D progression problems is complete and Monte Carlo reference solutions have been provided from both MCNP and Serpent for all 2D lattice problems. MCNP reference solutions have been provided for the 2D mini-core problem. A future version of this report will contain Serpent results for the mini-core problems.

In addition to the 2D progression problems a couple of preliminary 3D GE-14 bundle problems have been developed. Reference solutions have been provided for these 3D problems using MCNP. Again, a future update to this document will contain Serpent results for these 3D problems.

For all progression problems VERA, MCNP, and Serpent inputs are provided in a public Github repository: <https://github.com/cdlawing1/BWRProgressionProblemInputs>. Additionally, the MCNP and Serpent results are provided in HDF5 files that can be visualized with VERAView. These files will allow for easy comparison for future results using VERAView. This is especially important for the mini-core and 3D problems where it would be impractical to provide detailed fission rate distributions in this report.

The final report on the VERA BWR progression problems, with full specifications for various 2D and 3D problems will be completed by sometime in September 2020.

6. REFERENCES

- [1] General Electric systems and technology manual: Chapter 2.2 fuel and control rods system. Technical report, US NRC. URL <https://www.nrc.gov/docs/ML1125/ML11258A302.pdf>.
- [2] Spent nuclear fuel for disposal in the kbs-3 repository. Technical report, Svensk Kärnbränslehantering AB, December 2010. URL <https://skb.se/upload/publications/pdf/TR-10-13.pdf>. TR-10-13.
- [3] UK ABWR generic design assessment. Technical Report UE-GD-0182, GE-Hitachi, 2014.
- [4] Michael Fensin. Optimum boiling water reactor fuel design strategies to enhance reactor shutdown by the standby liquid control system. Master's thesis, University of Florida, 2004.
- [5] Andrew Godfrey. Vera core physics benchmark progression problem specifications. Technical Report CASL-U-2012-0131-004, CASL, August 2014. URL <https://www.casl.gov/sites/default/files/docs/CASL-U-2012-0131-004.pdf>.
- [6] MegaWatSoft Inc. Steam tables online. URL <https://www.steamtablesonline.com/Steam97Web.aspx>.
- [7] D.J. Kelly. Depletion of a BWR lattice using the RACER continuous energy monte carlo code. In *Proceedings of the International Conference on Mathematics and Computations, Reactor Physics, and Environmental Analyses*. American Nuclear Society, 1995.
- [8] J. Leppänen, M. Pusa, T. Viitanen, V. Valtavirta, and T. Kaltiaisenaho. The serpent monte carlo code: Status, development, and applications in 2013. *Annals of Nuclear Energy*, 82:142–150, 2015.
- [9] *MCNP Users Manual - Code Version 6.2*. Los Alamos National Laboratory, 2017. LA-UR-17-29981.
- [10] Scott Palmtag, Andrew Godfrey, Mark Baird, and Erik Walker. Vera common input user manual. Technical Report CASL-U-2014-0014-003, CASL, July 2019.
- [11] Jorge Solis, Kostadin Ivanov, and Baris Sarikaya. Boiling water reactor turbine trip (tt) benchmark, volume i final specifications. Technical report, OECD NEA, February 2001.
- [12] H.E. Williamson and D.L. Zimmerman. Effects of irradiation on B₄C filled stainless steel tubes in the dresden nuclear power station. Technical Report APED-4426, GE, March 1964.

Appendices

A Number Densities For all Materials

Number densities for all materials used in the BWR progression problems are provided in the following sections. Isotopes are referenced using the ZAID format used in MCNP. All number densities are in units of *atom/barn – cm*.

A.1 Structural Material for the Peach Bottom 6 Lattice

Number densities for the structural materials in the Peach Bottom 6 lattice are provided in the following listing. For the Peach Bottom 6 lattice, a specific zircaloy density (6.5514 g/cc) was provided in [11]. This density matches the number densities shown here.

Zircaloy-4		Zircaloy-2		B₄C	
24050	3.2968866141E-06	24050	3.2968866141E-06	5010	1.5209107996E-02
24052	6.3577105908E-05	24052	6.3577561664E-05	5011	6.1218387852E-02
24053	7.2091359200E-06	24053	7.2091210153E-06	6000	1.9106892039E-02
24054	1.7945095672E-06	24054	1.7944876240E-06		
26054	8.6716696590E-06	26054	5.5746761283E-06		
26056	1.3612707909E-04	26056	8.7510768952E-05		
26057	3.1437631362E-06	26057	2.0210029618E-06		
26058	4.1837688557E-07	26058	2.6895496406E-07		
40090	2.1857820282E-02	28058	2.5168392905E-05		
40091	4.7666719010E-03	28060	9.6948943550E-06		
40092	7.2859564333E-03	28061	4.2142787756E-07		
40094	7.3836454528E-03	28062	1.3437099713E-06		
40096	1.1895401226E-03	28064	3.4220074608E-07		
50112	4.6745084653E-06	40090	2.1862296412E-02		
50114	3.1806027268E-06	40091	4.7676267110E-03		
50115	1.6384932071E-06	40092	7.2874160028E-03		
50116	7.0069536357E-05	40094	7.3851579439E-03		
50117	3.7010617333E-05	40096	1.1897828288E-03		
50118	1.1671854166E-04	50112	4.6745437217E-06		
50119	4.1396077147E-05	50114	3.1806096543E-06		
50120	1.5700601411E-04	50115	1.6384966407E-06		
50122	2.2312399102E-05	50116	7.0069536357E-05		
50124	2.7902567370E-05	50117	3.7010617333E-05		
72174	3.5367440362E-09	50118	1.1671820703E-04		
72176	1.1627038879E-07	50119	4.1396077147E-05		
72177	4.1114602978E-07	50120	1.5700634316E-04		
72178	6.0301550100E-07	50122	2.2312463831E-05		
72179	3.0106525787E-07	50124	2.7902535529E-05		
72180	7.7543042177E-07	72174	3.5367440362E-09		
		72176	1.1627038879E-07		
		72177	4.1114602978E-07		
2004	2.6480209540E-05	72178	6.0301550100E-07		
		72179	3.0106525787E-07		
		72180	7.7543042177E-07		

A.2 Structural Materials for all Problems Problems except the Peach Bottom 6 Lattice

For all problems except the Peach Bottom 6 lattice, a specific density for Zircaloy was not provided, thus, the default density for Zircaloy from [10] (6.56 g/cc) is used in all other problems. This results in some slight but non-negligible differences in the Zircaloy number densities.

Zircaloy-4		Zircaloy-2		B₄C	
24050	3.3012144257E-06	24050	3.3012144257E-06	5010	1.5209107996E-02
24052	6.3660563353E-05	24052	6.3661019708E-05	5011	6.1218387852E-02
24053	7.2185993277E-06	24053	7.2185844034E-06	6000	1.9106892039E-02
24054	1.7968652137E-06	24054	1.7968432416E-06		
26054	8.6830529296E-06	26054	5.5819939862E-06		
26056	1.3630577263E-04	26056	8.7625644034E-05		
26057	3.1478899432E-06	26057	2.0236559253E-06		
26058	4.1892608745E-07	26058	2.6930802030E-07		
40090	2.1886512966E-02	28058	2.5201431366E-05		
40091	4.7729290946E-03	28060	9.7076208091E-06		
40092	7.2955206830E-03	28061	4.2198108447E-07		
40094	7.3933379385E-03	28062	1.3454738547E-06		
40096	1.1911016278E-03	28064	3.4264995181E-07		
50112	4.6806446763E-06	40090	2.1890994972E-02		
50114	3.1847778929E-06	40091	4.7738851580E-03		
50115	1.6406440514E-06	40092	7.2969821685E-03		
50116	7.0161516394E-05	40094	7.3948524151E-03		
50117	3.7059201042E-05	40096	1.1913446526E-03		
50118	1.1687175769E-04	50112	4.6806799790E-06		
50119	4.1450417634E-05	50114	3.1847848296E-06		
50120	1.5721211536E-04	50115	1.6406474895E-06		
50122	2.2341688511E-05	50116	7.0161516394E-05		
50124	2.7939194974E-05	50117	3.7059201042E-05		
72174	3.5413867078E-09	50118	1.1687142262E-04		
72176	1.1642301652E-07	50119	4.1450417634E-05		
72177	4.1168573974E-07	50120	1.5721244484E-04		
72178	6.0380707735E-07	50122	2.2341753325E-05		
72179	3.0146046519E-07	50124	2.7939163090E-05		
72180	7.7644832659E-07	72174	3.5413867078E-09		
		72176	1.1642301652E-07		
		72177	4.1168573974E-07		
2004	2.6871394453E-05	72178	6.0380707735E-07		
		72179	3.0146046519E-07		
		72180	7.7644832659E-07		

A.3 Fuels

The number densities for all fuels are given in this section. A separate listing is provided for each bundle type and the fuels are labeled following the rod labels provided in tables in the problem descriptions.

A.3.1 Peach Bottom Type 6

The fuel names here match the rod labels from Table 3.

Fuel: 1	Fuel: 2	Fuel: 3
92235 7.0155366968E-04	92235 5.1743125385E-04	92235 4.3585660109E-04
92234 6.2705860564E-06	92234 4.6248738276E-06	92234 3.8957480283E-06
92236 3.2134519291E-06	92236 2.3700830495E-06	92236 1.9964320566E-06
92238 2.2310983408E-02	92238 2.2495514040E-02	92238 2.2577269552E-02
8016 4.6044042232E-02	8016 4.6039880502E-02	8016 4.6038036666E-02
Fuel: 4	Fuel: 5	
92235 3.3796585825E-04	92235 6.8152675969E-04	
92234 3.0207867051E-06	92234 6.0915826986E-06	
92236 1.5480455539E-06	92236 3.1217190862E-06	
92238 2.2675377327E-02	92238 2.1674082661E-02	
8016 4.6035824036E-02	64152 1.3596568956E-06 64154 1.4820017148E-05 64155 1.0061252739E-04 64156 1.3915845081E-04 64157 1.0639132099E-04 64158 1.6886620921E-04 64160 1.4860810463E-04 8016 4.5749372650E-02	

A.3.2 GE9

The fuel numbers here match the rod labels from Table 5.

Fuel: 1		Fuel: 2		Fuel: 3	
92235	3.6368330841E-04	92235	4.5460133817E-04	92235	5.0005993347E-04
92234	3.2506529168E-06	92234	4.0632911430E-06	92234	4.4696065058E-06
92236	1.6658437971E-06	92236	2.0822919333E-06	92236	2.2905140794E-06
92238	2.2079156652E-02	92238	2.1988037049E-02	92238	2.1942477667E-02
8016	4.4895512914E-02	8016	4.4897567940E-02	8016	4.4898595443E-02
Fuel: 4		Fuel: 5		Fuel: 6	
92235	5.4551824904E-04	92235	5.9097628490E-04	92235	6.3643404104E-04
92234	4.8759193684E-06	92234	5.2822297309E-06	92234	5.6885375931E-06
92236	2.4987349443E-06	92236	2.7069545280E-06	92236	2.9151728304E-06
92238	2.1896918567E-02	92238	2.1851359746E-02	92238	2.1805801206E-02
8016	4.4899622940E-02	8016	4.4900650430E-02	8016	4.4901677915E-02
Fuel: 7		Fuel: 8		Fuel: 9	
92235	6.8189151747E-04	92235	8.1826226850E-04	92235	8.6371862610E-04
92234	6.0948429553E-06	92234	7.3137440414E-06	92234	7.7200394034E-06
92236	3.1233898516E-06	92236	3.7480332280E-06	92236	3.9562451245E-06
92238	2.1760242946E-02	92238	2.1623569848E-02	92238	2.1578012710E-02
8016	4.4902705393E-02	8016	4.4905787789E-02	8016	4.4906815241E-02
Fuel: 10		Fuel: 51		Fuel: 52	
92235	8.9781071075E-04	92235	8.5117615190E-04	92235	7.7575965692E-04
92234	8.0247592842E-06	92234	7.6079329926E-06	92234	6.9338496797E-06
92236	4.1124032061E-06	92236	3.8987945834E-06	92236	3.5533509035E-06
92238	2.1543845040E-02	92238	2.0424803245E-02	92238	2.0500386945E-02
8016	4.4907585827E-02	64152	2.6419608770E-06	64152	2.6419608770E-06
		64154	2.8796901355E-05	64154	2.8796901355E-05
		64155	1.9550105763E-04	64155	1.9550105763E-04
		64156	2.7039996922E-04	64156	2.7039996922E-04
		64157	2.0672988062E-04	64157	2.0672988062E-04
		64158	3.2812536722E-04	64158	3.2812536722E-04
		64160	2.8876167193E-04	64160	2.8876167193E-04
		8016	4.4556412853E-02	8016	4.4554708209E-02

A.3.3 GE14

The fuel numbers here match the rod labels from Table 7. These fuel number densities are used in all GE-14, GE-14 with vanished rods, mini-core, and 3D GE-14 cases.

Fuel: 1		Fuel: 2		Fuel: 3	
92235	3.7581788989E-04	92235	6.5766916663E-04	92235	7.5161727982E-04
92234	3.3591135247E-06	92234	5.8783401531E-06	92234	6.7180616940E-06
92236	1.7214259941E-06	92236	3.0124398796E-06	92236	3.4427672495E-06
92238	2.2815845192E-02	92238	2.2533369025E-02	92238	2.2439212620E-02
8016	4.6393487243E-02	8016	4.6399857943E-02	8016	4.6401981458E-02
Fuel: 4		Fuel: 5		Fuel: 6	
92235	8.4556423684E-04	92235	9.2776687584E-04	92235	1.0334546825E-03
92234	7.5577729010E-06	92234	8.2925117303E-06	92234	9.2371643140E-06
92236	3.8730893237E-06	92236	4.2496167945E-06	92236	4.7337175851E-06
92238	2.2345057374E-02	92238	2.2262672484E-02	92238	2.2156750358E-02
8016	4.6404104946E-02	8016	4.6405962977E-02	8016	4.6408351845E-02
Fuel: 7		Fuel: 5G		Fuel: 6H	
92235	1.1508838627E-03	92235	8.3631047188E-04	92235	9.5183163669E-04
92234	1.0286762957E-05	92234	7.4750614393E-06	92234	8.5076059709E-06
92236	5.2715994919E-06	92236	3.8307026466E-06	92236	4.3598449289E-06
92238	2.2039060827E-02	92238	2.0068086731E-02	92238	2.0406793171E-02
8016	4.6411006103E-02	64152	5.4173621766E-06	64152	4.0630216324E-06
		64154	5.9048279466E-05	64154	4.4286209599E-05
Fuel: N		64155	4.0087650210E-04	64155	3.0065737658E-04
92235	1.6677147196E-04	64156	5.5445732697E-04	64156	4.1584299522E-04
92234	1.4906270352E-06	64157	4.2390129459E-04	64157	3.1792597094E-04
92236	7.6389324357E-07	64158	6.7282372311E-04	64158	5.0461779233E-04
92238	2.3025355085E-02	64160	5.9210814709E-04	64160	4.4408111032E-04
8016	4.6388762155E-02	8016	4.5894365941E-02	8016	4.5790204522E-02
Fuel: 6K		Fuel: 7G		Fuel: 7H	
92235	9.8220924212E-04	92235	1.0374332727E-03	92235	1.0599861699E-03
92234	8.7791253104E-06	92234	9.2727255165E-06	92234	9.4743065060E-06
92236	4.4989889160E-06	92236	4.7519414343E-06	92236	4.8552445090E-06
92238	2.1058073804E-02	92238	1.9866518023E-02	92238	2.0298398849E-02
64152	2.0315108162E-06	64152	5.4173621766E-06	64152	4.0630216324E-06
64154	2.2143104800E-05	64154	5.9048279466E-05	64154	4.4286209599E-05
64155	1.5032868829E-04	64155	4.0087650210E-04	64155	3.0065737658E-04
64156	2.0792149761E-04	64156	5.5445732697E-04	64156	4.1584299522E-04
64157	1.5896298547E-04	64157	4.2390129459E-04	64157	3.1792597094E-04
64158	2.5230889617E-04	64158	6.7282372311E-04	64158	5.0461779233E-04
64160	2.2204055516E-04	64160	5.9210814709E-04	64160	4.4408111032E-04
8016	4.5630732324E-02	8016	4.5898911931E-02	8016	4.5792649145E-02

A.4 Smeared Grid and Nozzle Number Densities

The spacer grids and nozzles are all smeared into coolant using the data from Table 11 to perform volume weighted averaging on the number densities. The lower nozzles are always smeared into coolant at 0% void because they exist below the point where active fuel begins to heat the coolant. Top nozzles are smeared into coolant at the exit void and spacer grids are smeared into coolant at a void that matches their local conditions. For spacer grids, the lattice as well as the void concentrations are specified. The lattice is specified because the fuel pin array determines the flow area for the coolant inside of the channel box and thus determines the volume of coolant to smear the grid into. For example, the flow area is greater in regions with vanished rods.

A.4.1 Smeared Structures for 3D HZP Case

Lower Nozzle (0% void)		Upper Nozzle (0% void)		Inconel Grid in NAT lattice (0% void)	
6000	5.6097557583E-05	6000	3.7398371722E-05	14028	4.8455867324E-04
14028	2.7655369472E-04	14028	1.8436912982E-04	14029	2.4615956802E-05
14029	1.4049142402E-05	14029	9.3660949350E-06	14030	1.6246006069E-05
14030	9.2721341107E-06	14030	6.1814227404E-06	22046	2.5427482863E-05
15031	1.2236062806E-05	15031	8.1573752043E-06	22047	2.2930966364E-05
24050	1.3371944635E-04	24050	8.9146297568E-05	22048	2.2721382262E-04
24052	2.5786516234E-03	24052	1.7191010823E-03	22049	1.6674264520E-05
24053	2.9239838400E-04	24053	1.9493225600E-04	22050	1.5965377119E-05
24054	7.2784008622E-05	24054	4.8522672415E-05	24050	7.3987683390E-05
25055	3.0660469832E-04	25055	2.0440313221E-04	24052	1.4267784160E-03
26054	6.0272515204E-04	26054	4.0181676803E-04	24053	1.6178553861E-04
26056	9.4614920805E-03	26056	6.3076613870E-03	24054	4.0271740042E-05
26057	2.1850651465E-04	26057	1.4567100977E-04	26054	4.3246016469E-05
26058	2.9079296625E-05	26058	1.9386197750E-05	26056	6.7887022896E-04
28058	9.2801922734E-04	28058	6.1867948490E-04	26057	1.5678133523E-05
28060	3.5747076177E-04	28060	2.3831384118E-04	26058	2.0864604063E-06
28061	1.5538965018E-05	28061	1.0359310012E-05	28058	4.9978449496E-03
28062	4.9545201910E-05	28062	3.3030134606E-05	28060	1.9251648359E-03
28064	1.2617711867E-05	28064	8.4118079111E-06	28061	8.3685495010E-05
1001	4.0652712052E-02	1001	4.3523465861E-02	28062	2.6682627689E-04
8016	2.0326356026E-02	8016	2.1761732930E-02	28064	6.7952704122E-05
				1001	4.3368978076E-02
				8016	2.1684489038E-02

Zirc-4 Grid in PSZ/DOM/PLE lattice (0% void)		Zirc-4 Grid in VAN lattice (0% void)		Inconel Grid in PLEN lattice (0% void)	
24050	4.2900540501E-07	24050	3.8089940464E-07	14028	4.3022327457E-04
24052	8.2729330007E-06	24052	7.3452577003E-06	14029	2.1855676364E-05
24053	9.3808451341E-07	24053	8.3289354514E-07	14030	1.4424279897E-05
24054	2.3350948752E-07	24054	2.0732518457E-07	22046	2.2576202936E-05
26054	1.1283958442E-06	26054	1.0018645459E-06	22047	2.0359630284E-05
26056	1.7713455006E-05	26056	1.5727178229E-05	22048	2.0173547641E-04
26057	4.0908030375E-07	26057	3.6320858043E-07	22049	1.4804516107E-05
26058	5.4441042793E-08	26058	4.8336362539E-08	22050	1.4175118934E-05
40090	2.8442358322E-03	40090	2.5253008995E-03	24050	6.5691164319E-05
40091	6.2026033916E-04	40091	5.5070819890E-04	24052	1.2667883501E-03
40092	9.4808073690E-04	40092	8.4176885424E-04	24053	1.4364391361E-04
40094	9.6079246232E-04	40094	8.5305516576E-04	24054	3.5755917353E-05
40096	1.5478819923E-04	40096	1.3743121239E-04	26054	3.8396676904E-05
50112	6.0826762704E-07	50112	5.4006027499E-07	26056	6.0274593984E-04
50114	4.1387403350E-07	50114	3.6746477111E-07	26057	1.3920085050E-05
50115	2.1320795168E-07	50115	1.8930013681E-07	26058	1.8524977012E-06
50116	9.1177566421E-06	50116	8.0953480681E-06	28058	4.4374176725E-03
50117	4.8159845143E-06	50117	4.2759499364E-06	28060	1.7092888138E-03
50118	1.5187930645E-05	50118	1.3484850477E-05	28061	7.4301523603E-05
50119	5.3866398579E-06	50119	4.7826155357E-06	28062	2.3690603620E-04
50120	2.0430313977E-05	50120	1.8139385518E-05	28064	6.0332910126E-05
50122	2.9033876302E-06	50122	2.5778197824E-06	1001	4.4030118364E-02
50124	3.6308049432E-06	50124	3.2236690379E-06	8016	2.2015059182E-02
72174	4.6021670905E-10	72174	4.0861086699E-10		
72176	1.5129615019E-08	72176	1.3433074003E-08		
72177	5.3500131994E-08	72177	4.7500959631E-08		
72178	7.8467032542E-08	72178	6.9668227090E-08		
72179	3.9175937181E-08	72179	3.4782991017E-08		
72180	1.0090242131E-07	72180	8.9587850772E-08		
1001	4.2862802285E-02	1001	4.3580701981E-02		
8016	2.1431401143E-02	8016	2.1790350990E-02		

A.4.2 Smeared Structures for 3D HFP 40% Case

Lower Nozzle (0% void)		Upper Nozzle (40% void)		Inconel Grid in NAT lattice (40% void)	
6000	5.6097557583E-05	6000	3.7398371722E-05	14028	4.8455867324E-04
14028	2.7655369472E-04	14028	1.8436912982E-04	14029	2.4615956802E-05
14029	1.4049142402E-05	14029	9.3660949350E-06	14030	1.6246006069E-05
14030	9.2721341107E-06	14030	6.1814227404E-06	22046	2.5427482863E-05
15031	1.2236062806E-05	15031	8.1573752043E-06	22047	2.2930966364E-05
24050	1.3371944635E-04	24050	8.9146297568E-05	22048	2.2721382262E-04
24052	2.5786516234E-03	24052	1.7191010823E-03	22049	1.6674264520E-05
24053	2.9239838400E-04	24053	1.9493225600E-04	22050	1.5965377119E-05
24054	7.2784008622E-05	24054	4.8522672415E-05	24050	7.3987683390E-05
25055	3.0660469832E-04	25055	2.0440313221E-04	24052	1.4267784160E-03
26054	6.0272515204E-04	26054	4.0181676803E-04	24053	1.6178553861E-04
26056	9.4614920805E-03	26056	6.3076613870E-03	24054	4.0271740042E-05
26057	2.1850651465E-04	26057	1.4567100977E-04	26054	4.3246016469E-05
26058	2.9079296625E-05	26058	1.9386197750E-05	26056	6.7887022896E-04
28058	9.2801922734E-04	28058	6.1867948490E-04	26057	1.5678133523E-05
28060	3.5747076177E-04	28060	2.3831384118E-04	26058	2.0864604063E-06
28061	1.5538965018E-05	28061	1.0359310012E-05	28058	4.9978449496E-03
28062	4.9545201910E-05	28062	3.3030134606E-05	28060	1.9251648359E-03
28064	1.2617711867E-05	28064	8.4118079111E-06	28061	8.3685495010E-05
1001	4.0652712052E-02	1001	2.7000819399E-02	28062	2.6682627689E-04
8016	2.0326356026E-02	8016	1.3500409699E-02	28064	6.7952704122E-05
				1001	2.6904979219E-02
				8016	1.3452489610E-02

Zirc-4 Grid in PSZ/DOM/PLE lattice (40% void)		Zirc-4 Grid in VAN/NT lattice (40% void)		Inconel Grid in PLEN lattice (40% void)	
24050	4.2900540501E-07	24050	3.8089940464E-07	14028	4.3022327457E-04
24052	8.2729330007E-06	24052	7.3452577003E-06	14029	2.1855676364E-05
24053	9.3808451341E-07	24053	8.3289354514E-07	14030	1.4424279897E-05
24054	2.3350948752E-07	24054	2.0732518457E-07	22046	2.2576202936E-05
26054	1.1283958442E-06	26054	1.0018645459E-06	22047	2.0359630284E-05
26056	1.7713455006E-05	26056	1.5727178229E-05	22048	2.0173547641E-04
26057	4.0908030375E-07	26057	3.6320858043E-07	22049	1.4804516107E-05
26058	5.4441042793E-08	26058	4.8336362539E-08	22050	1.4175118934E-05
40090	2.8442358322E-03	40090	2.5253008995E-03	24050	6.5691164319E-05
40091	6.2026033916E-04	40091	5.5070819890E-04	24052	1.2667883501E-03
40092	9.4808073690E-04	40092	8.4176885424E-04	24053	1.4364391361E-04
40094	9.6079246232E-04	40094	8.5305516576E-04	24054	3.5755917353E-05
40096	1.5478819923E-04	40096	1.3743121239E-04	26054	3.8396676904E-05
50112	6.0826762704E-07	50112	5.4006027499E-07	26056	6.0274593984E-04
50114	4.1387403350E-07	50114	3.6746477111E-07	26057	1.3920085050E-05
50115	2.1320795168E-07	50115	1.8930013681E-07	26058	1.8524977012E-06
50116	9.1177566421E-06	50116	8.0953480681E-06	28058	4.4374176725E-03
50117	4.8159845143E-06	50117	4.2759499364E-06	28060	1.7092888138E-03
50118	1.5187930645E-05	50118	1.3484850477E-05	28061	7.4301523603E-05
50119	5.3866398579E-06	50119	4.7826155357E-06	28062	2.3690603620E-04
50120	2.0430313977E-05	50120	1.8139385518E-05	28064	6.0332910126E-05
50122	2.9033876302E-06	50122	2.5778197824E-06	1001	2.7315133355E-02
50124	3.6308049432E-06	50124	3.2236690379E-06	8016	1.3657566677E-02
72174	4.6021670905E-10	72174	4.0861086699E-10		
72176	1.5129615019E-08	72176	1.3433074003E-08		
72177	5.3500131994E-08	72177	4.7500959631E-08		
72178	7.8467032542E-08	72178	6.9668227090E-08		
72179	3.9175937181E-08	72179	3.4782991017E-08		
72180	1.0090242131E-07	72180	8.9587850772E-08		
1001	2.6590961003E-02	1001	2.7036327190E-02		
8016	1.3295480501E-02	8016	1.3518163595E-02		

A.5 Coolant Number Densities

H₂O: 0% Void	H₂O: 5% Void	H₂O: 10% Void
1001 4.9264973479E-02 8016 2.4632486739E-02	1001 4.6927189356E-02 8016 2.3463594678E-02	1001 4.4589405233E-02 8016 2.2294702616E-02
H₂O: 15% Void	H₂O: 20% Void	H₂O: 25% Void
1001 4.2251621110E-02 8016 2.1125810555E-02	1001 3.9913836986E-02 8016 1.9956918493E-02	1001 3.7576052863E-02 8016 1.8788026432E-02
H₂O: 30% Void	H₂O: 35% Void	H₂O: 40% Void
1001 3.5238268740E-02 8016 1.7619134370E-02	1001 3.2900484617E-02 8016 1.6450242309E-02	1001 3.0562700494E-02 8016 1.5281350247E-02
H₂O: 45% Void	H₂O: 50% Void	H₂O: 55% Void
1001 2.8224916371E-02 8016 1.4112458186E-02	1001 2.5887132248E-02 8016 1.2943566124E-02	1001 2.3549348125E-02 8016 1.1774674063E-02
H₂O: 60% Void	H₂O: 65% Void	H₂O: 70% Void
1001 2.1211564002E-02 8016 1.0605782001E-02	1001 1.8873779879E-02 8016 9.4368899395E-03	1001 1.6535995756E-02 8016 8.2679978780E-03
H₂O: 75% Void	H₂O: 80% Void	H₂O: 85% Void
1001 1.4198211633E-02 8016 7.0991058165E-03	1001 1.1860427510E-02 8016 5.9302137550E-03	1001 9.5226433869E-03 8016 4.7613216934E-03
H₂O: 90% Void	H₂O: 95% Void	H₂O: 100% Void
1001 7.1848592638E-03 8016 3.5924296319E-03	1001 4.8470751408E-03 8016 2.4235375704E-03	1001 2.5092910177E-03 8016 1.2546455089E-03